MASTER

~~CONFIDENTIAL~~

COMPREHENSIVE TECHNICAL REPORT

DIRECT AIR CYCLE | **AIRCRAFT NUCLEAR PROPULSION PROGRAM**

APEX-919

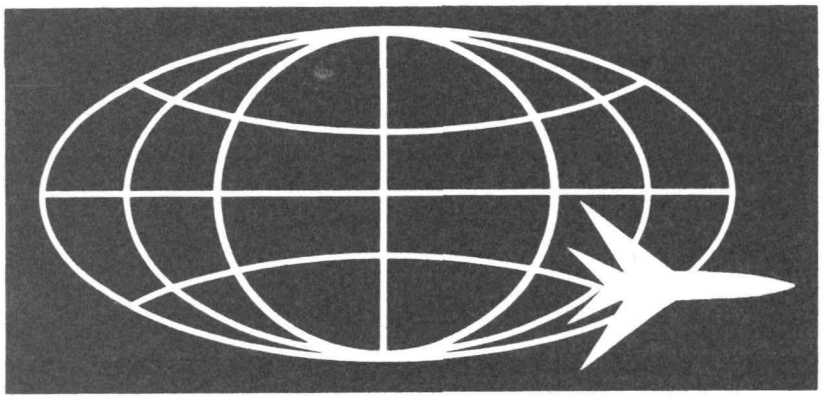

AEROTHERMODYNAMICS

FLIGHT PROPULSION LABORATORY DEPARTMENT

GENERAL ELECTRIC

DISCLAIMER

This is one of twenty-one volumes summarizing the General Electric Company's direct-air-cycle aircraft nuclear propulsion program. Additional copies are available from the United States Atomic Energy Commission, Division of Technical Information Extension, Oak Ridge, Tennessee.

The APEX number and title of each volume in the series is shown in the following list.

APEX-901 Program Summary and References
APEX-902 P-1 Nuclear Turbojet
APEX-903 Reactor Core Test Facility
APEX-904 Heat Transfer Reactor Experiment No. 1
APEX-905 Heat Transfer Reactor Experiment No. 2
APEX-906 Heat Transfer Reactor Experiment No. 3
APEX-907 XMA-1 Nuclear Turbojet
APEX-908 XNJ140E Nuclear Turbojet
APEX-909 Aircraft Nuclear Propulsion Systems Studies
APEX-910 Aircraft Nuclear Propulsion Application Studies
APEX-911 Remote Handling Equipment
APEX-912 Controls and Instrumentation
APEX-913 Metallic Fuel Element Materials
APEX-914 Ceramic Reactor Materials
APEX-915 Shield Materials
APEX-916 Moderator Materials
APEX-917 Organic, Structural and Control Materials
APEX-918 Reactor and Shield Physics
APEX-919 Aerothermodynamics
APEX-920 Applied Mechanics
APEX-921 Nuclear Safety

APEX-919

COMPREHENSIVE TECHNICAL REPORT GENERAL ELECTRIC DIRECT-AIR-CYCLE RCRAFT NUCLEAR PROPULSION PROGRAM

AEROTHERMODYNAMICS

Author: R. N. NOYES

Contributors: G. A. GAST, C. S. LANKTON, S. C. SKIRVIN, L. W. HABEL, C. W. MOON, W. R. TERRILL, R. R. JORDAN, A. G. ROBISON

Editor: R. GEHRING

December 6 ,1961

United States Air Force — Contract No. AF 33(600)—38062

United States Atomic Energy Commission — Contract No. AT(11-1)—171

AEC RESEARCH AND DEVELOPMENT REPORT

GENERAL ELECTRIC

NUCLEAR MATERIALS AND PROPULSION OPERATION
(Formerly Aircraft Nuclear Propulsion Department)
FLIGHT PROPULSION LABORATORY DEPARTMENT
Cincinnati 15, Ohio

DISTRIBUTION

INTERNAL

C. L. Chase
D. Cochran
E. B. Delson
M. C. Leverett
W. H. Long
H. F. Matthiesen
A. J. Rothstein (6)
D. R. Shoults
G. Thornton
Library (6)

EXTERNAL DISTRIBUTION

Col. Ola P. Thorne
Pentagon, Washington 25, D. C.

Capt. Hendricks
Andrews AFB, Md.

Lt. Col. Stanley Valcik (2)
A. S. D.
Wright-Patterson AFB, Ohio

Dr. Frank Pittman
AEC
Washington 25, D. C.

DTIE (14) plus reproducible master
Oak Ridge, Tennessee

ABSTRACT

This is one of twenty-one volumes summarizing the Aircraft Nuclear Propulsion Program of the General Electric Company. This volume summarizes the methods and techniques developed for use in the thermal design of nuclear reactors associated with that program.

Information and references are given on the analytical and experimental work required to design and evaluate the proposed high performance air cooled fuel elements. Methods of optimizing the thermal designs, particularly by the use of high speed electronic digital computing equipment, are discussed. The computer programs developed to provide accurate performance predictions, are identified and described. Details of the computing programs may be found in the referenced material.

Means for matching the coolant-flow to the predicted internal heat generation rates in the non-fueled components are discussed. Test methods and results are indicated and significant equipment and instrumentation information provided.

The relationships of reactor pressure losses and of localized perturbances to power plant performance are indicated, and the detailed analyses which were required to identify and predict these effects are discussed.

ACKNOWLEDGEMENTS

Acknowledgement is made of the contribution of Paul E. Lowe.

PREFACE

In mid-1951, the General Electric Company, under contract to the United States Atomic Energy Commission and the United States Air Force, undertook the early development of a militarily useful nuclear propulsion system for aircraft of unlimited range. This research and development challenge to meet the stringent requirements of aircraft applications was unique. New reactor and power-plant designs, new materials, and new fabrication and testing techniques were required in fields of technology that were, and still are, advancing very rapidly. The scope of the program encompassed simultaneous advancement in reactor, shield, controls, turbomachinery, remote handling, and related nuclear and high-temperature technologies.

The power-plant design concept selected for development by the General Electric Company was the direct air cycle turbojet. Air is the only working fluid in this type of system. The reactor receives air from the jet engine compressor, heats it directly, and delivers it to the turbine. The high-temperature air then generates the forward thrust as it exhausts through the engine nozzle. The direct air cycle concept was selected on the basis of studies indicating that it would provide a relatively simple, dependable, and serviceable power plant with high-performance potential.

The decision to proceed with the nuclear-powered-flight program was based on the 1951 recommendations of the NEPA (Nuclear Energy for the Propulsion of Aircraft) project. Conducted by the Fairchild Engine and Airplane Corporation under contract to the USAF, the five-year NEPA project was a study and research effort culminating in the proposal for active development of nuclear propulsion for manned aircraft.

In the ensuing ten years, General Electric's Aircraft Nuclear Propulsion Department carried on the direct air cycle development until notification by the USAF and USAEC, early in 1961, of the cancellation of the national ANP program. The principal results of the ten-year effort are described in this and other volumes listed inside the front cover of the Comprehensive Technical Report of the General Electric Direct Air Cycle·Aircraft Nuclear Propulsion Program.

Although the GE-ANPD effort was devoted primarily to achieving nuclear aircraft power-plant objectives (described mainly in APEX-902 through APEX-909), substantial contributions were made to all aspects of gas-cooled reactor technology and other promising nuclear propulsion systems (described mainly in APEX-910 through APEX-921). The Program Summary (APEX-901) presents a detailed description of the historical, programmatic, and technical background of the ten years covered by the program. A graphic summary of these events is shown on the next page.

Each portion of the Comprehensive Report, through extensive annotation and referencing of a large body of technical information, now makes accessible significant technical data, analyses, and descriptions generated by GE-ANPD. The references are grouped by subject and the complete reference list is contained in the Program Summary, APEX-901. This listing should facilitate rapid access by a researcher to specific interest areas or

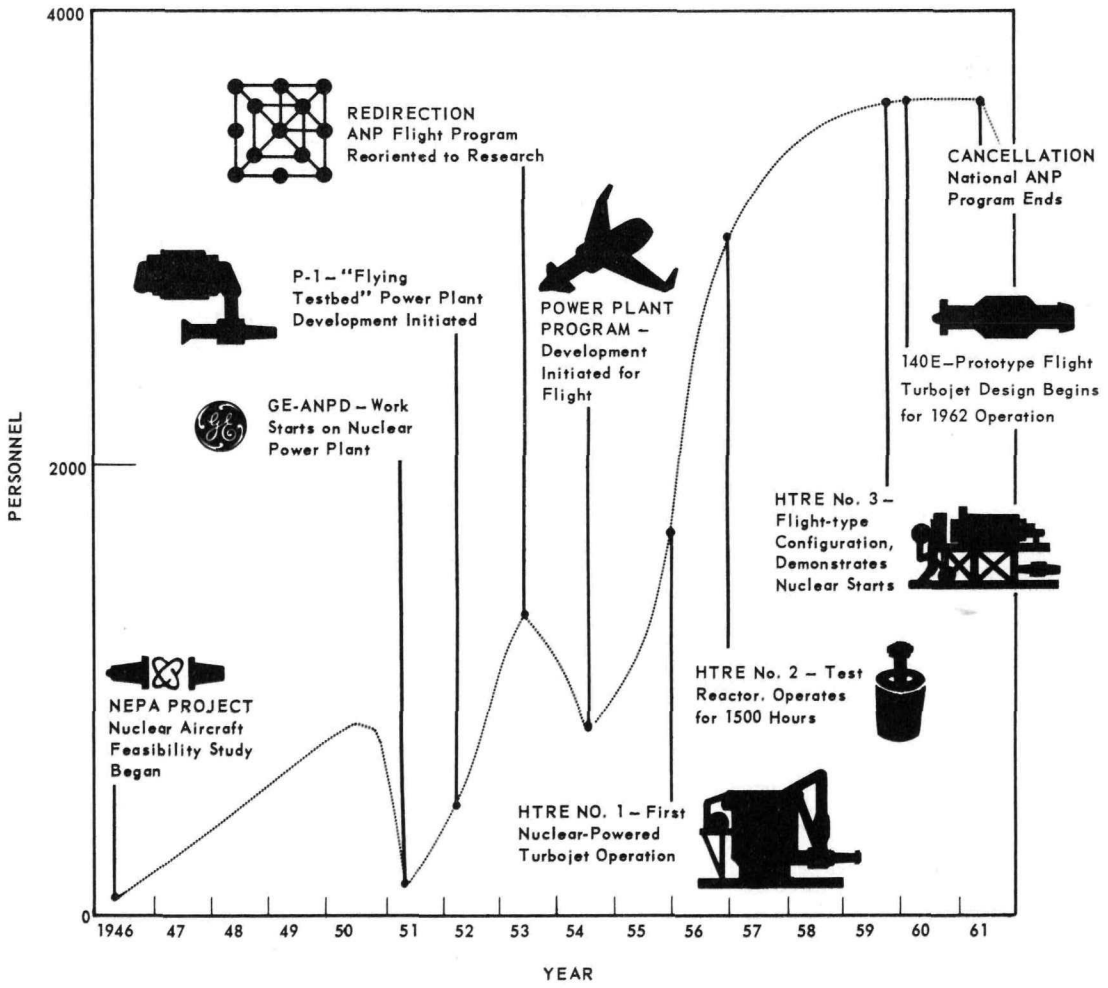

Summary of events – General Electric Aircraft Nuclear Propulsion Program*

*Detailed history and chronology is provided in Program Summary, APEX-902. Chronology information extracted from: Aircraft Nuclear Propulsion Program hearing before the Subcommittee on Research and Development of the Joint Committee on Atomic Energy, 86th Congress of The United States, First Session, July 23, 1959, United States Government Printing Office, Washington 1959.

sources of data. Each portion of the Comprehensive Report discusses an aspect of the Program not covered in other portions. Therefore, details of power plants can be found in the power-plant volumes and details of the technologies used in the power plants can be found in the other volumes. The referenced documents and reports, as well as other GE-ANPD technical information not covered by the Comprehensive Report, are available through the United States Atomic Energy Commission, Division of Technical Information Extension, Oak Ridge, Tennessee.

The Report is directed to Engineering Management and assumes that the reader is generally familiar with basic reactor and turbojet engine principles; has a technical understanding of the related disciplines and technologies necessary for their development and design; and, particularly in APEX-910 through APEX-921, has an understanding of the related computer and computative techniques.

The achievements of General Electric's Aircraft Nuclear Propulsion Program were the result of the efforts of many officers, managers, scientists, technicians, and administrative personnel in both government and industry. Most of them must remain anonymous, but particular mention should be made of Generals Donald J. Keirn and Irving L. Branch of the Joint USAF-USAEC Aircraft Nuclear Propulsion Office (ANPO) and their staffs; Messrs. Edmund M. Velten, Harry H. Gorman, and John L. Wilson of the USAF-USAEC Operations Office and their staffs; and Messrs. D. Roy Shoults, Samuel J. Levine, and David F. Shaw, GE-ANPD Managers and their staffs.

This Comprehensive Technical Report represents the efforts of the USAEC, USAF, and GE-ANPD managers, writers, authors, reviewers, and editors working within the Nuclear Materials and Propulsion Operation (formerly the Aircraft Nuclear Propulsion Department). The local representatives of the AEC-USAF team, the Lockland Aircraft Reactors Operations Office (LAROO), gave valuable guidance during manuscript preparation, and special appreciation is accorded J. L. Wilson, Manager, LAROO, and members of his staff. In addition to the authors listed in each volume, some of those in the General Electric Company who made significant contributions were: W. H. Long, Manager, Nuclear Materials and Propulsion Operation; V. P. Calkins, E. B. Delson, J. P. Kearns, M. C. Leverett, L. Lomen, H. F. Matthiesen, J. D. Selby, and G. Thornton, managers and reviewers; and C. L. Chase, D. W. Patrick, and J. W. Stephenson and their editorial, art, and production staffs. Their time and energy are gratefully acknowledged.

THE EDITORIAL BOARD:

Paul E. Lowe
Arnold J. Rothstein
James I. Trussell

November 8, 1961

CONTENTS

FIGURES

1. INTRODUCTION AND SUMMARY

This volume summarizes the aerothermodynamic work performed from early 1952 to early 1961, in conjunction with the General Electric Company's Aircraft Nuclear Propulsion (ANP) Program.

More specifically, the volume describes the technology of fluid dynamics and heat transfer developed in the course of designing a series of air-cooled reactors for aircraft nuclear propulsion.

The methods used for prediction of performance of reactor components and systems, and the confirming experimentation, formed the data-and-methods file on which detailed power plant thermal designs were based. This volume, together with its references, is thus intended to provide a repository of aerothermodynamic techniques which might readily be drawn upon for a variety of needs.

The authors have assumed that the reader is familiar with elementary heat transfer and fluid flow theory, and has a general acquaintance with the principles of nuclear reactors and turbojet engines. Some acquaintance with the uses of digital computing machines will further increase the reader's understanding of the presented material. Use of some of the jargon peculiar to the project has been unavoidable but care has been taken to provide definitions.

A basic factor in reactor thermal design for direct cycle power plants is the relatively low density and low heat capacity and conductivity of the air as a heat transfer medium. Thus the key problem in the thermal design of ANP reactor systems was repeatedly found to be the inter-relating of the heat transfer and associated fluid dynamics requirements with the nuclear and structural requirements.

The degree of sophistication utilized in optimizing these conflicting requirements varied. For the preliminary and advanced design studies, rough methods of calculation were used to obtain a relatively quick evaluation of alternatives and the initial sizing. As the work progressed through detailed design to final fabrication, the analysis methods used became much more detailed and complex, and much more precise.

For example, for the concentric ribbon type of fuel elements used in the Heat Transfer Reactor Experiments (HTRE), initial sizing and performance predictions were obtained by assuming that the fuel cartridge could be characterized by an average hydraulic diameter; therefore, a single passage wall temperature and a bulk-air temperature were computed as a function of axial location of the fuel tube in the reactor core. As the design progressed, radial variations in fuel-ring temperature and bulk-air temperature were computed within a single fuel tube. Finally, a map was obtained with both radial and cir-

cumferential temperature and flow as a function of axial position in a number of tubes, in the core cross section, which were identified as controlling.

The degree of sophistication also increased with the major program steps; the early systems tests being much less demanding than the later ones which approached flight prototypes. This was particularly true for the moderator and shield cooling requirements which, if not sufficiently optimized, could result in penalties of lower effluent temperature and increased weight.

The existing basic technologies of turbulent gas flow and of convective heat transfer were found, as expected, to be valid for the ANP systems. However, most of the ANP configurations were unique and the value of greater optimization was higher, in terms of improved performance, than for more conventional power plants. It was, therefore, generally found necessary to determine experimentally the characteristic aerothermodynamic coefficients in order to obtain the required precision in performance analysis and prediction. Existing literature did provide, in most cases, some approximate comparisons which guided initial estimates of size requirements and performance.

There were two fundamental reasons for the high degree of sophistication in thermal design as the mechanical design neared completion. First, it was recognized that in order to maximize the power for a given weight limit and given materials limitations, it was necessary to approach optimum aerothermodynamic performance as closely as possible. Thus, in the final design, an ambitious attempt was made to obtain an isothermal core - one which would have the same safe maximum wall temperature at all positions in the core. The total pressure drop through the reactor was minimized at the same time. Second, it was realized that very localized perturbations could lead to unacceptably high fuel element temperatures which would impair the safety of reactor operation or shorten fuel element life. Detailed analyses and experiments were therefore conducted to identify and predict such local effects and to propose remedies wherever practical.

The four major parts of this volume cover the following areas: section 2, the digital computer programs which were conceived and perfected for the analysis of nuclear reactors and nuclear reactor components; section 3, the basic analytical and experimental investigation of components; section 4, the more important heat transfer and fluid flow instrumentation techniques; and section 5, the miscellaneous supplementary investigations. The references at the end of each section are intended to be selective rather than exhaustive, giving the most important documents which were generated in accomplishing this work. No attempt has been made to assemble a bibliography on basic heat transfer and fluid dynamics since many good ones are already in existence.

Section 2 of this volume deals with the analysis "tools," that is, digital computer programs, which have been found to be of major value. These programs apply the capabilities of the IBM 704 and 7090 digital computers to the otherwise insurmountable arithmetic of detailed analyses of ANP power plants. The authors' approach is to describe the program in general terms, indicate the required input data, and point out the uses of the program. Consultation of the appropriate reference is required to obtain detailed familiarity with the program.

Section 3 covers the significant fuel element configurations which were considered for aircraft nuclear reactor applications. The references deal with the detailed analytical methods. Some comparisons are made of ANP analyses results and similar information from the available literature. Considerable detail is given on reactor aerothermodynamics, describing how fuel elements were sized, the means of achieving the required flow distribution and the approaches to determining local fuel element temperature perturbation.

Also discussed are the means for determining cooling requirements for removal of gamma and neutron heat from the shielding and non-fueled reactor components.

Section 4 is a short discussion of temperature and flow instrumentation. Some of the problems are indicated, as are the means of determining the probable error in observation. Information on instrumentation of specific power plants is contained in the APEX covering that power plant. Problems of fuel element temperature measurements are discussed in APEX-920 as well as in the indicated references.

Section 5 of this report is a brief discussion of some generally applicable analytical studies; e.g., the procedure for determining temperature in a non-concentric annulus with unequal heat release from the bounding walls, and the evaluation of the "Coanda Effect" in place of turning vanes.

2. AEROTHERMODYNAMIC COMPUTER PROGRAMS

The programs discussed in this section were developed for use in the analyses of direct cycle; i.e., air-cooled flight-type nuclear reactor systems. In general, the latest techniques and methods were applied to obtain a high degree of optimization in the design of these high-porosity, high-power-density, high-temperature reactors. Use was made of IBM 704 and 7090 digital computers to permit handling the otherwise impossible volume of arithmetic associated with detailed analyses of the complex systems. This section provides general descriptions of the programs and their uses. Detailed information on a program can be obtained from the appropriate reference.

2.1 OFF-DESIGN PROGRAM

The Off-Design Program (ANP 443) for the IBM 704 digital computer utilizes a one-dimensional approach to determine the compressible-flow characteristics with friction, area change and heat addition in a single flow passage. The analysis and program[1*] employs an approximate integrated form of the differential equation for pressure loss. The approximate form approaches the exact form as the increment in passage length tends to zero. Entrance and exit total pressure losses are calculated as specified fractional coefficients of the entrance and exit dynamic pressures, respectively. Heat release is prescribed longitudinally in the form of a power profile.

Major input data consists of incremental lengths (called stages), stagewise hydraulic diameters and free-flow areas, power profile, inlet total pressure, inlet and exit total temperatures and mass flow. Normal output data include system exit total and static pressure, stagewise average Reynolds numbers, and the following quantities evaluated at the exit of each stage: total temperature, total pressure, surface temperature, dynamic pressure, static pressure, and Mach number.

The program was originally conceived as a means of estimating the off-design-point aerothermal performance of nuclear reactor cores. Subsequently, it has also been applied with good results to the preliminary design of nuclear reactor cores, sizing of shielding and control rod coolant passages, and to virtually any kind of flow passage. Because it was intended as a preliminary, fast-running design tool, all physical properties are evaluated at the total bulk temperature (a very minor error at the low Mach numbers of interest) and flow is considered to be choked if the Mach number reaches 0.9 or higher.

2.2 HEATED ANNULI AND ANSECTOR COMPUTER PROGRAMS

During development of the concentric-ring type fuel cartridge, the heated-annuli computer program was devised in order to analytically compute aerothermal performance for this particular fuel element design. The cartridge consisted of a number of distinct

*Superscripts refer to the reference lists that appear at the end of each section.

stages, each separated from its neighbor by a fixed gap. Each stage, in turn, consisted of a number of fueled concentric rings. The concentric-ring design is described fully in 3.1.3.

The thermal analysis of the concentric-ring element consisted of making a heat balance on each of the fuel element rings within a stage. In this balance, the assignable heat was assumed to be circumferentially uniform, and when generated in any ring was dissipated in four ways: (1) transfer of heat by convection to the adjoining outer annuli, (2) transfer of heat by convection to the adjoining inner annulus, (3) transfer of heat by radial radiation to the immediate neighboring outer rings, and (4) transfer of heat by radial radiation to the immediate neighboring inner rings. A heat balance may also be made on each annular flow passage in a stage. Here the enthalpy rise, from inlet to exit within a given annulus of a stage, was equated to the heat transferred by convection from the two rings forming the annulus.

From the process described above, it is possible to write, for any stage, a set of N nonlinear algebraic equations for N unknown temperatures which consists in part of annulus-exit bulk temperature and temperatures at the trailing edge of the fuel ring. In addition to the unknown fuel-ring and bulk temperatures, the equation set also contains unknown temperatures in the radial direction through the moderator section associated with the fuel cartridge hole, and finally, the moderator coolant temperature. These equations are all nonlinear because they involve both thermal radiation interchange and a nonlinear dependence of heat transfer coefficient on surface and bulk temperature.

To solve this equation set, trial values are assigned to the temperatures and the nonlinear temperature-dependent coefficients are evaluated. The equation set is now linear and a first solution is obtained. With these new temperatures, the coefficients are re-evaluated and a second solution to the set is obtained. This process is repeated until convergence is achieved.

The temperature solution for the first stage, as described above, is based on an assumed average mass-flow velocity through each annulus. After this solution is obtained, the pressure loss (compressible flow with friction and arbitrary heat addition) is evaluated for each annulus. In general, this results in different annuli stage-exit static pressures. The assumption is made that the correct mass-flow velocity distribution among the annuli in a stage is such that all static pressures at the stage-exit plane are equal. Consequently, adjustments are made to the initial assumed mass-flow velocity distribution, and the entire temperature and pressure-drop calculation is repeated. The procedure is iterated until all exit static pressures are the same. Thus a unique flow and temperature distribution is obtained for the first stage.

This final mass-flow velocity distribution becomes the initial trial distribution into the second stage, and the second-stage calculations are carried out in identically the same manner described for the first. Ultimately, the aerothermal performance for the entire cartridge is obtained. During the process of flow readjustment among the annuli that takes place in the gap region between two successive stages, the attendant enthalpy addition or deletion associated with these flow changes is suitably accounted for, in order to maintain an over-all heat balance. In addition, provisions are made to preserve continuity of flow, and to allow for continual geometry changes from stage-to-stage.

The original temperature analysis for this program was previously reported.[2] This original analysis was a more ambitious attempt to ascertain the actual variation of wall and bulk temperature with axial position through a stage. This procedure was coded for operation on an IBM 650 computer. The running time for a full cartridge was found to be prodigious, even when extrapolated to the speed of an IBM 704. This led to the compro-

mise analysis qualitatively described in this section and previously reported.[3] The IBM 704 program number associated with this analysis is ANP 23.

With the completion of the heated-annuli program, attention was directed to the advanced problem of determining the effect on ring temperatures, bulk temperatures, and flow characteristics of circumferential power variation within the fuel rings. This resulted in the conception and design of the "ansector" program.[4] In essence, this program is an iterative application of the heated-annuli program. The 360 degrees of circumference within a stage is divided into six 60-degree sectors, and the heated-annuli technique is applied to each sector portion of an annulus - hence the name ansector. As in the heated-annuli program, the final flow distribution is assumed to be that which results in all ansectors of a stage having the same exit static pressure, and in which an enthalpy balance and continuity of mass flow is maintained. The IBM 704 program number associated with the ansector problem is ANP 2.

2.3 REACTOR CORE TRANSIENT TEMPERATURE PROGRAM

The purpose of this program is to make a simultaneous gross transient analysis of two reactor components, such as fuel and solid moderator or fuel and reflector, each having variable internal heat generation and a cooling flow passage. A single flow passage cannot be used to cool both components. The program is written assuming air to be the coolant for both components. The program could be adapted to other fluids by changing various empirical constants. Transient temperature and pressure distributions are computed only for the longitudinal direction, which is the direction of cooling flow; i.e., radial and circumferential variations within a component are not determined. However, heat transfer by conduction from one component to the other, through an arbitrary resistance separating them, can be considered. Longitudinal conduction is considered in the analysis of one component and not in the other so that a dual analysis of a single physical component can be made to investigate this effect. Radiation is not considered. Variable material properties may be given as input. Friction-factor and heat-transfer coefficient correlations may be given for laminar, transition, and turbulent flow, and the critical Reynolds numbers for determining the flow type may be given arbitrarily and independently for each component.

An added feature of the program is the determination of cooling flow redistribution for a configuration in which the cooling flow enters the two components from a common plenum and exhausts to a common plenum. Since, in general, the two components will have different heat-generation rates as a function of time, the magnitude of flow resistance will vary for the cooling passages of the two components. Thus, a portion of cooling flow will shift from one passage to the other where there exists a smaller flow resistance. The program adjusts the cooling-flow split as a function of time in order to effect equal static pressures at the exit of both cooling passages.

Although the program does not give a detailed solution, it does give insight into problems which do not apply directly, such as radial thickness in a component where the radial gradient is of concern; or a series of fuel plates where only an "average" solution is obtained. In such conditions, the program will indicate the critical position in space and time which may be subsequently investigated in detail. Because of the redistribution of cooling flow, this position would be difficult to determine by a hand calculation. The most significant advantage of this program relative to a general nodal-point, relaxation program (see section 2.4) is that less time is involved to set up the input data, and computer operating time is greatly reduced.

The method of analysis is to write a heat balance about an incremental length of each component and the cooling passage of each component. The derivatives of temperature with respect to distance and time are then approximated by dividing the core length into four equal segments and using finite-difference techniques. The result is a system of twenty simultaneous linear equations involving twenty unknown temperatures which can be solved at each time throughout a transient solution.

The output data of the program for each component are the following: component surface temperature, cooling-air temperature, total and static pressure, Mach number, and Reynolds number at the five longitudinal positions (x/L = 0, 0.25, 0.5, 0.75, 1.0); maximum component surface temperature and its x/L location; and the cooling-flow distribution.

The required inputs are tables of component material properties (air properties are built-in), time intervals to be investigated, and total cooling flow as a function of time (an option is to give the flow split-up if it is known). In addition, the following data are required for each passage: length, hydraulic diameter, free-flow area, heat-transfer perimeter, and volume; inlet and exit pressure-loss coefficients; friction-factor and heat-transfer coefficient correlations; and heat-generation rate, inlet-air temperature, and inlet pressure as functions of time.

A detailed description of this analysis was published.[5] The digital program number is ANP 330.

2.4 TRANSIENT HEAT TRANSFER (THT) PROGRAM

2.4.1 Version A (THTA)

The Transient Heat Transfer (THT) Program permits the analysis of complex transient and steady-state heat transfer problems that can involve radiation, convection and conduction.[6] The program is based upon the finite difference technique of dividing the geometry of the problem into a one-, two-, or three-dimensional network of nodal volumes (up to 200 nodes may be used). Material properties are considered to be uniform within a given node and are evaluated at the temperatures at the centers of the nodes. The coordinate dimensions of each node, the physical properties of the node materials as functions of temperature, and the boundary conditions and internal heat generation as function of time and/or temperature make up the input data for the programs. The output consists of node temperatures for desired time intervals, measured from the beginning of the transient. The program calculates the surface areas and volumes of nodes, interpolates physical properties and boundary conditions from input tables, assembles a heat balance in the implicit form for each node and then solves the system of N equations relating the N unknown node temperatures. This process is repeated for each specified time step in the transient until temperatures at node centers have been computed for all the time steps.

Since the program is based upon the implicit form of finite difference equations, the solution is stable for any length-of-time step.

2.4.2 Version B (THTB)

The THTB program[7] is similar to the THTA program, with the following additions:

1. A generalized form of data storage is used whereby the data fields are not preassigned but are identified by the program on the basis of the data actually loaded. As a result, no memory locations are left unused and the node capacity can be as high as one thousand, the actual number being dependent on the number of boundary-condition, time-step, and material-property entries which have been made.

2. The option exists to recompute temperature-dependent properties, including thermal radiation coefficients, based on the temperatures at the middle of the time step rather than always at the beginning of the time step, as is the case in THTA. More accurate solutions are obtained by this technique.
3. The number of connections to thermal radiation sources or sinks is unlimited, compared to a maximum of three per node face in THTA.

2.5 ISOTHERMAL 90-DEGREE FOLDED FLOW PROGRAM

This program was devised to compute the flow distribution through a number of parallel channels of variable resistance which discharged into an exit manifold plenum. After discharging into the plenum the flow is forced to turn, due to the presence of the manifold wall. The turn angle may be as high as 90 degrees. The incompressible flow through the channels was assumed to be isothermal, and each channel had the same inlet pressure. The main input into the program consisted of assigning the resistance of each channel, the coordinates of the discharge plenum header wall, and the total weight flow. The output consisted of the weight flow distribution through the channels and the discharge plenum pressure, velocity and streamline pattern.

The main assumptions in the analysis for this program were: (1) the pressure was invariant in the exit plenum in a direction normal to the discharge plane of the multiple channels, (2) the flow along the exit manifold plenum wall was frictionless, and (3) the flow discharging from the exit channels incurred one dynamic head loss in making the primary turn in the manifold exit header.

The analysis and programming of this problem is available.[8] The digital program number is ANP 145.

2.6 FANTANA (Flow and Temperature Analysis-Version A) PROGRAM

This program[9] is similar in many respects to the THTA program described in Section 2.4. It employs the implicit form of the finite-difference heat balance and uses the accelerated Gauss-Seidel method of solving the resulting large system of simultaneous equations for both the transient and steady states. The manner of describing the nodes is exactly the same.

FANTANA, however, will also carry out compressible pressure drop computations for fluid passages adjacent to solid nodes or embedded in a matrix of solid nodes wherein either the mass-flow and exit static pressure level or only the inlet total and exit static pressure levels are prescribed. The analysis employed also accounts for "pumping energy" resulting from centrifugal force fields.

The program computes its own convective heat transfer coefficients at the interfaces between fluid and solid nodes. Alternatively, film coefficients can be prescribed, as in THTA.

FANTANA uses a generalized form of data storage whereby data fields are not preassigned but are identified by the program on the basis of the data actually loaded. As a result, the number of nodes which can be handled by the program ranges from 600 downward, depending on the number of boundary-condition, time-step, and material-property entries.

FANTANA is the only program available which can carry out flow calculations coupled with a transient thermal analysis for large systems. Consequently, it has been applied to

the transient analysis of many nuclear reactor components such as fuel elements, solid moderators, control rods, and shields.

2.7 COMPRESSIBLE FLOW NETWORK PROGRAM

This program (ANP 622) for the IBM 704 and 7090 digital computers will compute the compressible-flow distribution in arbitrarily-connected, non-isothermal networks. Networks may contain as many as 55 branches (characterized by the fact that all components in a branch carry the same mass flow), 40 internal junctions where two or more branches meet, and 30 external junctions which connect to external pressures and flow sources or sinks. Each branch can consist of as many as 25 stages, each of which may be an incremental length along a flow passage or may be some component whose pressure loss characteristics can be simulated by a fractional coefficient of the upstream dynamic pressure.

The analytical structure of the program,[10] is as follows: The pressure-drops along the individual branches are computed by the analysis described in section 2.1. An incompressible network is computed which is mathematically equivalent to the compressible network for the particular set of mass-flows and pressure-drops under consideration. Then, the consistency of incompressible network pressure-drops is checked by means of the analytical methods.[11] If the incompressible flow network pressure-drops are not consistent, a new set of mass-flows is computed and the compressible pressure-drops are recomputed.

Normal input to the program includes network connection data, detailed branch data, a heat transfer relationship, entrance and exit loss coefficients for the branches which must include flow-splitting and mixing losses, external pressure levels, and flow-source temperature levels. Normal output includes branch mass-flows, external flows, internal junction pressure and temperature levels, tolerances on the results of iterative calculations, and optionally, detailed output for the branches similar to that described for the Off-Design Program in section 2.1.

The Compressible Flow Network program can easily handle complex systems which otherwise would probably have been built and tested in preference to application of the extremely tedious and involved iterative techniques previously required for the solution of such problems.

2.8 ISOTHERMALIZE PROGRAM

This program (ANP 439 and 743)[12] is an outgrowth and extension of the Off-Design Program. It enables the aerothermal designer to apply directly the design constraints such as pressure-drops and maximum surface temperatures, rather than limiting him to the normal input of the Off-Design Program. Prior to availability of the Isothermalize program, it was necessary to do considerable cross-plotting of the results of Off-Design calculations in order to match design criteria. The Isothermalize Program calculations are carried out by means of a system of numerical interpolations and/or extrapolations whereby the program will systematically vary two of the normal input variables to an "Off-Design" calculation routine until the design constraints, which are ordinarily dependent upon the normal input, are satisfied by the results of the Off-Design calculations.

Two versions of the Isothermalize program are available, one each for the IBM 704 and 7090 digital computers. The 704 version (ANP 430) is limited to circular passages and accepts the following as normal input: pressure-drop in the form of ratio-of-exit static or exit total to inlet total pressure, maximum surface temperature, either bulk-discharge

total temperature or passage hydraulic diameter, total cross section for flow and solid associated with the passage, and virtually complete passage description. Normal output includes all normal Off-Design output plus a separate tabulation of the hydraulic diameter, discharge total temperature, mass velocity, and total heat release, and, optionally, tables of volumetric heating rates, and stress levels, for cylindrical tubes.

The 7090 version (ANP 743) has additional options: one allows the use of non-circular cross section passages (rectangular, elliptical, etc.) while another option permits the designation of total heat release as a design constraint, and allows inlet pressure to be calculated when geometry, flow, exit pressure and maximum surface temperature are predetermined, as in a nuclear rocket core. Output is similar to that from the 704 version except that no stress levels are calculated for the additional cross sections.

The 7090 version actually embodies the General Flow Passage Program (see section 2.9) rather than the Off-Design Program and superimposes an additional level of iteration in order to satisfy the additional design constraints.

2.9 GENERAL FLOW PASSAGE PROGRAM

This program (ANP 663)[13] is a growth version of the Off-Design Program (see section 2.1). It utilizes the same analysis and deals with a flow passage of fixed geometry. Instead of being limited to the same input variables as the Off-Design Program, however, it will accept as input any combination of the Off-Design input-output variables which can be satisfied by suitable iteration of either the inlet total pressure or the mass flow. It also provides, optionally, for automatic computation of interstage expansion or contraction losses if an area change is encountered, or for arbitrary interstage loss coefficients to be prescribed. Input and output are generally similar to that for the Off-Design Program.

2.10 REFERENCES

1. Delaney, J. A., et al., "Off-Design and Modified Off-Design Programs," GE-ANPD, DC 60-7-12, July 1960.
2. Noyes, R. N., "Method for Solution of Turbulent Flow in a Heated Annulus Adaptable to Digital Computation," GE-ANPD, DC 56-3-97, March 1956.
3. Clark, N., et al., "Heated Annuli Computer Program," GE-ANPD, DC 59-4-26, April 1959.
4. Clark, N., "Ansector Computer Program," GE-ANPD, DC 61-5-63, May 1961.
5. Gast, R. A., "A Generalized Reactor Core Transient Temperature Analysis," GE-ANPD, XDC 59-10-22, October 1959.
6. Vollenweider, D. B and Campbell, D. J., "Program THT for the IBM 704 Computer to Solve General Transient Heat Transfer Problems," GE-AGT, R 58-AGT 665, October 30, 1958.
7. Stephens, G. L. and Campbell, D. J., "Program THTB for Analysis of General Heat Transfer Systems," GE-FPD, R 60 FPD 647, April 21, 1961.
8. Brunso, J., "Isothermal 90^{o} Folded Flow Program," GE-ANPD, DC 59-2-193, January 29, 1959.
9. Vollenweider, D. B. and Campbell, D. J., "Flow and Temperature Analysis Program (FANTAN) for the IBM 704 Computer," GE-FPD, R 59 FPD 795, October 30, 1959.
10. Skirvin, S. C., "Compressible Flow Network Computer Program," GE-ANPD, APEX-661, August 1961.
11. Delaney, J. A., "Incompressible Flow Network Subroutine: FLONET," GE-ANPD, APEX-662.
12. Skirvin, S. C., "Isothermalize (IBM 704) and Isothermalize 90 (IBM 7090): Computer Programs to Size Coolant Passages or Evaluate Coolant Passage Aerothermal Performance with Multiple Design Constraints (ANP 439 and 743)," GE-ANPD, APEX-663.
13. Skirvin, S. C., "General Flow Passage: A Computer Program to Calculate Aerothermal Performance of an Arbitrary Flow Passage of Fixed Geometry," GE-ANPD, APEX-664.

3. ANALYTICAL AND EXPERIMENTAL COMPONENT INVESTIGATION

The complexity of an aircraft nuclear power plant, with the attendant high cost of full-scale tests, dictated considerable reliance on system-analysis and on component development. This portion of the report summarizes the fuel element configurations which were given serious consideration and the means of determining their characteristic coefficients. It also discusses fluid-dynamic and heat-transfer considerations of ANP reactors and of reactor auxiliaries.

3.1 FUEL ELEMENT CONFIGURATIONS

3.1.1 Parallel Flat Plate Fuel Elements

One of the first fuel element configurations seriously considered in the direct cycle system used parallel plates as in the R-1 reactor (see APEX-902). One of the several geometry arrangements, for which the heat transfer and pressure drop characteristics were investigated, is that shown in Figure 3.1.

Preliminary evaluation of heat transfer performance of several parallel plate configurations[1] indicated that data could be reasonably correlated by an equation of the form

$$\frac{h}{C_p G} = 0.025 \left(\frac{DG}{\mu}\right)^{-0.2} \qquad (1)$$

Where

h = heat transfer coefficient
C_p = specific heat of air
G = mass flow velocity
D = hydraulic diameter
μ = viscosity of air

Both C_p and μ are evaluated at exit bulk-air temperature. The corresponding best correlation of friction-factor data was achieved by the use of a multiplier of 1.5 on the usual friction-factor relationship for flow in rough pipes.

Intermediate appraisals of more heat transfer data[1, 2, 3] indicated that improvement in correlation could be obtained by assuming

$$h = A \frac{T_b^{0.8} G^{0.8}}{T_f^{0.7} L^{0.2}} \qquad (2)$$

where A is an experimentally determined constant, T is the temperature, L is the stage length, and the subscripts b and f refer to bulk and film conditions at the stage exit. Equation (2) was an attempt to factor in thermal entrance-region length effects on the heat transfer coefficient.

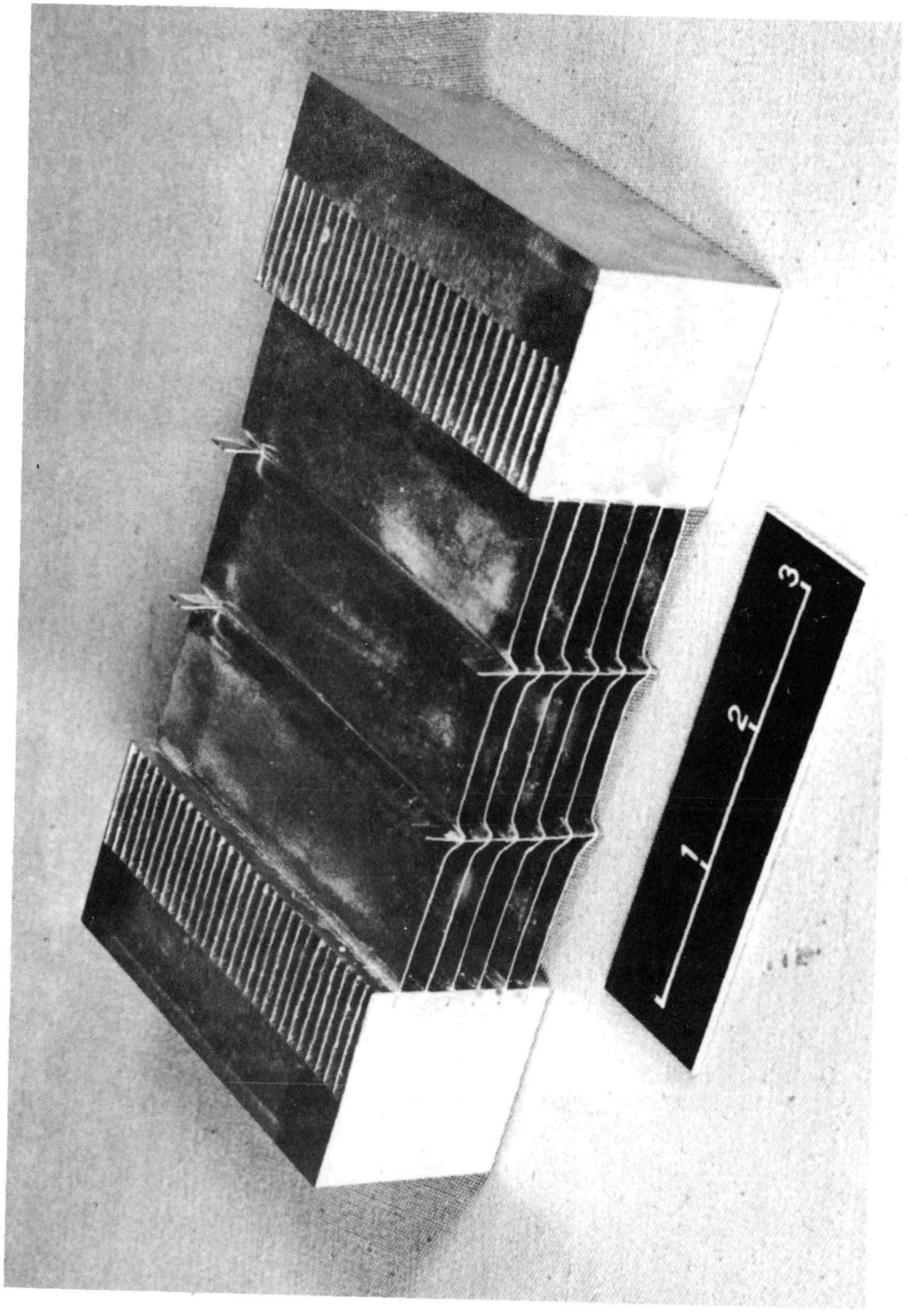

Fig. 3.1 – Typical parallel plate fuel element configuration

With continued over-all analysis on flat-plate systems, it became apparent that the ratio of stage length to average hydraulic diameter would be 10 or greater. Since in turbulent flow, the heat transfer coefficient is essentially fully-developed when this ratio is about 10, stage trailing-edge heat transfer coefficients were determined to be best correlated by

$$h = A \frac{G_b^{0.8}}{D^{0.2}} \frac{T_b^{0.8}}{T_f^{0.56}} \qquad (3)$$

where the mass-flow velocity G_b is based on the average fluid velocity and the exit bulk density.[4]

From an evaluation of the performance of a ceramic-plate fuel element,[5] it was concluded that an exit bulk temperature of 2030°F, from a 13-stage cartridge, could be realized with a maximum plate temperature of 2640°F. The attendant total pressure loss through the core was 15 percent of the inlet pressure.

A simplified series of graphic calculations suitable for rapid analysis of thermodynamic design problems associated with the use of plate-type fuel elements in direct-air-cycle reactors were developed.[6]

3.1.2 Pebble-Bed Fuel Element Matrices

To achieve higher heating-surface temperatures and smaller cores, consideration was given to the concept of using enriched UO_2 - BeO pellets in a pebble-bed matrix.

A preliminary thermodynamic study was made of a ceramic pebble-bed fuel element proposed for a tubular-type reactor.[7] The study indicated that because of the interrelation and mutual sensitivity of these design limitations, sizing and performance should be determined by a combined study of heat transfer, pressure losses, and thermal stress. The thermodynamic study consisted of a parametric investigation of the effects of bed porosity, pebble size, airflow rate, fuel inventory and cladding thickness on pebble temperature, exit air temperature, and pebble stress. The published results of the study[7] summarize the most appropriate equations for the determination of heat transfer coefficient and friction factor.

A thorough review of unclassified literature, a compilation of source material, and a detailed examination of the equations to predict heat transfer and pressure drop resulted in a published guide for packed-bed design work.[8]

A qualitative study of factors (variation in local porosity, support effects, etc.) which influence pressure loss evaluations was conducted.[9] In this study, GE-ANP tests were conducted on beds 1/4 and 1/2 inch in thickness which contained steel balls 1/16 and 1/8 inch in diameter. The tests were made with both straight and diffuser entrance sections. The main conclusion drawn from this investigation was that a generalized formulation for the accurate determination of pressure loss through any type of bed geometry is not possible and that good data correlation can only be achieved for a specific geometry and pebble packing.

A GE-ANP hydraulic flow test using water was conducted on a specific pebble bed in both normal and oblique flow.[10] The bed contained steel balls 1/16 inch in diameter, had frontal dimensions of 2 inch by 1 inch, and a depth of 5/16 inch. In the oblique flow test, the angle between the bed face and the inlet water flow direction was 3.6 degrees. The results of this test indicated that the pressure drop in this particular oblique flow configuration was about 1.6 times that in normal flow and that the test pressure drop coefficient fell in the theoretical band range developed in "Aerodynamics of Propulsion" by Kucheman and Weber.

3.1.3 Concentric Ring Fuel Elements

This configuration received possibly the greatest amount of development effort, principally because of its good structural integrity as proven during operation of HTRE No. 1, No. 2, and No. 3. A typical cartridge assembly is that shown in Figure 3.2.

As can be seen in Figure 3.2, the cartridge, which fitted into a core fuel tube, contained a number of fuel element stages in the active core region. The cartridge design used in HTRE No. 1, contained 18 stages. Each stage was 1.5 inch long and was separated from its neighbor by a gap of 1/8 inch. Each stage was composed of a number of concentric-fueled metallic rings, and the coolant air passed through the annular spaces formed by these rings.

Using the basic aerothermal relationships developed for the design of concentric ring elements[11] the predicted performance for the cartridge design used in HTRE No. 1 is derived.[12] Specifically, it is shown how the final design necessitates a consideration of the inter-relation of engine variables, fuel element aerothermodynamic relations, nuclear characteristics of the active core and pressure and heat-loss characteristics of the auxiliary systems connecting the engine to the reactor.

An approximate method of predicting both the drag and the pressure loss of a concentric-ring fuel element in a circular duct is feasible.[13] This method is based on a momentum analysis which considers the drag or pressure drop distribution of each individual component of the fuel element. This method predicts pressure losses that agree within 20 percent of experimental results.

An experimental evaluation was made of the airflow characteristics of a system of parallel flat plates.[14] The test rig was a nearly exact model of a concentric-ring element approximately eight times element size. The main conclusions drawn from this test were:

1. The presence of gaps between stages adds about 25 percent to the pressure drop.
2. Rounded leading edges reduce pressure drop by 10 to 12 percent as compared with square edges.
3. Three sets of parallel plates in series have an over-all pressure drop about 2-1/2 times that across a single set of plates.
4. Pressure drops within the stages are not appreciably influenced by induced turbulence at entrance of the first stage, or angle-of-attack of entrance flow.

An experimental investigation, using room temperature air, was made to determine the effect of variation in stage length and interstage gap on pressure loss.[15] The results showed that the pressure loss through four 1-1/2 inch long elements was approximately 1.6 times the loss through one 6-inch long element. The pressure losses caused by a 0.125 inch interstage gap were 10 percent greater than when the interstage gap between elements was reduced to zero.

The possibility of lowering radial leading-edge deformations in a concentric-ring stage by staggering the rings was investigated.[16] The deformations were believed to be due to nonsymmetric vena contracta effects at the entrance of a stage. The purpose of the tests was to determine the comparative pressure losses for the following two designs: (1) rings staggered so that the leading edge of every other ring was 0.1 inch behind the ring adjacent to it on either side, and (2) rings staggered so that the profile of the leading edges formed a cone. In either of the above two designs, three identical stages were tested in series. The results indicated that there was a pressure loss of approximately 1.45 times the upstream dynamic head (for three stages) with no discernible difference in loss between the two designs.

Initial designs of concentric-ring fuel elements incorporated channel spacers to maintain ring concentricity. To enhance structural integrity, a design was conceived in which

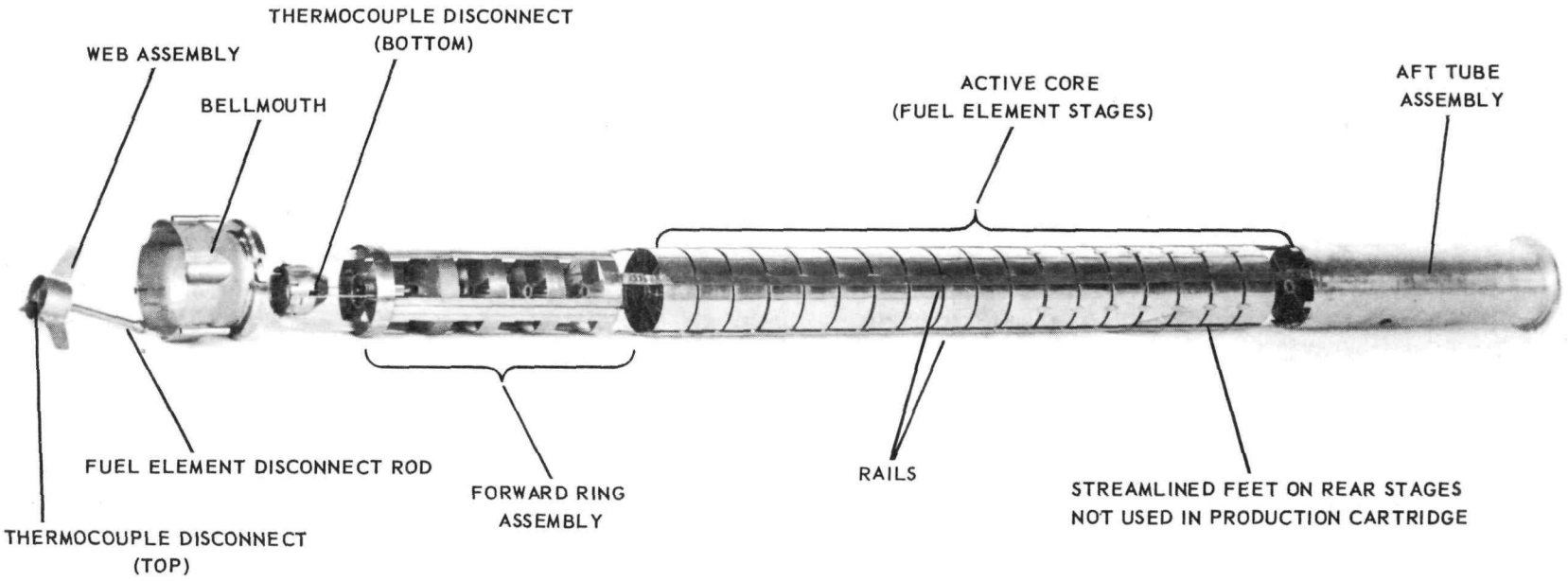

Fig. 3.2 – Typical concentric ring fuel assembly (A-2)

combed ribs were substituted for spacers on the front face of a stage and spacers elsewhere in the annuli flow space were eliminated. One such design was aerodynamically tested.[17] This cold-flow test was conducted on two different such configurations; one with the front support combs and outside guide rails set normal to the face of the element, and one with the combs and rails set 20 degrees to the normal. The purpose of the canted combs and twisted rails was to produce a swirling flow which alternately washed over cold and hot surfaces as it passed through the fuel elements. Tests were conducted to determine the amount of swirl promoted by setting the combs at an angle of 20 degrees to the normal.[18] The pressure loss for the configuration with angled combs and rails was 20 to 35 percent greater, depending on Reynolds number, than that with straight combs and rails.[17]

A preliminary analytical evaluation was made of the effect of swirl flow on reduction of fuel-plate temperature overages due to circumferential power scallops.[19] This analysis indicated that for a maximum-to-average ratio of circumferential power of 1.15, a reduction in the hot-spot plate temperature of 250°F might be realized, neglecting any increase in pressure loss due to swirling. When swirl pressure losses are included, the hydraulic diameter must be increased to reduce the pressure loss so that it will be equal to that of the no-swirl case, thus leading to higher wall temperatures. It was predicted that if the additional losses due to swirling amounted to 50 percent of the no-swirl pressure loss, no gains due to swirl flow are possible.

Cold-flow pressure drop tests were conducted on a three-stage concentric-ring comb-type cartridge before and after it was subjected to 1900°F gas flow (products of combustion from propane and air) in the burner rig test station. The results of this test,[20] indicated that before burner rig testing, the friction factor was 1.54 times that for rough pipe. After testing, the multiplier had increased to 1.64. This increase was attributed to oxidation of surfaces and some structural deformation of the cartridge while in the burner rig.

Three concentric-ring cartridge designs were tested in cold flow to determine their pressure drop characteristics.[21] Two of these designs were ultimately used in HTRE No. 3, while the other was a preliminary design in the iteration process leading to the final design. In each of the three tests, Reynolds number was varied from 5×10^3 to 1×10^5, and inlet Mach number was varied from 0.01 to 0.27. Except at low Reynolds numbers (5000 or less), friction factors could be correlated, with a maximum band spread of ±3 percent for the preliminary design and ±2 percent for the HTRE No. 3 types by an equation of the form

$$f = \alpha \, Re^{-0.14} \tag{4}$$

where the constant α had the values 0.053 for the preliminary design and 0.048 and 0.049 for the two HTRE No. 3 designs. In addition to cartridge friction-factor determination, a correlation of inlet tube pressure losses in upstream hardware, is also presented for the HTRE No. 3 designs.[21]

Cold flow friction-factor data obtained from a 19-stage cartridge with rounded leading edges was compared to that obtained from square leading edges.[22] The results indicated that the square-edge element has a friction factor that is about 16 percent higher than the streamlined element for a range of Reynolds numbers from 15,000 to 65,000.

3.1.4 Shaped-Wire Fuel Elements

In the course of fuel element configuration development, attention was given to the use of semi-elliptical shaped wire as a possible means of improving heat transfer characteristics. A preliminary performance evaluation of a streamline wire fuel element in a typical core tube was made.[23] This study was based on the pressure drop data of Joyner and Palmer[24] which were for staggered banks of streamline tubes, and the single-wire heat transfer correlation presented in "Heat Transmission," McAdams, 2nd edition. The

analysis, based on flat reactor power, indicated that for a 30-inch length of fuel cartridge, an exit air temperature of 1700°F could be realized with a maximum wire temperature of 2200°F and a ratio of outlet-to-inlet total pressure of 0.907 in the tube.

In the first GE-ANP experimental investigation to determine the pressure loss characteristics of a shaped-wire fuel element, friction factors were obtained that were slightly higher than those obtained by Joyner and Palmer, and there was considerable scatter in the data. The geometry of the cartridge investigated is that shown in Figure 3.3. It was reported that better data correlation could be obtained by further examination of the effects on pressure drop of: (1) wire radial spacing, (2) wire pitch spacing, (3) wire shape, (4) wire size, and (5) length of test specimen.[25]

The results of tests on five different geometries in which the wire radial spacing and the wire pitch spacing was varied was reported.[26, 27] In all of these tests, the wire was semi-elliptical in shape and had major and minor axes of 0.160 inch and 0.020 inch respectively. All test specimens were six inches long. As a consequence of variation in radial and axial spacing of the wire, each of the five specimens had a different hydraulic diameter, resulting in a range of values from 0.133 inch to 0.196 inch.

The final correlation of the test data on the five specimens was published.[27] With the exception of 17 out of some 150 data points, friction-factor variation grouped in a band of width ±10 percent from a mean correlation line.

3.1.5 Corrugated Surface Fuel Elements

The corrugated surface was investigated as a potential fuel element design mainly because of its structural integrity and possible increased heat transfer performance. For this particular design, the coolant airflow was in a direction perpendicular to the corrugations of the fuel plate.

Three different designs incorporating the corrugated surface were investigated. These were (1) a stacked assembly of corrugated plates, (2) a corrugated concentric-ring assembly, and (3) a corrugated radial-vane assembly. Figure 3.4 shows the design of the corrugated concentric-ring element. In all the above designs, the wave of the corrugation is formed by two circular arcs joined tangentially. The principal parameters describing the geometry of corrugated systems are the amplitude-to-pitch ratio, the gap-to-amplitude ratio, the wave angle, and the diffusion angle. The wave angle is defined as the half angle swept by the radius in moving from one end of the arc, forming a corrugation to the other end. The diffusion angle is defined, for two separated parallel plates whose corrugations would be perfectly in phase if brought together, as the double angle between a perpendicular to the centerline of the passage and a perpendicular to either wall at the plane of minimum cross-sectional area.

Experimental results of pressure drop and heat transfer are reported in terms of the above parameters for a stacked assembly of corrugated plates.[28] The results of this investigation showed that an increase in heat transfer coefficient, above that realized in a straight duct, may be obtained in wavy passages. The friction factor, however, increases faster than the heat transfer coefficient. A measure of heat transfer effectiveness is the ratio of the Colburn j-factor to one-half the friction factor. For ideal smooth tubes, this ratio is unity. For all the corrugated configurations tested, this ratio varied from 0.95 to 0.30 for wave angles of from 10 to 40 degrees, respectively.

A two-dimensional analysis of subsonic potential flow between wavy walls whose shapes are sine waves of arbitrary amplitude and pitch was published.[29] The results of this analysis were used to evaluate the pressure coefficient along the walls of the passage. In addition to the two-dimensional flow analysis, the published report also contains a method of solution for a three-dimensional flow with axial symmetry.

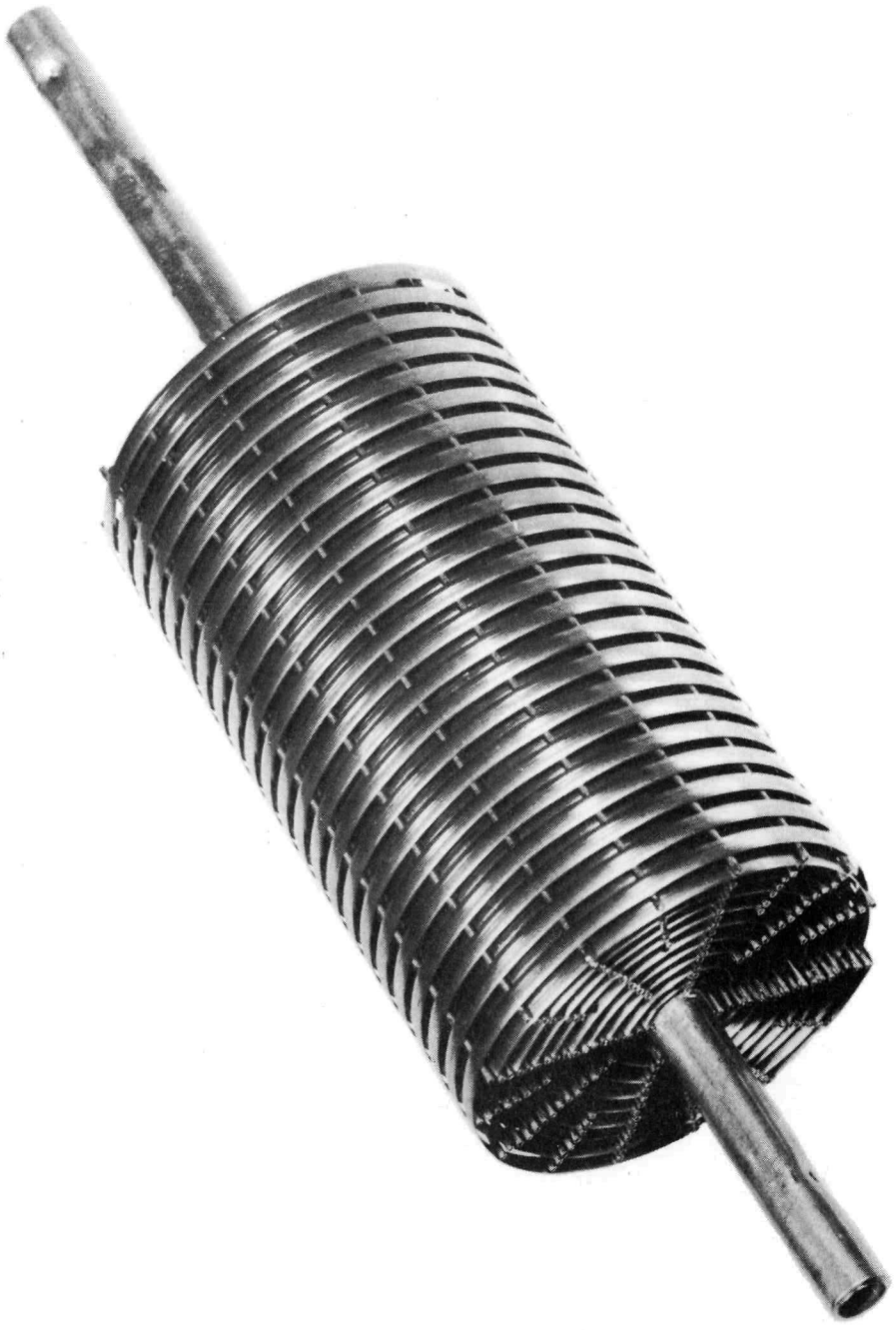

ACF - 2 MOCKUP NO. 3
18 Layers - .160" X .020" Elliptical Nichrome Wire.
192 - .062" O.D., .008" Wall, Type 304 S.S. Spacers.
Length = 6" (Approx.)
Outside Diameter = 3.5" (Approx.)
Pitch = .261"

Fig. 3.3 – Shaped wire fuel element test specimen

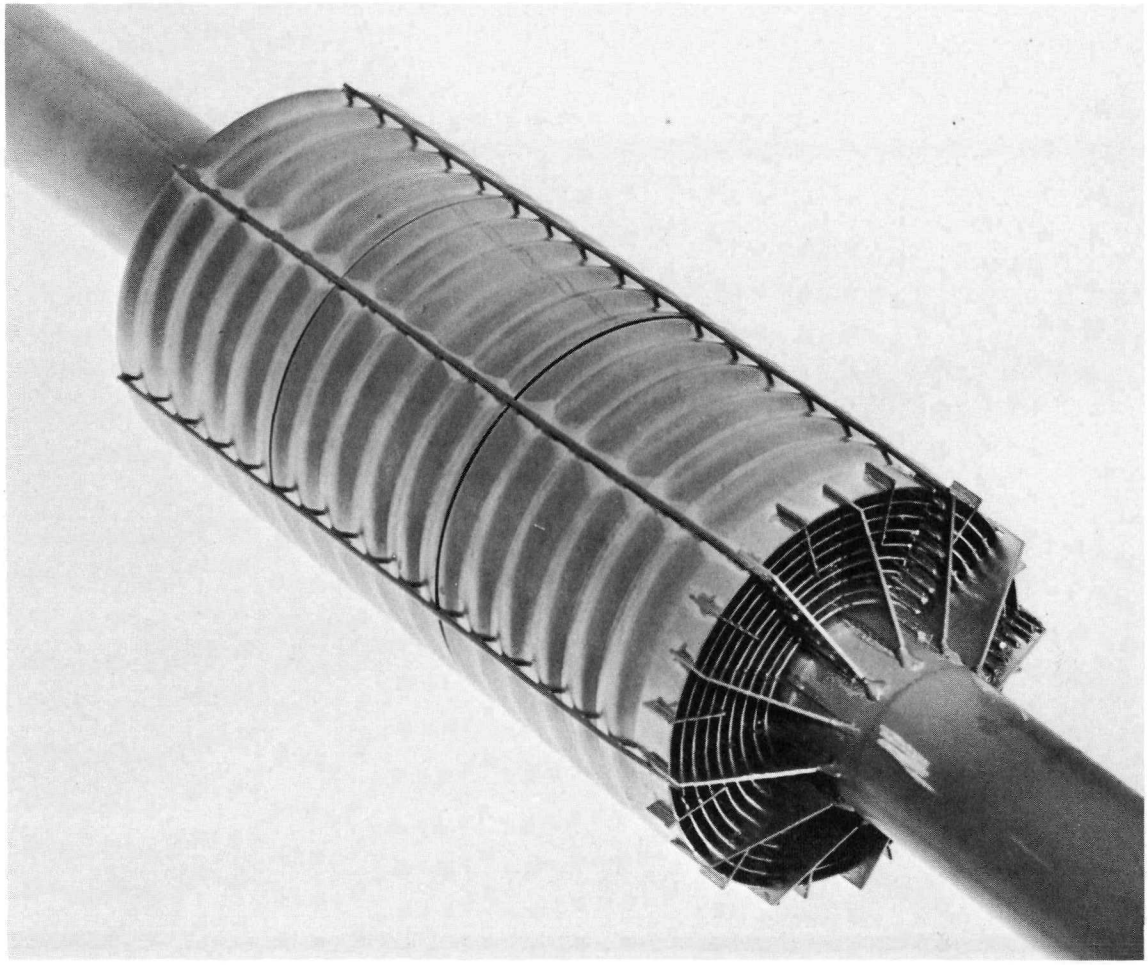

Fig. 3.4 – Corrugated concentric ring fuel element

The predicted aerothermal performance of a particular corrugated concentric-ring configuration were reported.[30] The results of experimental cold-flow pressure drop tests on the same design prior to nuclear testing in the MTR were published.[31] The experimental results indicated that the pressure drop would be approximately three times that predicted in the published report.[30] Care must be taken in interpreting these results because the sample tested was not of very good quality in terms of concentricity of of the rings, or uniformity of the corrugations, and the measured pressure drop included the additional drag of the leads of the attached thermocouples.

A detail of the recommended design procedures for corrugated concentric-ring configurations was reported.[32] The procedures proposed make use of the published experimental results of the two-dimensional tests.[28]

No experimental or analytical work was performed to determine the aerothermodynamic performance of the corrugated radial-vane assembly. A description and qualitative appraisal of the design was published.[33]

3.1.6 Screen and Screen Matrix Fuel Elements

The first wire configuration considered as a potential fuel element design consisted of parallel wire banks similar to tube banks. A summarization of existing technology regard-

ing heat transfer performance and pressure loss was made and applied to prediction of performance when used in the R-1 reactor.[34, 35]

As a result of experimental tests conducted at NACA, heat transfer and pressure drop data specifically applicable to screen banks in series was reported.[36] This data indicated that pressure loss could be satisfactorily correlated in terms of the dynamic head, the number of screen bank layers, and the free-flow fraction described from a one-dimensional frontal view of the screen bed. The heat transfer coefficient data was about 20 percent lower than that of the well-known Grimison data for flow over tube banks.

Increased attention was given to furthering the knowledge of the aerothermodynamic characteristics of wire screen matrices with the advent of the P-123 folded-flow power plant concept (see APEX-909). Early appraisals of the screen matrix as a potential fuel element configuration[37, 38] used the heat transfer and pressure drop relations of Tong.[39] Later experimental data which became available was that of London et. al.[40]

Although consistent correlation was obtained for a large spectrum of screen geometries, this correlation was open to some doubt as to its application to a completely heated matrix at temperatures in the neighborhood of 2000°F. The London heat transfer data were obtained by a transient technique on a single heated rod within the matrix at temperature levels just above ambient.

As a consequence of the uncertainty of applicability of the London data, an experimental program was undertaken to evaluate the heat transfer and pressure drop characteristics of a brazed in-line crossed-rod screen matrix having essentially uniform power generation, and operating at temperature levels of 1700° to 2000°F. The results of this investigation were published.[41] A summary of the test results of this investigation is shown in Figure 3.5.

Also shown in Figure 3.5 are the test results from the data of London for a geometrically similar configuration. A comparison of the published results[41] to those of London, show that the heat transfer coefficient was about 20 percent lower, and the friction factor was 40 to 115 percent higher than London's. The friction-factor data were considerably higher than those of London because the screen matrix was held together by braze material at wire junctions (crossings), and the results were obtained from tests after certain amounts of dust had been injected into the coolant air stream, as shown by samples 7 and 8 of Figure 3.5.

An analysis of the detailed temperature distribution that would exist in an average wire at the exit face of the screen-bed matrix of the P-123 system was reported.[42] The analysis, based on design-point operation, indicated that a temperature difference of 13°F would exist in any one wire between the hottest and coldest positions in an average square formed by the intersection of four wires.

Temperature perturbations due to clogging of the wire mesh were reported.[43] In this test, clogging was simulated by the "potting" of ceramic cement on the inlet face of the screen. For a clog about 1/2 inch in diameter, the magnitude of the temperature perturbation varied linearly with heat generation in the screen matrix and had a value of about 490°F, when the exit-screen surface temperature was 2250°F and the power level was 876 kilowatts per square foot.

Additional studies on clogging effects within the screen matrix due to dust contamination in the coolant air were made.[44, 45] These studies were concerned with the mechanism and the percentage of dust collection by a bank of wires at various temperature levels. The results indicated a serious increase in dust collection with screen temperature, approaching 90 percent capture efficiency at temperatures above 1700°F.

Analytical and experimental studies were made of the channel flow of air through porous resistances inclined at slight angles to the longitudinal axis of the channels. An evaluation

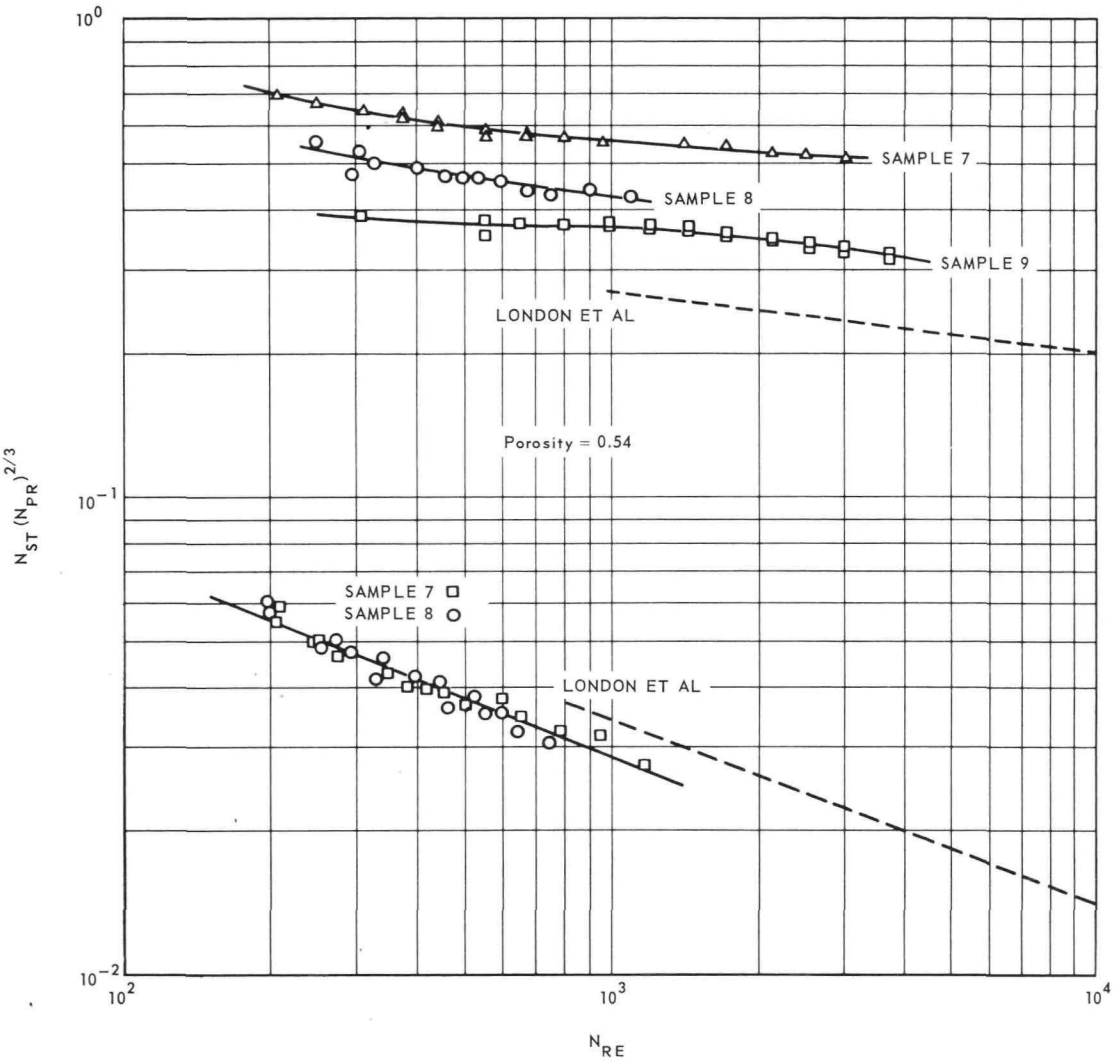

Fig. 3.5 – Heat transfer and pressure drop characteristics of brazed wire screen matrices

was made of the flow characteristics through a resistance bed that was inclined at an angle of 3-1/2 degrees to the flow direction with the downstream side of the bed discharging to the atmosphere.[46] Tests on twenty-seven 180-degree folded-flow duct configurations that lead into and out of a porous bed were reported.[47] The results of this testing definitely indicated that the flow distribution through the bed is influenced by the shape of the inlet and outlet ducts as well as by the relative widths of the ducts. Analytical studies of 180-degree folded-flow systems were published.[48, 49]

3.1.7 Cylindrical Coolant Flow Channels

With the advent of the XNJ140E ceramic-core reactor in which the air coolant flows through longitudinal cylindrical holes, attention was focused on the determination of variation in local heat transfer coefficient and friction factor with longitudinal position in the core.

For fully-developed turbulent flow with constant heat flux, a local heat transfer coefficient may be calculated from the usual Nusselt relation:

$$\frac{hD}{k_f} = 0.0205 \left(\frac{\rho_f DV}{\mu_f}\right)^{0.8} \left(\frac{C_p \mu}{k}\right)_f^{0.4} \qquad (5)$$

where the subscript f denotes evaluation of fluid properties at film temperature. As a result of thermal entrance region effects and heat-flux variation through the tube length, the fully developed heat transfer coefficient for constant heat flux has to be modified. The analytical determination of the effects of thermal entrance region and arbitrary heat flux on the local heat transfer coefficient were derived for the cases of laminar and turbulent flow respectively.[50, 51] In particular, it is shown that for a longitudinal power profile closely approximating that of the XNJ140E core, the ratio of local-to-fully-developed turbulent heat transfer coefficient is 1.06 and 0.91 just inside the active core entrance and at the active core exit, respectively.[51] (The XNJ140E core is described in APEX-908.)

The results of an experimental investigation to determine local friction factors in production ceramic tubes of various wall finishes were published.[52] Less detailed tests were previously reported.[53, 54] Specifically, the following type tubes were tested: fueled BeO tubes - alumina coated; fueled BeO tubes - uncoated; and non-fueled BeO tubes - uncoated.

These three types had average ratios of root mean square surface roughness-to-tube diameter of 0.00044, 0.00011, and 0.00005, respectively. Their respective curves of friction factor versus Reynolds number all fell slightly above the usual minimum friction factor curve for a smooth tube, with the alumina-coated tubes having the highest f value (an increase of 19 percent over smooth-tube performance at a Reynolds number of 5×10^4). For purposes of XNJ140E design analysis, a multiplier of 1.15 was applied to the smooth-tube value irrespective of Reynolds number level.

The amount of flow that passes through the interstitial spaces between hexagonal tubes in a bundle was investigated and reported.[55] From these tests it was estimated that in a ceramic core composed of hexagonal tubes having internal bores of 0.200 inch, the interstitial flow would be about 0.4 percent of the total flow.

A comparison of round-tube to concentric-ring fuel elements was made.[56] This analysis indicated that a 5 to 10 percent gain in thrust-to-weight ratio could be realized with round tubes if the tube diameter could be as small as 0.1 inch. For tube diameters larger than 0.15 inch, little gain may be realized over that achieved with concentric-ring cartridges. Ceramic tubes can, however, operate at higher temperatures with the resultant increase in power.

For high tube-wall temperatures, heat transfer by radiation tends to approach the order of magnitude accomplished by convection. In addition, if there is an appreciable longitudinal gradient in wall temperature, conductive heat transfer must also be considered. The computational mechanics for determining the heat transfer characteristics in tube flow under the combined influence of fully-developed radial convection, axial conduction, and radiation were reported.[57] The nonlinearity of the problem necessitates the repetitive solution of a linear simultaneous equation-set until convergence is achieved.

An analytical solution for the temperature distribution in a cross-section of a fuel rod matrix was obtained.[58] The fuel rod consisted of a right circular cylindrical solid containing a uniformly distributed heat source, a central coolant hole channel, and k symmetrically placed coolant hole channels located on a bolt circle of arbitrary radius. The outer surface of the rod is surrounded by a solid annular ring having a different uniform heat source and an insulated outer boundary. This analysis was chosen because it appeared to offer a simpler method than the THT program for determining effects of geometry perturbations on temperature distribution.

3.2 REACTOR AEROTHERMODYNAMICS

Significant experimental data and significant analytical work in reactor aerothermodynamics not specifically related to a particular design will be reported here.

3.2.1 External Influences

Design of flow passages external to the reactor may influence entrance and exit pressure losses, inlet velocity profiles and reactor flow distribution. Final performance predictions for reactor operations have been based largely on experimental data obtained from isothermal flow tests of scale-model simulations of reactor and shield configurations.

Matching of fuel element power to fuel element airflow is a significant step in the design of reactors for high-performance nuclear power plants for aircraft. A mismatch of 5 percent in a local coolant channel can lead to an additional fuel element temperature requirement of about $100^{\circ}F$, or alternately, for a given fuel element temperature limit, the turbine inlet temperature would have to be reduced by about $60^{\circ}F$ which in some power plants may be equivalent to about a 5 percent reduction in thrust.

ANP design practice has been to design external ducting so that the influence on core flow distribution will be relatively small - no more than about 5 percent deviation from average flow. Flow distributions as measured in the scale-model tests are then used in the design specifications that control power distribution. Any imperfect matching that is predicted in the design process is accounted for in the prediction of maximum calculated fuel element temperature. Uncertainties in flow measurement are estimated and the corresponding temperature effects are statistically added to temperature effects resulting from other measurement uncertainties; e.g., critical-experiment flux, fuel loading, and flow-passage dimensions, to determine an allowance in fuel element temperature for measurement uncertainties. The sum of this allowance and the maximum calculated temperature become the prediction of the maximum fuel element temperature or the hot-spot temperature.

The HTRE No. 1 reactor configuration as tested in the Core Test Facility (CTF) was characterized by relatively large plenums above and below the core (about 1 foot axial depth for the upper plenum and a depth in excess of 1 foot for the bottom plenum).

Data for core inlet Mach number range of 0.048 to 0.153, from test runs on a scale model, indicate that there are no regions of significant flow deficiency nor any pattern of maldistribution. Description of the test apparatus and a summary of data were published.[59]

The HTRE No. 3 reactor was the first reactor operated in a flight configuration shield. Design objectives of low weight and small external envelope led to plenums of significantly smaller axial height than those of the HTRE No. 1 design. Again, extensive scale model tests led to acceptable flow passage designs at either end of the reactor. This experimental program and the resulting data were reported.[60] Typical flow distributions for HTRE No. 3 are summarized in Figure 3.6. The HTRE No. 3 final design and two alternative configurations were investigated. Significantly, the flow maldistribution was limited to the same magnitude as was realized in the HTRE No. 1 design even though the shield plugs were located only a few inches from the ends of the reactor.

Porous wavy-wall shield plugs were introduced in the XMA-1A power plant design. Flow distribution data within the reactor core along with other experimental data for a series of configurations have been published.[61] Horizontal and vertical orientations of both the front and rear wavy-wall shield plug passages were investigated together with the effect of simulated compressor swirl. Magnitude of deviation of flow from average value did not vary significantly with several configuration modifications. However, location of maximum and

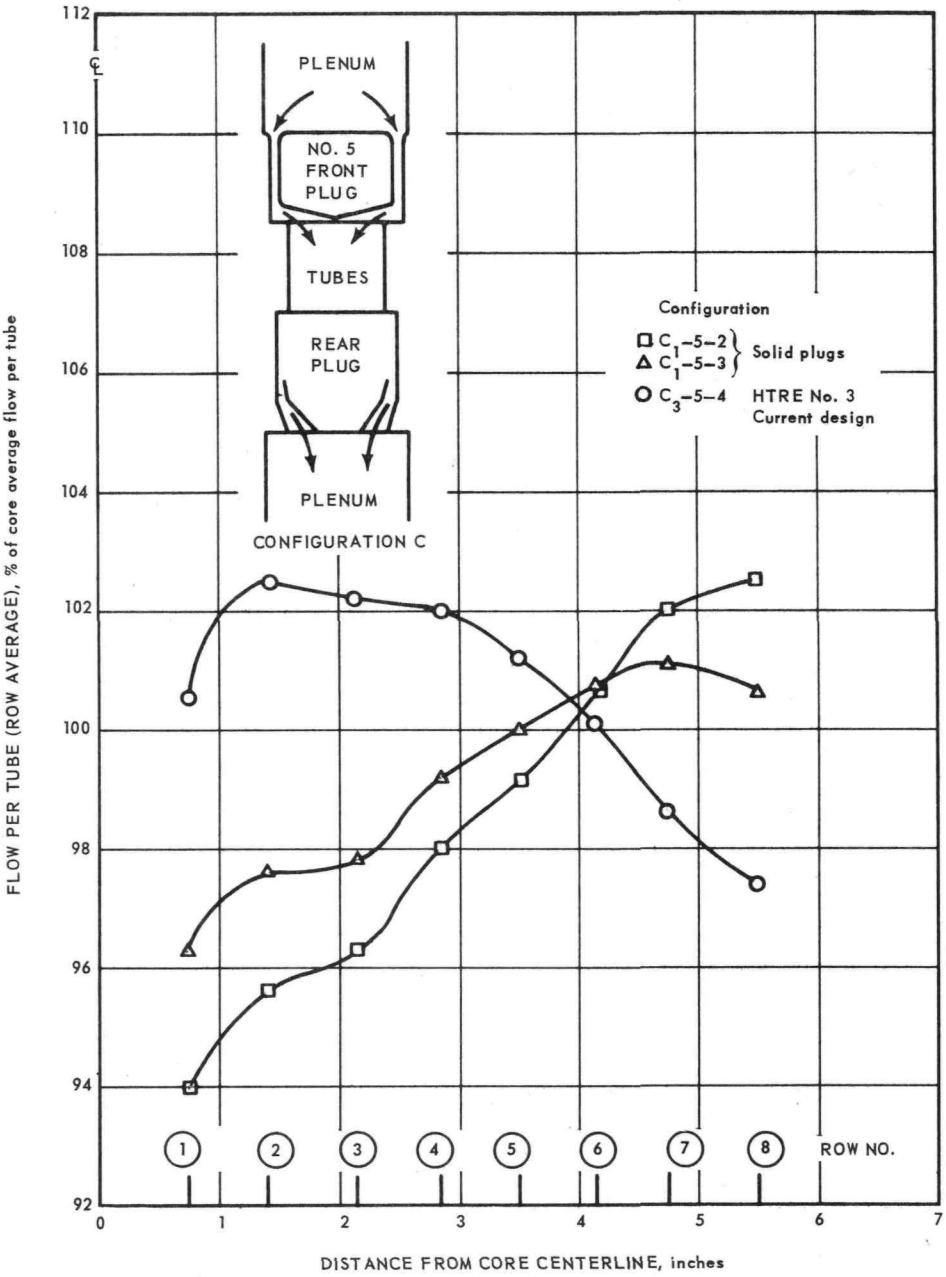

Fig. 3.6 – Weight flow distribution radially in core for various rear plugs

minimum flow regions within the frontal area of the core did vary, depending on the rotation of the front plug. Flow distribution data for the XMA-1A plug orientations are shown in Figure 3.7. Flow deficiencies are generally 2 percent or less.

The data shown above indicate that for several duct configurations external to the reactor, designs yielding flow distributions uniform within approximately 2 percent are possible. An alternative design philosophy would be to design ducts for better shielding effectiveness; i.e., lower-volume plenums. This approach might well lead to nonuniform reactor flow distribution. Although it is conceivable that reactor power could be matched to a nonuniform flow distribution, this design approach has not been used, for the reason that measurement of flow distribution in cold flow tests, followed by analytical interpretation for the heat-addition case, might lead to significantly larger uncertainties in design predictions than exist for the situation of near-uniform core flow distribution.

The adoption of the annular shield duct in the forward plug of the HTRE No. 3 power plant results in a situation wherein the air flows radially across the front of the reactor and encounters a 90 degree turn entering the fuel tubes. This turn produces a non-axisymmetric velocity profile approaching the fueled elements. Flow distribution is further influenced by whether the inlets are sharp or rounded, by tube position within the core, and by thermocouple disconnects and supporting structure located in the entrance region. Reasonably successful attempts were made to measure total pressure distribution within the inlet of tubes in the HTRE No. 3 scale model used for the previously described flow distribution studies. In an attempt to obtain more complete flow mapping, total head measurements were also made in a two-dimensional full-scale tube-inlet model. Data from both these tests, shown in Figures 3.8, 3.9, 3.10, and 3.11, were published.[60] Data like these (circumferential and radial maldistributions within a tube) when used as input data for the Ansector program (see section 2.2) result in higher fuel element temperatures downstream from the low inlet-velocity areas than would result from an assumption of uniform inlet flow velocity.

3.2.2 Fuel Element Sizing Techniques

Extensive use was made of the Off-Design Computer Program (see section 2.1) for final sizing of tubular fuel elements and for identifying average hydraulic diameter and total fuel element flow area per stage for concentric-ring fuel elements. Because hydraulic diameter and flow area are input data, the program is used parametrically in many instances. Final determination of hydraulic-diameter variations within a concentric-ring fuel element to accommodate nonuniform ring-to-ring power distribution is accomplished by iterative use of the Heated-Annuli Program (see section 2.2). During design studies, "rules-of-thumb" or short-cut estimating procedures were evolved to minimize computer costs. For example, in the XMA-1A reactor, design philosophy was to fuel-load each ring in a stage in a manner that would result in uniform ring-to-ring power distribution. The outermost annulus is bounded by a fueled ring and an unfueled cylinder. One effective "rule-of-thumb" that evolved was that a reduction of 30 percent in outer annulus size relative to other annuli in that stage would restrict the flow enough to raise the temperature of the outer ring to the same level as the temperature of the other rings.

The Ansector Program (see section 2.2) is useful in relating circumferential power-flow maldistributions to circumferential variations of fuel element temperatures. These relationships make possible a choice of circumferential variation of poison shim stock around the fuel cartridge in a manner that will limit circumferential temperature deviations to acceptable values without using excessive amounts of poison.

Sizing techniques not requiring the use of computing machines are available and generally yield results sufficiently accurate for preliminary design. A step-by-step standard method of designing concentric-ring type fuel elements with particular application to the HTRE No. 1

$$D = \left(\frac{\text{weight flow per tube}}{\text{average weight flow per tube}}\right) \times 100$$

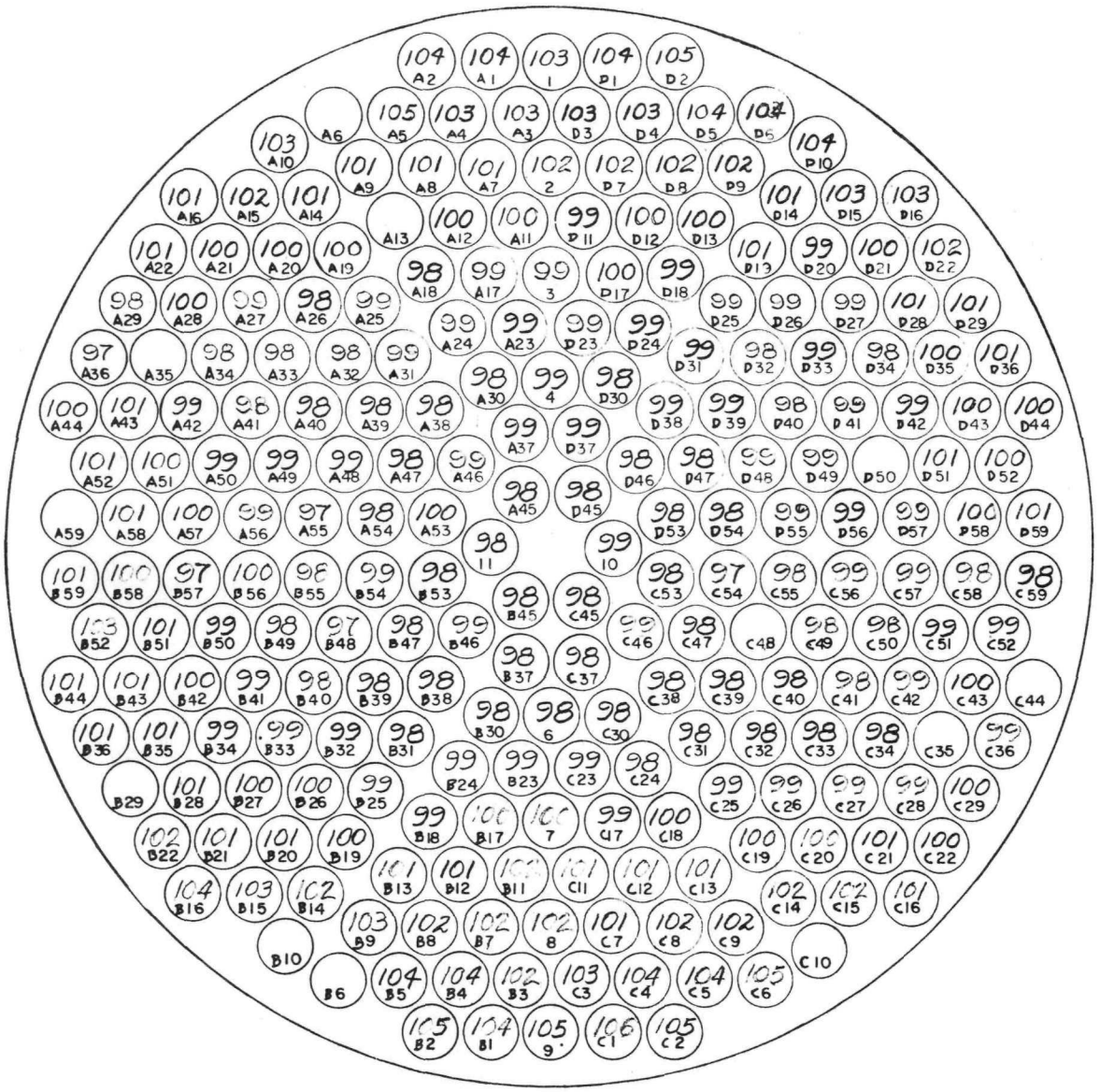

Fig. 3.7 – Weight flow distribution D in tube bundle, configuration 0213, front plug horizontal, rear plug horizontal, with extension fins. Complete model including swirl and simulated "choke" plates

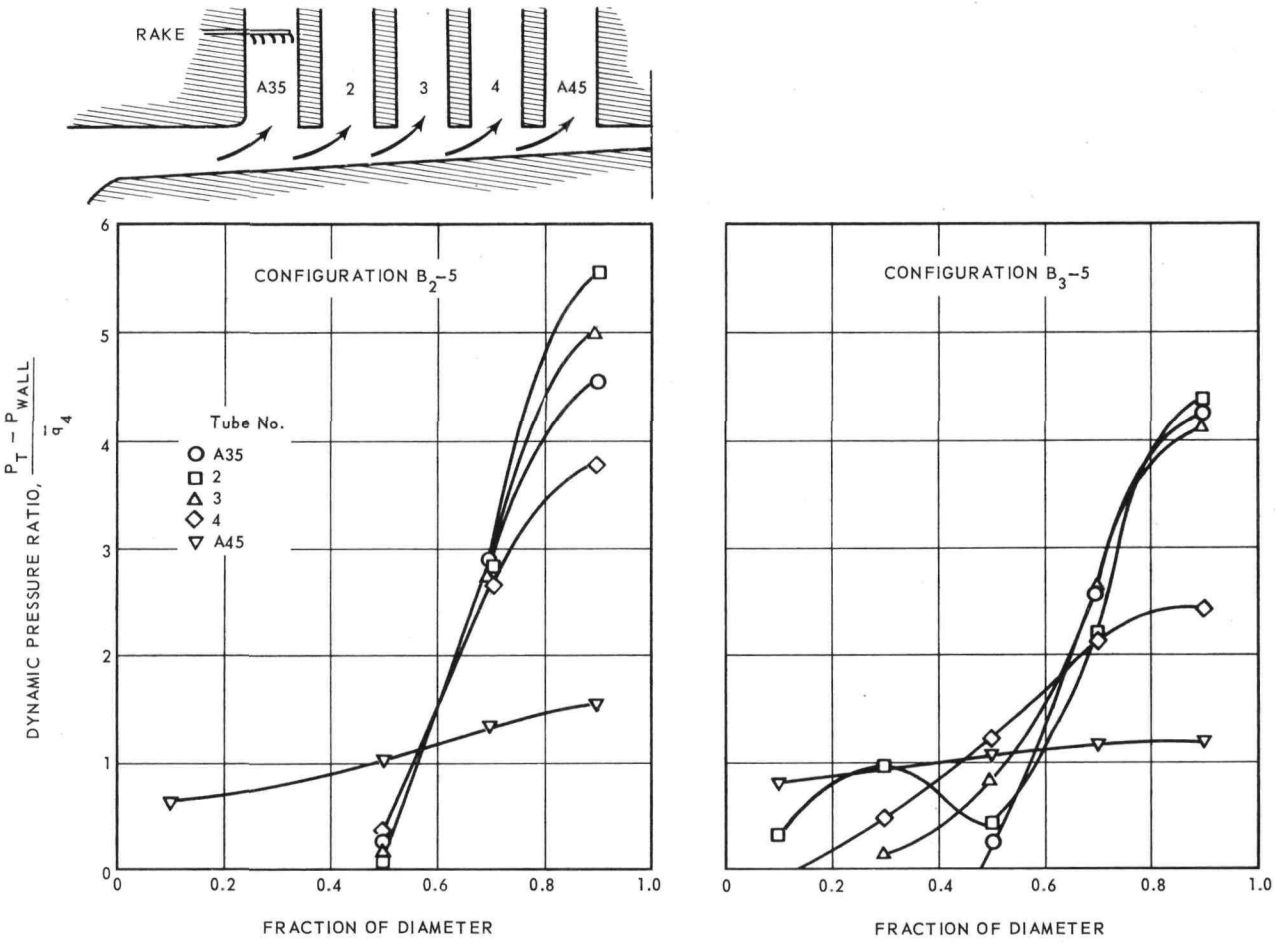

Header No. 5
sharp inlets

Header No. 5
rounded inlets

Fig. 3.8 – Inlet total pressure profiles for various entrance conditions

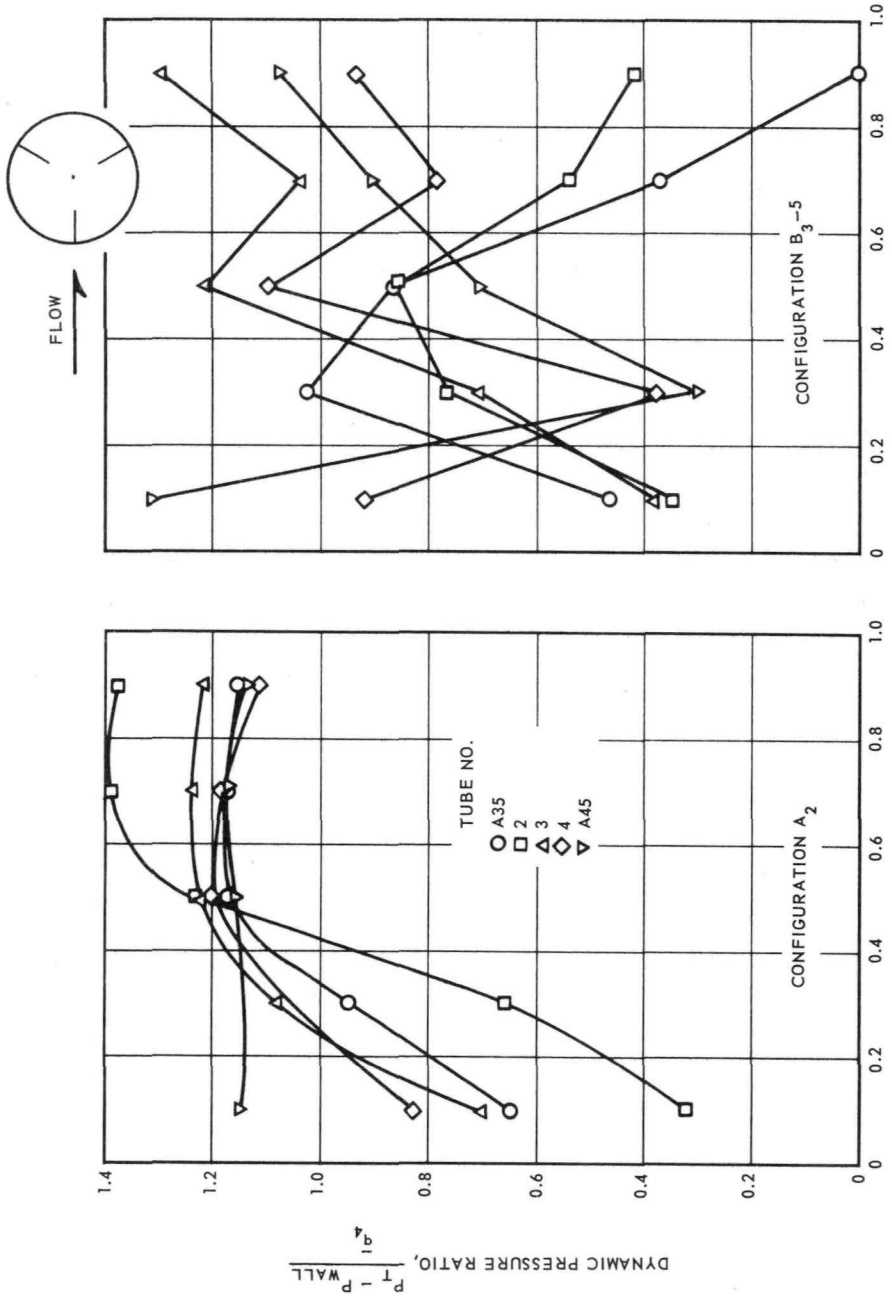

Plenum feed
sharp inlets

Header No. 5, rounded inlets,
and disconnect inserts

Fig. 3.9 – Inlet total pressure profiles for various entrance conditions

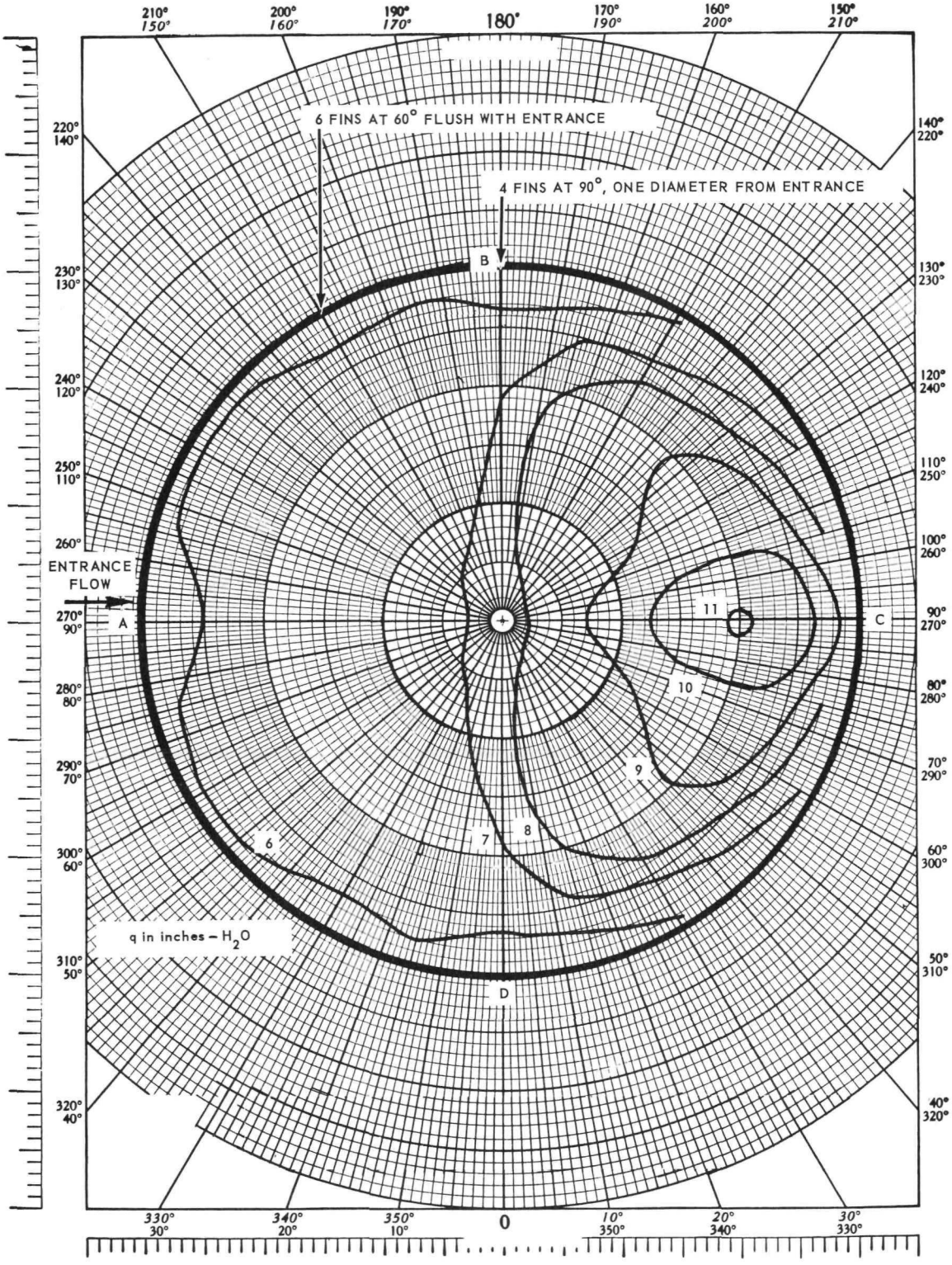

Fig. 3.10 – ISO-Q plots from two-dimensional flow results for a tube-in-core location similar to that of tube A35 with nose and fin inserts

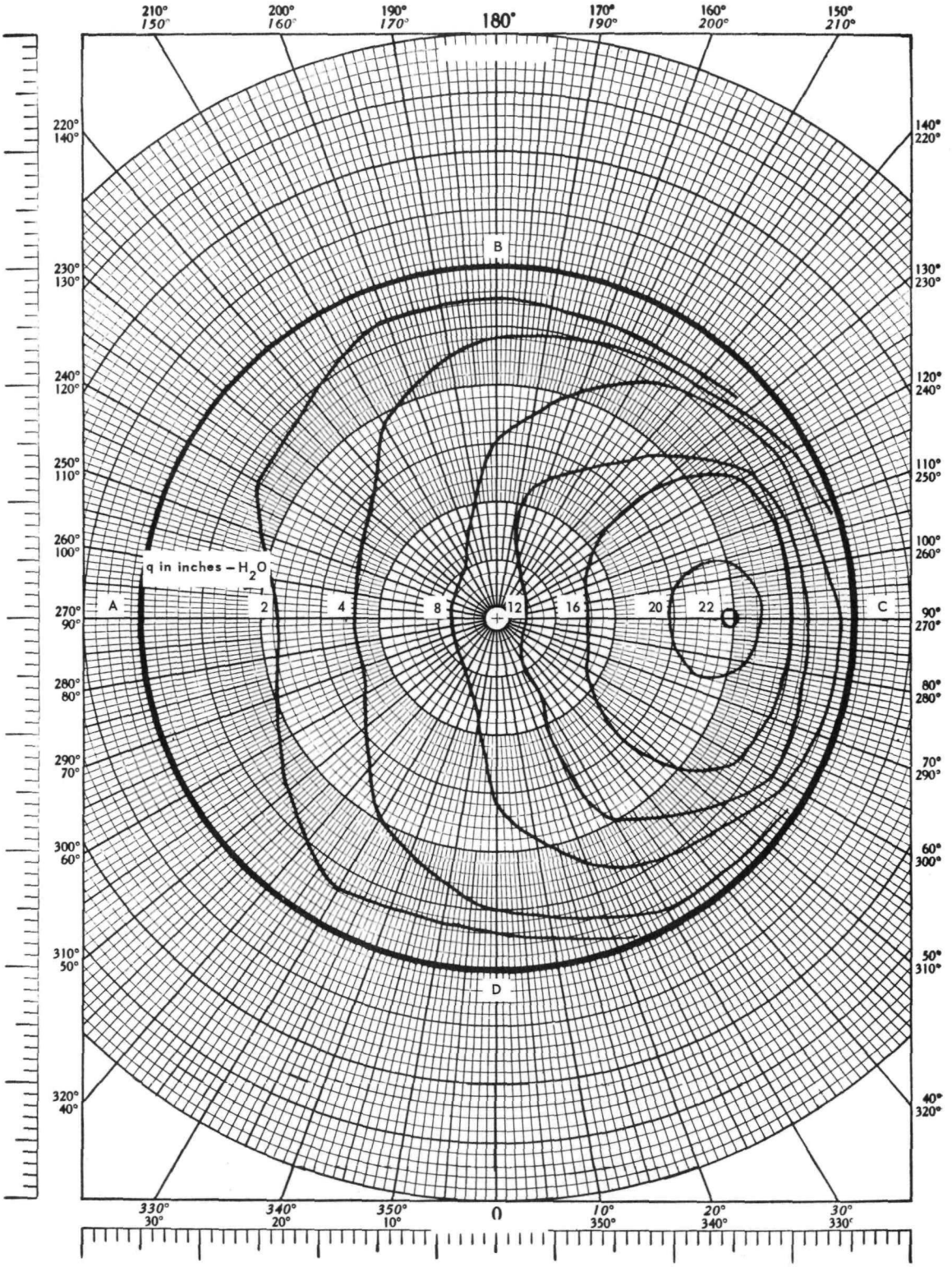

Fig. 3.11 – ISO-Q plots from two-dimensional flow results for a tube-in-core location similar to that of tube A35 without nose and fin inserts

core was published.[62] Data applicable to the design procedure are included. Generalized thermal design relationships and generalized pressure loss computations for air in conduits were reported.[63, 64] Included is an analysis that establishes relationships among reactor component geometry, power level and distribution, coolant-flow rates and resultant temperatures.[63] These formulations can be used for typical thermal design problems such as basic coolant-channel sizing, worth of power shaping, off-design performance, and temperature-perturbation studies. Typical examples of such studies are included. Although the specific presentations are for the case of turbulent flow of air in conduit type passages, this approach can be utilized to develop the same type of presentation for alternative coolants and types of coolant passages. Generalized data for pressure loss in air, treated as a compressible fluid, flowing in a constant-area, high-friction duct is presented.[64] The graphs included lend themselves to the sizing and rating of air-heat exchanger ducts and reactor coolant passages. Two groupings of parameters are presented; one to be used for establishing design and one to be used for off-design predictions.

3.2.3 Fuel Element Temperature Perturbations

Prediction of fuel element temperature perturbations is a part of the reactor design process and involves considerations of power distribution, flow distribution, fabrication tolerances, measurement uncertainties and heat transfer. Discussion here will be limited to aerothermodynamic phenomena that have an influence on fuel element temperature perturbations.

The Ansector Computer Program is sufficiently flexible with regard to input data that six circumferential temperatures can be computed for the trailing edge of each fuel ring in each stage for the situation wherein unique geometries and power loadings are specified in each of six sectors. The maximum amount of detailed analysis could be accomplished by taking all the measured conditions; i.e., inspection data, inlet velocity distribution, etc., and by use of the Ansector Program, predicting a detailed core temperature map. Time and cost requirements preclude this action, however. Additionally, the reactor designer tends to limit his primary concern to "hot channels"; in this case, hot ansector channels. In practice then, the Ansector Program is used for a few typical cases from which simplified and more approximate temperature-perturbation factors are derived. For example, in the HTRE No. 3 design a factor Γ_i was evaluated for the hottest sector of the tenth ring in each fuel cartridge for the highest-temperature stage.[65] This factor Γ_i was defined as being proportional to the temperature of the hot-ring sector less the inlet air temperature. Approximation of Γ_i as a simple ratio of percent-power deviation-to-percent-flow deviation was proven by HTRE No. 3 operation to be a sufficiently accurate approximation.

An analysis was made of the possible alleviation in peak bulk air and fuel plate temperatures that would occur because of thermal diffusion in the air stream in the outer annulus of an XMA-1A concentric-ring type fuel cartridge.[66] A particular calculation showed only approximately 8°F alleviation, or about 10 percent of the temperature perturbation that would occur in the absence of thermal diffusion. Actually, in computing the alleviation, angular conduction within the fuel ring was also included. Because this effect is small, it is normally omitted from reactor predictions. The concept of swirl flow (discussed in 3.1.3) was considered as a means of reducing circumferential temperature scallops but was never used in a reactor design because of lack of performance improvement.

In the initial phases of the design of tubular fuel element reactors, it was recognized that a flow channel formed by tubes placed end-to-end would experience an increase in core pressure loss if there was lateral displacement of the holes at the connecting ends. Also a channel that includes such misalignments would pass less airflow than one with no misalignments. This would lead to a temperature perturbation in the channel with misaligned holes. Information for predicting pressure losses for flow through sections of tubing having sharp lateral misalignments at the connecting ends was published.[67] Loss coefficient data

are presented in the form of an empirical equation containing dimensionless displacement as one parameter and two other parameters that are functions of upstream Mach number.

Utilization of transition pieces at the inlet and exit of the core in the XNJ140E-1 design introduced two additional flow distribution questions. The first pertains to flow distribution within the cluster of 19 fuel tubes associated with one transition piece. The second pertains to the effect of misalignment between transition piece and forward reflector, and between transition piece and aft retainer. An experimental program to investigate these effects was devised but because of the program cancellation, was not implemented.[68]

Another factor that can lead to temperature perturbations is nonuniform change of surface roughness and flow area with operating life. A particular experiment with Nichrome concentric-ring fuel elements indicated a pressure loss increase of 10 percent due to oxidation that occurred during a structural integrity test at operating temperatures.[69] Sensitivity of oxidation rates to temperature level were not determined in sufficient detail to make possible an integration of the effects over the longitudinal temperature distribution for evaluation of the possible resulting flow and temperature perturbation effects.

Ceramic fuel tubes have on occasion been observed to experience one or more of several types of geometry changes; namely, growth or swelling, clad blistering, rippled clad, and hydrolysis. As an aid to understanding the influence of these effects on pressure loss, an axial static pressure profile traverser and recorder was designed to measure and record the longitudinal static pressure along the axis of a fuel tube and to detect local changes in the static pressure. A description of the operation of this test unit, including a discussion of the types of static profiles obtained, and interpretation of the profiles in relationship to tube damage was published.[70]

3.2.4 Moderator Cooling

In air-cooled moderators, design philosophy has been to design coolant passages to allow flow of air in excess of the predicted requirements. This procedure permits the design of coolant channels to be sized early in the design sequence. As experimental data are obtained for nuclear heating rates and for flow resistance, the prediction of actual flow requirement can be made. Typically, flow resistances or orifices are provided in a range of sizes so that actual flow rate can be set at the time of reactor assembly. If the reactor is properly designed for remote handling, the actual flow rate can be changed after initial operation at design conditions. This procedure tends toward slightly excessive void volume in the reactor but is considered to be the practical approach for the design of the first reactor of a given type. It is anticipated that for subsequent designs, flow areas for moderator cooling can be reduced.

Results of an experimental investigation of the HTRE No. 3 moderator flow configuration were published.[71] Friction factors for the cooling slot, and loss coefficients for the slotted entrance and several exit orifice sizes were determined.

Procedures for sizing and positioning coolant holes in the XMA-1A tri-flute moderator were developed.[72] The extruding process used for fabrication resulted in elliptical holes instead of round holes as originally intended. Convective heat transfer rates were computed by the use of correlations for round tubes, wherein an equivalent or hydraulic diameter equal to four times the flow area divided by the heat transfer perimeter was used. For typical hole patterns, temperature predictions as computed with the THT computer program (see section 2.4) are shown. Also an approximate expression to determine local porosity is developed.

3.2.5 Control Rod Cooling

Use of air-cooled control rods in the HTRE No. 3 and subsequent reactors resulted in a requirement for a control rod design with some freedom to deflect and adapt to axial

distortions of the containing guide tube. The HTRE No. 3 strapped and segmented rod filled this requirement and also the requirement that excessive bearing loads would not result from thermal bowing associated with nonuniform heat removal from the surface. Temperature predictions were determined from the computer programs discussed in sections 2.4 and 2.6. The method of computation is necessarily complex because of the requirement for detailed strap temperature distributions, the possibility of eccentric positioning of the rod relative to the guide tube, and the flow of a non-specified amount of heat into the external surface of the guide tube.

Although effective friction factors can be estimated, pressure loss predictions are confirmed by flow experiments using close simulations of the design configurations. Typical of the experimental data are those reported for the XMA-1A control rod cooling passage.[73] An effective friction factor 38 percent larger than that for a smooth tube was identified for the strapped portion of the rod. The definition of flow area and hydraulic diameter was rather complex; basically, it involved an averaging of flow areas and perimeters over the length. Hence, this increase of 38 percent is a measure of the increased pressure loss associated with strapped rods relative to continuous one-piece rods, or more appropriately, it is indirectly a measure of the increased void required. Similar data are reported for the XNJ140E-1 control rod.[74] The equivalent friction factor for the strapped portion of this rod was about 45 percent greater than that for smooth tubing.

The tests of the HTRE No. 3 control rod also included calibration of four different flow restrictor sizes (mounted on top of the control rod) and determination of friction factor in the open portion of the guide tube and in the smooth annulus forward of the strapped region.[73]

3.2.6 Air-Cooled Aft Retainer Assembly

A three-phase experimental program was established to determine heat transfer coefficients within the flow passage of the XNJ140E-1 aft retainer assembly. Although conditions within the flow passage consist essentially of flow normal to a bank of tubes for which heat transfer data are available, specialized data were considered necessary for the following reasons: (1) the tubes are very short ($L/D < 1.4$), (2) the flow passage is nonsymmetrical and convergent as seen in Figure 3.12, and (3) data are not readily available for the side plates which are the critical structural members of the XNJ140E-1 design.

Phase one of the experiment was designed to determine, exclusively, the heat transfer coefficient for individual tubes in the tube bank. This was accomplished by insulating selected tubes from the plates, heating them electrically, and measuring the heat dissipated to the air stream.

Phase two, using a different test model, was to determine the heat transfer coefficient for the exposed areas of the side plates.

Phase three was designed to heat both the tubes and plates so that upon calculating an over-all heat balance, the results of phases one and two could be verified. Upon obtaining this verification, the cooling air-flow distribution was to be computed from the heat transfer coefficient data of phases one and two and local air temperature measurements of phase three. Because of contract termination, phase three tests were not made.

Figure 3.12 shows the arrangement of tubes in the test model, the 29 tube locations and the 9 plate locations which were investigated, the number-letter position coordinates, and the tube row designation to which reference will be made below. The tubes were 0.87 inch in diameter, 1.1 inch in length, and were spaced on the apexes of equilateral triangles with a pitch of 1.09 inch. A detailed description of the test procedure and test model, including drawings and photographs was published.[75] The results of the test data of all of the individual test locations which were investigated are reported. In all cases, for both tubes and plates, the data are represented by plotting Nusselt number versus Reynolds number,

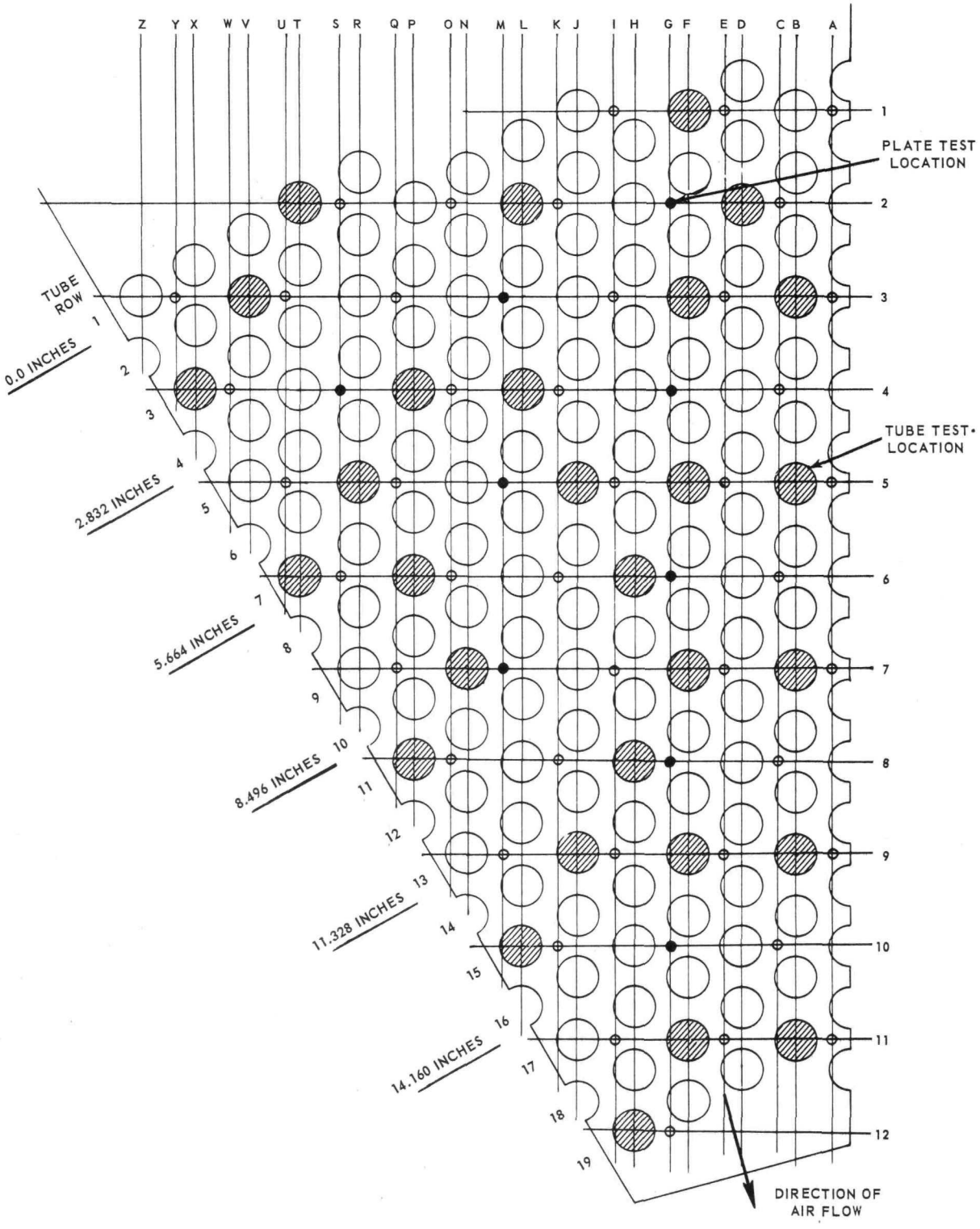

Fig. 3.12 – XNJ140E-1 aft retainer assembly test model

defined by hD_T/k_f and $G_{EM}D_T/\mu_f$ respectively. In these definitions, h is the local heat transfer coefficient, D_T is the outside diameter of the tube, k_f is the air-film thermal conductivity, G_{EM} is the maximum mass velocity established at the exit of the retainer assembly, and μ_f is the air-film viscosity.

Figure 3.13 presents a correlation of the test data for the tube bank wherein the Reynolds number is based on the local maximum mass velocity, G_{LM}, within the tube row in which the particular tube being investigated is positioned. The local maximum velocity was computed by multiplying the exit mass velocity by the ratio of free-flow area of the exit tube row (row 19 in Figure 3.12) divided by the free-flow area of the tube row being investigated. This calculation assumes a uniform mass velocity within a tube row which is not rigorous because of the nonsymmetrical nature of the flow passage. The design equation, which was derived from the data, is

$$\left(\frac{hD_T}{k_f}\right) = 0.0907\left(\frac{G_{LM}D_T}{\mu_f}\right)^{0.7}\left(\frac{c_p\mu}{k}\right)_f^{1/3} \qquad (6)$$

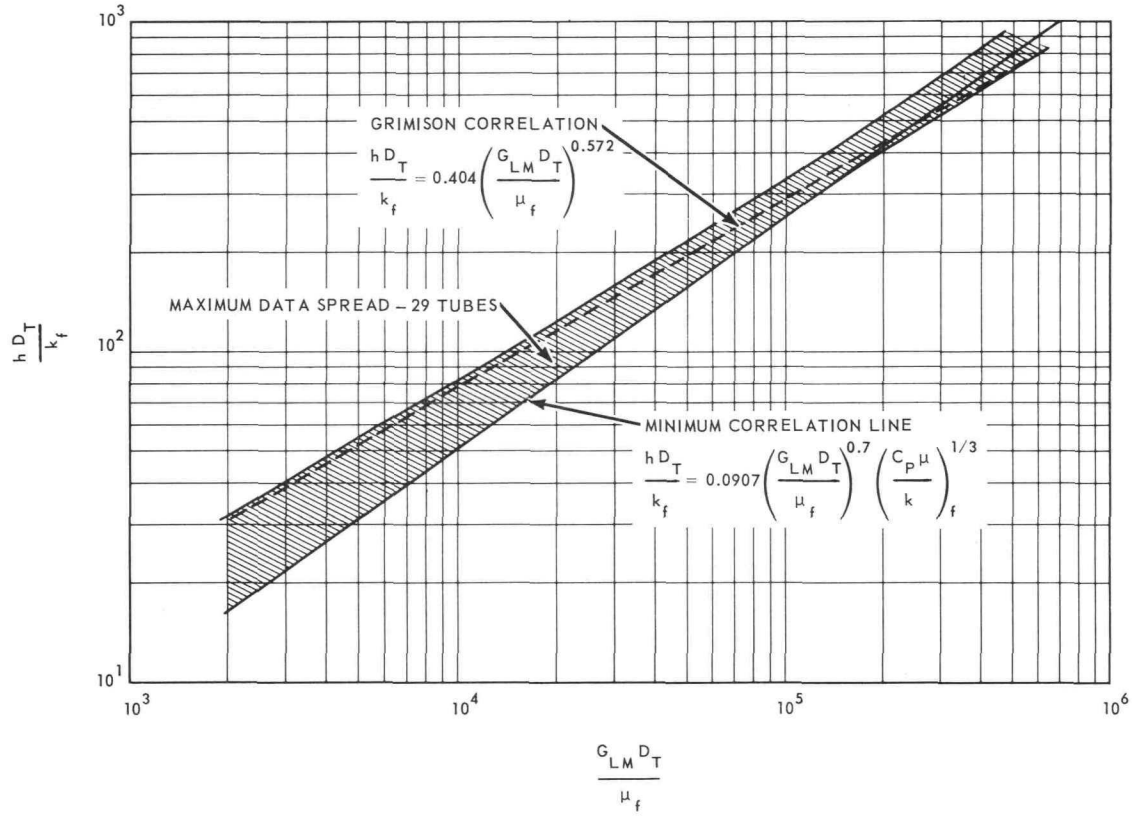

Fig. 3.13 – Correlation of heat transfer data for tubes of XNJ140E-1 aft retainer assembly

It is significant that the above equation represents a minimum correlation of the data, and its use will result in conservative cooling requirements. Also shown in Figure 3.13 is the correlation for the mean heat transfer coefficient for a tube bank where $S_T/D_T = 1.25$ and $S_L/D_T = 2.0$; S_T and S_L being defined as the transverse and longitudinal tube spacing, respectively.

A preliminary analysis of the test data for the exposed surfaces of the side plates resulted in the following design equation for predicting minimum plate heat transfer coefficients

$$\left(\frac{hD_T}{k_f}\right) = 0.000392\left(\frac{G_{EM}D_T}{\mu_f}\right)^{1.19}\left(\frac{c_p,\mu}{k}\right)_f^{1/3} \qquad (7)$$

In order to compare the test results with existing literature data for turbulent flow parallel to a flat plate, the data were also correlated by plotting hx/k_f versus $G_{LM}\,x/\mu_f$, where x is the distance from the plate leading edge to the point under investigation. Figure 3.14 presents the results of the correlation and the corresponding minimum design equation:

$$\left(\frac{hx}{k_f}\right) = 0.0567\left(\frac{G_{LM}x}{\mu_f}\right)^{0.805}\left(\frac{c_p,\mu}{k}\right)_f^{1/3} \qquad (8)$$

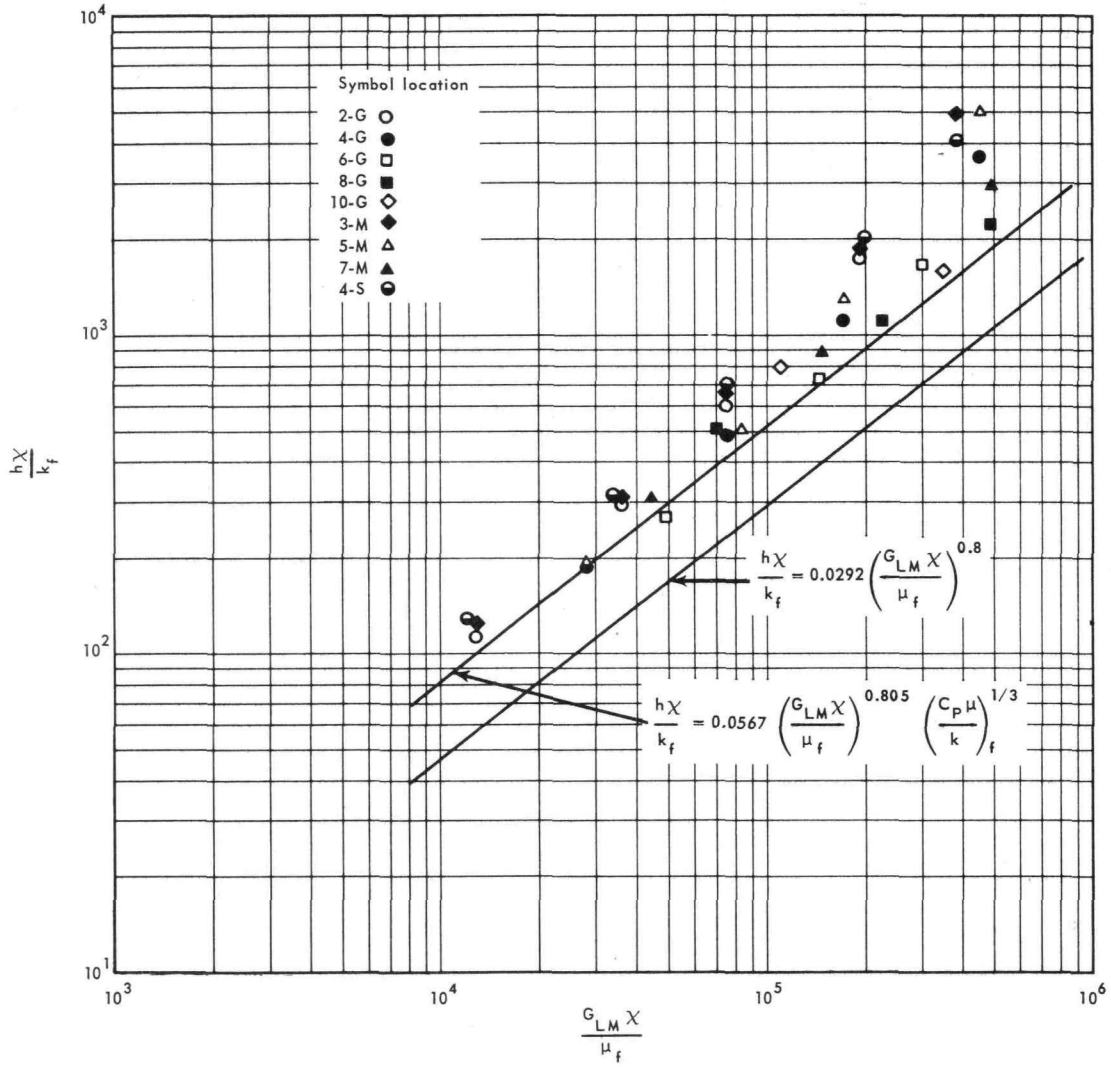

Fig. 3.14 – Correlation of heat transfer data for side plates of the XNJ140E-1 aft retainer assembly

The solution of the integral energy equation for turbulent flow parallel to flat plates, assuming constant wall temperature, is given by

$$\left(\frac{hx}{k_f}\right) = 0.0292\left(\frac{G_{LMx}}{\mu_f}\right)^{0.8} \qquad (9)$$

The solution is also shown in Figure 3.14. Thus it is seen that the added turbulence, effected by the tube bank, increases the local plate heat transfer coefficient by approximately 80 percent. In addition, there appears to be a strong entrance effect, particularly for high Reynolds numbers, which cannot be fully evaluated because the local mass velocity is not accurately known. It was planned, in phase three of the experimental program, to determine the mass velocity distribution and obtain a correlation which would more accurately represent local conditions. Phase three was not completed and the most useful results of the experiment as conducted are the design equations for predicting minimum heat transfer coefficients.

3.3 SHIELD AEROTHERMODYNAMICS

To maintain the integrity of a direct-air cycle reactor shield system, provision must be made for removal of the secondary heat generated within the shield. Passages are provided in the shield for guiding the primary reactor coolant flow before it enters the active core and after it passes through the active core.

Frequently, the extent of the shield (size, shape, and material) is considered to be largely a nuclear design problem, the integrity to be a mechanical design problem, and the ducting and cooling to be an aerothermodynamic design problem. However, because each of these areas is so closely related to the others, integration of all is necessary. It is the intent here to concentrate on those aspects affecting aerothermodynamic design.

Factors that govern the aerothermal design include such items as:

1. Maximum allowable size and weight of reactor and shield.
2. Maximum allowable quantity of secondary coolant to be utilized for dissipation of heat generated within the shield.
3. Maximum allowable pressure loss in the primary coolant while it passes through the shield and flows to and from the reactor fuel elements.
4. Maximum allowable deviation from specified flow distribution to the reactor fuel elements, to match inherent variations in core power; the basic requisite being to have the lowest possible perturbation in fuel element temperature above core average for a given core-exit coolant temperature.

For convenience, the shield has been divided into three general areas. These are the front shield, rear shield, and side shields. Sometimes the front and rear shields are referred to as the front and rear plugs. In most systems considered by GE-ANP, the reactor was a right cylinder contained within another hollow right cylinder called the pressure shell. Generally, the front and rear shields also had a right cylinder shape and fitted within the pressure shell. The pressure shell normally contained the whole assembly of front shield, reactor, and rear shield. The side shield, which is of a hollow right cylindrical shape, fitted over the pressure shell.

The earlier HTRE shielding systems (see APEX-904, 905, and 906) consisted of a number of tanks containing alternate layers of water and lead. The heat generated within the water and lead was dissipated by an auxiliary pump system which circulated the water through the shield tanks and then through a water cooler.

Later systems such as the XMA-1A (see APEX-907) and the XNJ140E-1 (see APEX-908) had air-cooled shields. The front and rear shields were cooled by either the primary air stream or by air bled from the primary air stream. The side shield was air-cooled by an independent auxiliary flow circuit.

3.3.1 Side Shields

In the thermodynamic design of side shield systems employing lithium hydride as the shielding material, prime emphasis was placed on efficient removal of internal heat with a minimum of coolant flow and pressure loss.

Acceptable temperature gradients and differentials throughout the side shield system must be maintained. Since the LiH is supported by metallic structure, and contained within metallic cladding, the temperature patterns existing within the LiH at steady-state operation strongly manifest themselves on the metallic components which are imbedded in, or in contact with the LiH. Since the heat energy must transverse thicknesses of LiH before being removed, an improper design resulting in a poor temperature distribution sets up thermal stresses which must be accommodated in the mechanical design. This was the major thermal restraint in the design of the XNJ140E-1 side shield, a lightweight metallic structure which employed minimum cladding thicknesses, and was capable of operation at 800° to 1000°F.

System transient operational effects must also be considered in side shield design. Nuclear starts and scrams can impose significant radial temperature differentials. At normal steady state operation heat generation rates at the inner radial regions are often 8 to 10 times higher than those at the outer radial regions. The steady state requirements, imposed by these conditions, must be met by designing for a much higher cooling capability at the inner radial region. This, coupled with the poor thermal conductivity of Lithium Hydride (2 to 4 BTU/hr-ft-°F) and the thermal inertia of the system, leads to a mismatch during the above mentioned transient operation. Thus, during a nuclear start, the inner regions will lead the outer regions in temperature level with time and a temperature difference builds up. A scram leads to a more rapid cooling of the inner radial regions, where the inherent cooling capacity is higher, and again a temperature difference builds up. Designing for high-temperature-level operation at steady state tends to aggravate this situation even more. One approach to this particular problem is to design for the steady-state high-temperature-level requirement using intermittent coolant flow to accommodate the critical transient operation.

The specifics of the various aspects of the system design will be discussed separately in the following paragraphs.

3.3.1.1 Side Shield Coolant Flow Passages - As previously mentioned, the HTRE series of power plants had independent water-cooling circuits for the side shields. The XMA-1A and XNJ140E-1 side systems, however, were to be air-cooled and the flow was to be provided by ram-air pressure during flight, and blowers during ground test operations. In each of the latter two systems, the objective was to minimize the amount of coolant flow and associated pressure loss without exceeding maximum prescribed temperature levels and temperature differentials. The basic difference in the cooling-flow designs of these two systems was that the XMA-1A used concentric-annulus flow passages while the XNJ140E-1 used tubes.

No flow tests were conducted on the XNJ140E-1 system prior to the time of contract termination. However, a test series was planned for evaluation of flow distribution through the array of cooling tubes in the XMA-1A design. The following is a summary of the more significant flow tests completed for the XMA-1A design.

Results of tests to determine circumferential flow distribution of the XMA-1A external side-shield entrance and exit plenums were published.[76] Cooling air to the XMA-1 side

shield was delivered by eight circular ducts. The coolant-flow spaces in the shield consisted of small annular shaped passages. The transition from the eight discrete circular ducts to the annular passages had to be accomplished in a manner to assure reasonably uniform circumferential flow distribution in the annular passages. A plenum was provided as a means of making the transition, and a series of tests of a 180-degree, 1/4-scale model of the top half of the shield were conducted to evaluate the plenum size requirements.

Two different size plenums were tested which could be distinguished from each other by considering the radial distance from the outer edge of the trunnion ring to the outer surface of the plenum. For the first plenum investigated, this distance was 7 inches (full scale) and for the second, it was 10 inches (full scale). Initial tests with the smaller of the two plenums resulted in excessive flow distortions opposite the piping inlets. Tests with the larger plenum did not have as much distortion. Subsequent testing was with the larger plenum and a range of simulated annular passage flow resistances. The larger entrance plenum, tested separately, incurred a flow perturbation of +4.5 percent to -4.8 percent. The larger exit plenum, tested separately, incurred a perturbation of +7.4 percent to -10 percent. If these effects were to be additive the total distortion would be a variation of the average weight flow from +11.9 percent to -14.8 percent.

An experimental evaluation of the pressure-loss, flow-distribution characteristics in the XMA-1A side-shield assembly was made.[77] Because of the uncertainties involved in predicting flow distributions and pressure losses in this system, cold flow tests were conducted on a 21.6 inch flattened sector of the borated steel portion of the side-shield assembly. The purpose of the testing was twofold:

1. To determine the over-all pressure drop characteristics of the model.
2. To determine the radial flow distribution among the several parallel cooling channels of the model.

A schematic diagram of the side-shield flow model is shown in Figure 3.15. Figure 3.16 shows a plot of the over-all pressure loss parameter as a function of weight flow through the model.

For any given value of pressure loss parameter, the experimental weight flow is approximately 15 percent greater than the predicted value. A flow of 1.7 pounds per second through the model is representative of the flow that could be expected in a similar flow sector of the shield system when the total flow for the entire shield system was approximately 45 pounds per second.

The radial flow distribution in the several parallel cooling channels of the model is shown in a plot of individual channel flow rate (Wc) versus total flow rate (Wt) in Figure 3.17. Table I gives a comparison of predicted and actual values for the flow distribution along with percent deviation in the two values.

The disagreement in the predicted and experimental values for Channel 3 and Channel 4 deserves some consideration. Measurements of channel dimensions were taken to compare the actual flow area of each channel with the design flow area. The measurements taken showed the height of Channel 4 to be 3.2 percent larger than the design value. In addition, Channel 3 was also slightly larger (1.5 percent) than the design specifications.

All other channels showed only slight differences in actual and design values. One possible reason for the differences existing in these particular channels was the difficulty in maintaining close tolerances on the struts which control the height of these channels.

The difference in actual and design dimensions of Channels 3 and 4 does not fully account for the difference in predicted and experimental values of the flow distribution. However, in the case of Channel 4, it does tend to compensate in the proper direction.

		PASSAGE WIDTH – SECTION C-C				
CHANNEL	HEIGHT	A	B	C	D	E
3	0.40	1.28	3.12	3.12	3.12	1.28
4	0.35	1.30	3.18	3.18	3.18	1.30
5	0.47	1.33	3.27	3.27	3.27	1.33

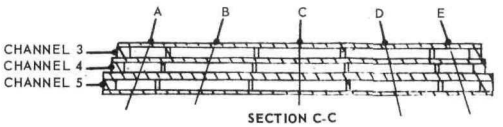

SECTION C-C

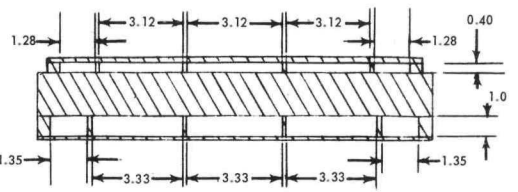

SECTION A-A

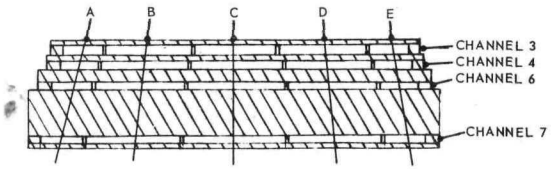

SECTION B-B

		PASSAGE WIDTH – SECTION B-B				
CHANNEL	HEIGHT	A	B	C	D	E
3	0.40	1.28	3.12	3.12	3.12	1.28
4	0.35	1.30	3.18	3.18	3.18	1.30
6	0.30	1.33	3.26	3.26	3.26	1.33
7	0.30	1.41	3.44	3.44	3.44	1.41

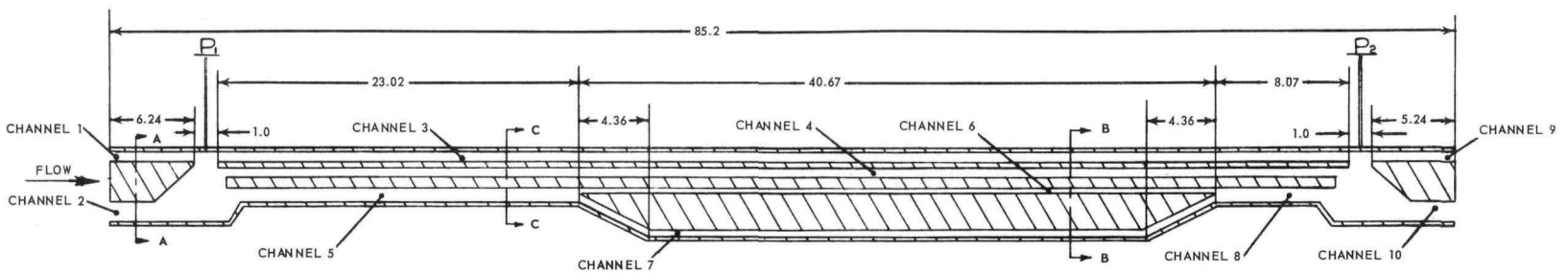

SIDE SHIELD MODEL

Fig. 3.15 – Schematic diagram of XMA-1A side shield flow model

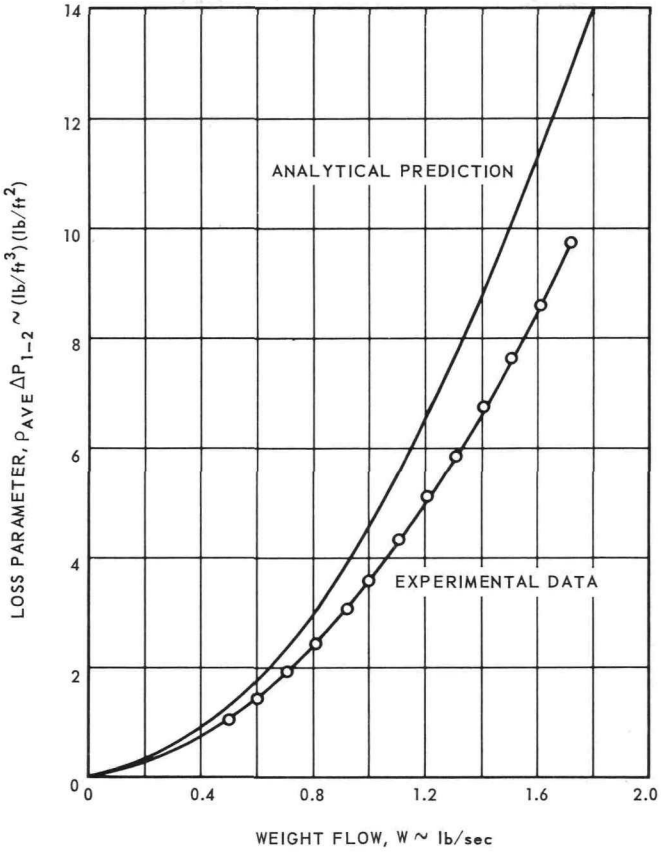

Fig. 3.16 – Pressure loss versus weight flow in XMA-1A side shield flow model

TABLE I

ANALYTICAL PREDICTIONS[a]

Channel	Total Flow (Wc) % (Actual)	(Predicted)	Deviation, % = (Actual - Predicted) x 100 / Actual
1	31.5	-	-
2	68.5	-	-
3	30	32.5	-7
4	32.3	27.6	+17
5	41	40	+2.5
6	20.6	20	+3.0
7	19	20	-5.0
8	41	40	+2.5
9	30	-	-
10	70	-	-

[a]Analytical predictions of flow distribution were based on the design dimensions shown in Figure 3.15.

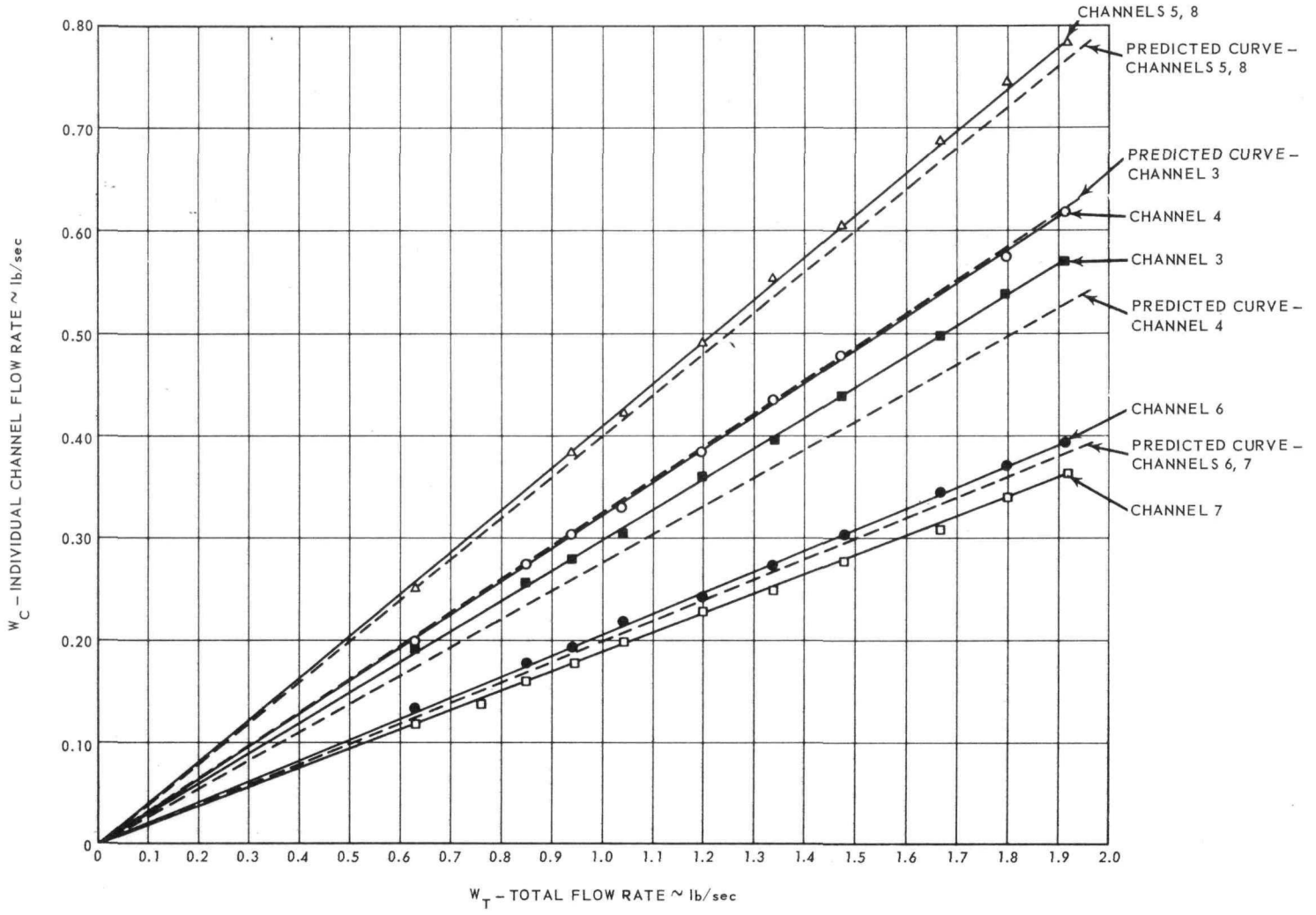

Fig. 3.17 – Individual channel flow rates versus total flow rate

The above emphasizes the importance of holding close tolerances on the channel dimension of the prototype assembly. It was estimated that a change of 0.003 inch in the height of some channels would cause a 1 percent change in the flow through that channel.

3.3.1.2 Methods for Estimating Side Shield Cooling Requirements - No significant system heat transfer tests were conducted on either the XMA-1A or the XNJ140E-1 shields. At the time of contract termination, however, there was a test series planned in which a typical shield sector of the XNJ140E-1 design was to be tested in a nuclear environment. Tests were made to evaluate the thermal conductivity of the lithium hydride shield material under various circumstances.

Heat transfer analyses of the XNJ140E-1 system were accomplished utilizing the "THT" and "Fantan" computer programs discussed in sections 1.4 and 1.6 respectively.

Heat transfer analyses of the XMA-1A shield system was accomplished through the utilization of a special computer program.[78, 79] This program gives the steady-state radial and longitudinal temperature variations and the radial heat fluxes in a system of nuclearly-heated, concentric, cylindrical shields using one-dimensional radial conductors. Axial discontinuities in the flow channels, varying the number of shields, and changes in shield thicknesses necessitate separate computer runs; any other variations in physical geometry are handled in consecutive stations with altered input.

A simplified method was used for the determination of the internal temperature distribution in solid rings for any shield geometry and for any heat-generation rate at the inner surface of the shielding.[80] In this method, the radial distribution of nuclear heating rate is approximated by an exponential expression which decays with increasing radius. Axial heat conduction was not considered.

3.3.2 End Shields

As previously discussed, the two major areas of aerothermodynamic concern are the passage of primary-coolant flow through the shield to the reactor and the removal of the nuclearly-generated heat in the shield. These are discussed in the following sections.

3.3.2.1 End Shield Primary Flow Passages - The objective of the primary flow passage of the front shield was to collect the flow forward of the front shield, duct it through or around the shield and suitably distribute it among the heated passages in the core.

Two basic passage configurations were utilized in GE-ANP systems. One was an annulus duct shape which was located near the outer perimeter of the front shield and the other was a "porous-plug" design. The porous-plug configuration provided many independent flow passages through the shield. Several variations of a porous-plug configuration were considered.

The rear-shield primary flow passages also have been of the annular duct and porous-plug type of design. Their function is to collect the flow as it leaves the reactor, duct it through or around the rear shield, and finally deliver it to the turbine. In both annular ducts or porous-plug ducts, diffusers must be employed to slow down the flow before it enters the core.

The results of an analytical and experimental study of two dimensional diffusers were published.[81] The analytical results are based on estimated diffuser-transition losses and are presented in terms of thrust-to-weight ratio for a range of diffuser length and area ratios. Diffuser efficiency and total head losses determined experimentally for several configurations and modifications are presented and related to velocity-head distribution in the diffuser.

One of the earlier experimental appraisals of annular duct flow characteristics analyzed the results of a 1/4-scale model test of the Core Test Facility No. 1 (CTF No. 1) ducting

and core in several different configurations to determine pressure drop and flow distribution characteristics.[82] The test covered evaluation of exit-torus performance, both with and without turning elbows, for various arrangements of elbows and with round or square exit ducts from the torus, and for both one- and two-engine air flow conditions. A sketch of the system tested is presented in 3.4.2.2.

The results of the tests showed no indication of pressure loss or flow distribution which would have detrimental effects on the operation of the CTF in HTRE No. 1 system.

The results of flow tests on an offset-reactor design configuration which comprised a flow geometry necessitating an annular-compressor discharge air flow passage between the shield and the reflector were published.[83, 84] A schematic of the test rig is shown in Figure 3.18. The air flow had to be turned toward the reactor centerline and directed toward the core face. Aerodynamically-controlled turning of this airflow through 180 degrees, and near-uniform radial and circumferential flow distribution were the objectives. In order to facilitate power plant design, by eliminating a radial bulge in the turning region, cylindrical pressure shells were maintained at the inner and outer diameter of this annular passage.

Three configurations were tested. The first configuration had three annular turning vanes and an annular ring. The second had only one vane (adjacent to the annular ring) and the annular ring; the third had no vanes. In each of these configurations, the axial spacing of the header contour with respect to the plane of the simulated core inlet was not changed. Therefore, in each case the header volume increased from configuration one through three, by the volume formerly occupied by the vanes.

The conclusions reached as a result of this testing were:

1. It is feasible to use an annular-vaned turning region to direct the airflow from an annular passage between the reflector and shield into the reactor core face. It is also possible to use a turning passage without vanes with some sacrifice in reactor flow distribution.
2. The total pressure loss from the annulus to a station inside the tube bundle for the three-vaned configuration was found to be on the order of 1 percent of the inlet pressure, one annulus dynamic pressure, or 0.8 of tube bundle dynamic pressure. For the configuration using the one vane, the total pressure drop was found to be on the order of 0.9 percent of the inlet pressure, 0.8 of annulus dynamic pressure, or 0.7 of tube bundle dynamic pressure. In the configuration with no vanes the values were 0.7, 0.8, and 0.7 respectively.
3. The flow distribution through the simulated reactor core was within a range of 2 percent for the first configuration, 2.5 percent for second, and 3 percent for the third.

The results of an experimental investigation using air at ambient temperature to determine the aerodynamic characteristics of an approximate 1/4-scale model of the HTRE No. 3 reactor shield assembly were published.[85] A schematic of the test configuration is shown in Figure 3.19.

A combination of front-plug and rear-plug geometries were developed that produced a reactor flow distribution within ±2.5 percent of being constant in a radial direction. No circumferential variations in reactor flow are noted which could be attributed to the front-plug inlet scroll with either one- or two-engine operation.

The results of a series of experimental flow tests of a model of the XNJ140E-1 configuration are shown in Figure 3.20. The objectives of this test series were to establish the basic geometry of header and collector shapes necessary to obtain an acceptable uniform flow distribution within the simulated reactor in both radial and circumferential directions, while sustaining the minimum loss in total pressure.[86]

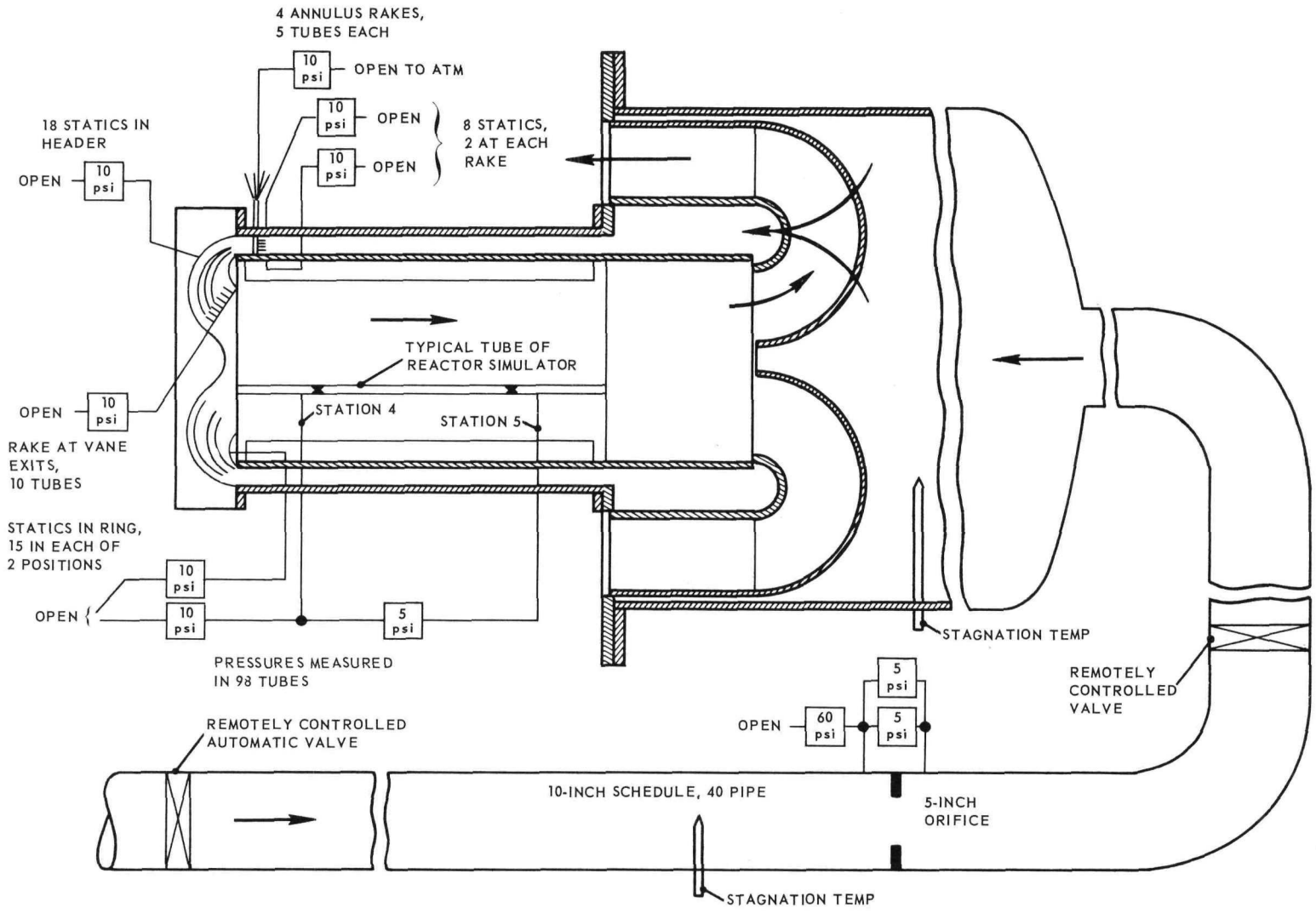

Fig. 3.18 – Schematic diagram of airflow circuit

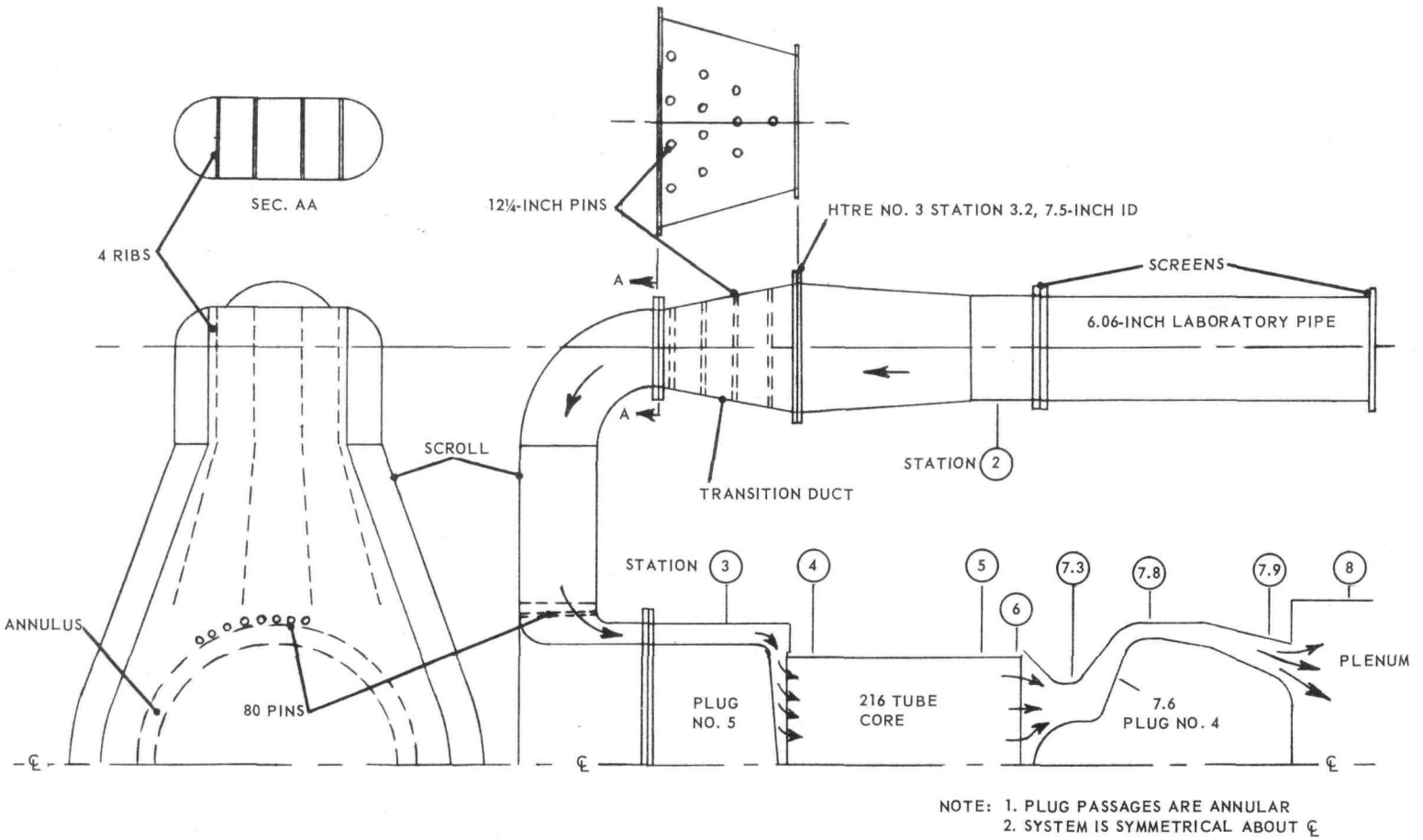

Fig. 3.19 – Sketch of complete 1/4-scale scroll-shield-tube bundle mockup for experimental aerodynamic performance investigation

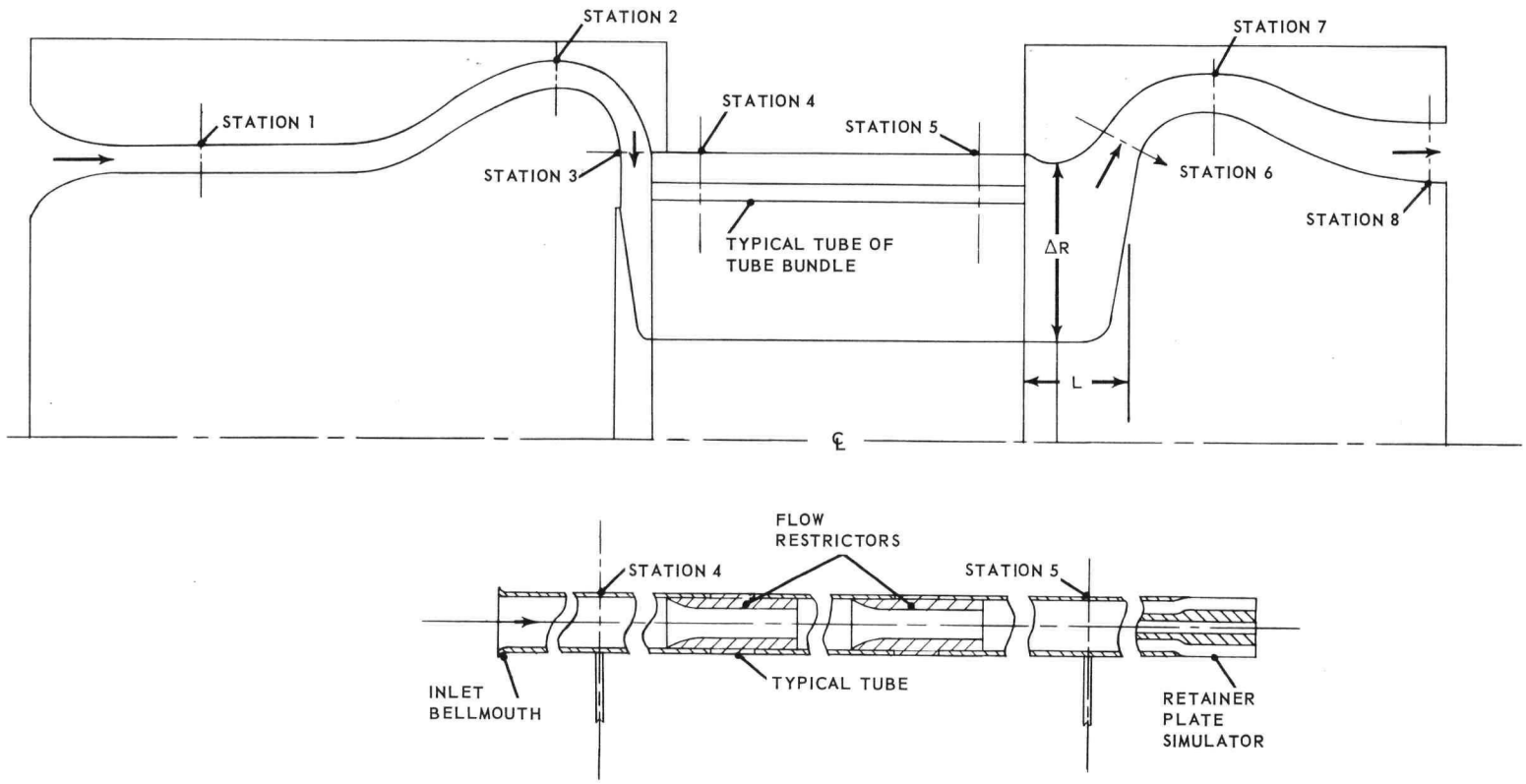

Fig. 3.20 – Flow mockup of XNJ140E-1 primary duct passage

The conclusions from this test were:

1. The results of these tests indicated that for each header design there is a particular collector shape which results in uniform flow distribution for the tube bundle. Such combinations are:

A_3/A_1	$L/\Delta R$
.96	.4
1.21	.5
1.51	.6

   The area ratio (A_3/A_1) is defined as the ratio of the inlet header area to the referenced annulus area at the model entrance. The spacing ($L/\Delta R$) is defined as the mean axial spacing of the rear collector from the exit plane of the tube bundle divided by the difference between the outer and inner radii of the tube bundle.
2. The total pressure loss from station one (the inlet station of the test model) to station four (the station forward of the two restrictors in the tube bundle) is a function of the inlet header geometry. The prescribed design total pressure ratio was achieved for an A_3/A_1 of 1.21. A slight improvement in performance is obtained for the largest value of A_3/A_1, while lower values of A_3/A_1 cause significant reductions in the resultant total pressure recovery. Station designations of the test model are identified by Figure 3.20.
3. The annular front duct basic pressure loss due to friction, diffusion, and turning, from station one to station three (the header inlet) is quite small since P_{t3}/P_{t1} is approximately 0.985 at the design Mach number. A non-clean configuration, with irregularities such as struts and guide tubes, will cause this pressure ratio (P_{t3}/P_{t1}) to be on the order of 0.975.
4. The entry loss from the header to station four is significantly higher because the flow is approaching the tube bundle at an angle. For the design configuration, the pressure ratio (P_{t4}/P_{t3}) is equal to 0.975. By comparison, a zero angle of approach has resulted in an equivalent value for P_{t4}/P_{t3} of 0.995.
5. The flow distribution for the tube bundle is not a function of the Mach number at station one. The flow distribution for each hexagonal row remains essentially constant regardless of the inlet Mach number for any given configuration.
6. The pressure taps on the rear face of the tube bundle did not act as static pressure taps. Because of the ejector action, these ten taps read significantly lower pressure than the actual static pressure. Computations involving the tube bundle exit-plane reference area, weight flow, total temperature, and use of a static pressure consisting of an arithmetic average of the ten pressures, resulted in computed values for flow function, Mach number and total pressure. This computed value of total pressure was significantly lower than that at station six; hence, the pressures obtained experimentally must be lower than the static pressures existent at this station and the data serves only as an indication of the base drag of the tube bundle.
7. Simulated flow extraction from the front-duct outer annulus in amounts from zero to twenty percent of the system flow had negligible effects on flow distribution. Similar results were obtained for flow injection into the inner annulus of the rear collector using zero to six percent injection rates.
8. Test configuration runs with the simulation of a compressor discharge swirl-angle of 30 degrees and 10 degrees were run. A swirl-angle of 30 degrees provided an unacceptable flow distribution while a 10 degree swirl-angle caused hardly any significant changes in flow distribution.

An experimental study of airflow through a duct containing staggered rows of streamline struts was conducted.[87] (This study is discussed in section 5.2.)

A comparison was made of the experimentally determined airflow characteristics through porous plugs whose air channels are composed of either serpentine ducts or biconvex struts.[88] The conclusions from this comparison were:

1. The serpentine duct, through all ranges of void volume fraction considered, has a lower over-all pressure loss ratio than does the biconvex strut duct.
2. The flow distribution of the biconvex strut exit is better than that of the serpentine duct. Louvers are mandatory if the serpentine duct stream is to be made uniform across the diffuser mouth. By using louvers to direct the air stream, there will be additional losses in total pressure.
3. The serpentine duct has less tendency to choke. For void volume fractions below 0.375 the biconvex strut ducts showed a tendency to choke at design point flow. There is a decided penalty paid by the flow through the biconvex struts due to contraction and expansion losses. This condition could be at least partially alleviated if the biconvex struts were designed so that a constant flow cross section was maintained throughout the strut array.

An experimental study was made to determine the pressure drop across a 1/4-scale model of the front serpentine porous plug of the XMA-1 power plant.[89] These results were achieved in the first phase of a program designed to determine the aerodynamic characteristics of the XMA-1 power plant from compressor-exit to turbine-inlet. Figure 3.21 shows a cross section of the configuration tested. As a result of this testing, it was concluded that:

1. The pressure loss for the proposed front plug was well within the design objective (a test pressure ratio of 0.981 versus the design objective value of 0.975). Little additional improvement could be expected; i.e., the internal loss is not much larger than smooth-pipe loss, and possible diffuser improvement would not decrease over-all loss by more than about 10 percent.
2. The relatively large variations in diffuser transverse-exit velocity profile may pose a serious tube-bundle flow-distribution problem.

The results of additional experimental investigations made to determine the aerodynamic characteristics of a serpentine duct and of a diffuser at the exit of the duct were published.[90] Figure 3.22 is a sketch of the duct tested. As the wave lengths of the wiggles in the passages were not constant with passage length, air was introduced at one end and then at the other end by reversing the duct in the test rig to determine the effect of flow direction in the duct.

Results of the testing showed that in general the static-pressure readings taken at the top and bottom walls of a particular station in the duct did not agree. These differences were caused by the centrifugal effects of the air flowing through the wiggly duct. Figure 3.23 illustrates these differences by showing the variation of $\left(\frac{p_p - p_s}{p_p}\right)(100)$ with distance where p_p is the plenum pressure and p_s is the static pressure measured at either the top wall or the bottom wall. Total pressure traverses were taken at the various stations along the duct and these readings were used to plot total pressure profiles, which are shown in Figures 3.24 and 3.25. The side-wall values came from wall static-pressure readings at those stations. In interpreting the above figures, the serpentine passage was called a front duct when air was emitted from the compact wiggle end, and visa versa.

In addition to the above pressure surveys, data was obtained on effective friction factor and total pressure loss coefficient.[90]

The results of a series of cold-flow tests of a single-passage serpentine duct made to determine the effects of wall fabrication irregularities on pressure loss were reported.[91] Six distinct tests were made with walls having roughness of varying degree and type in

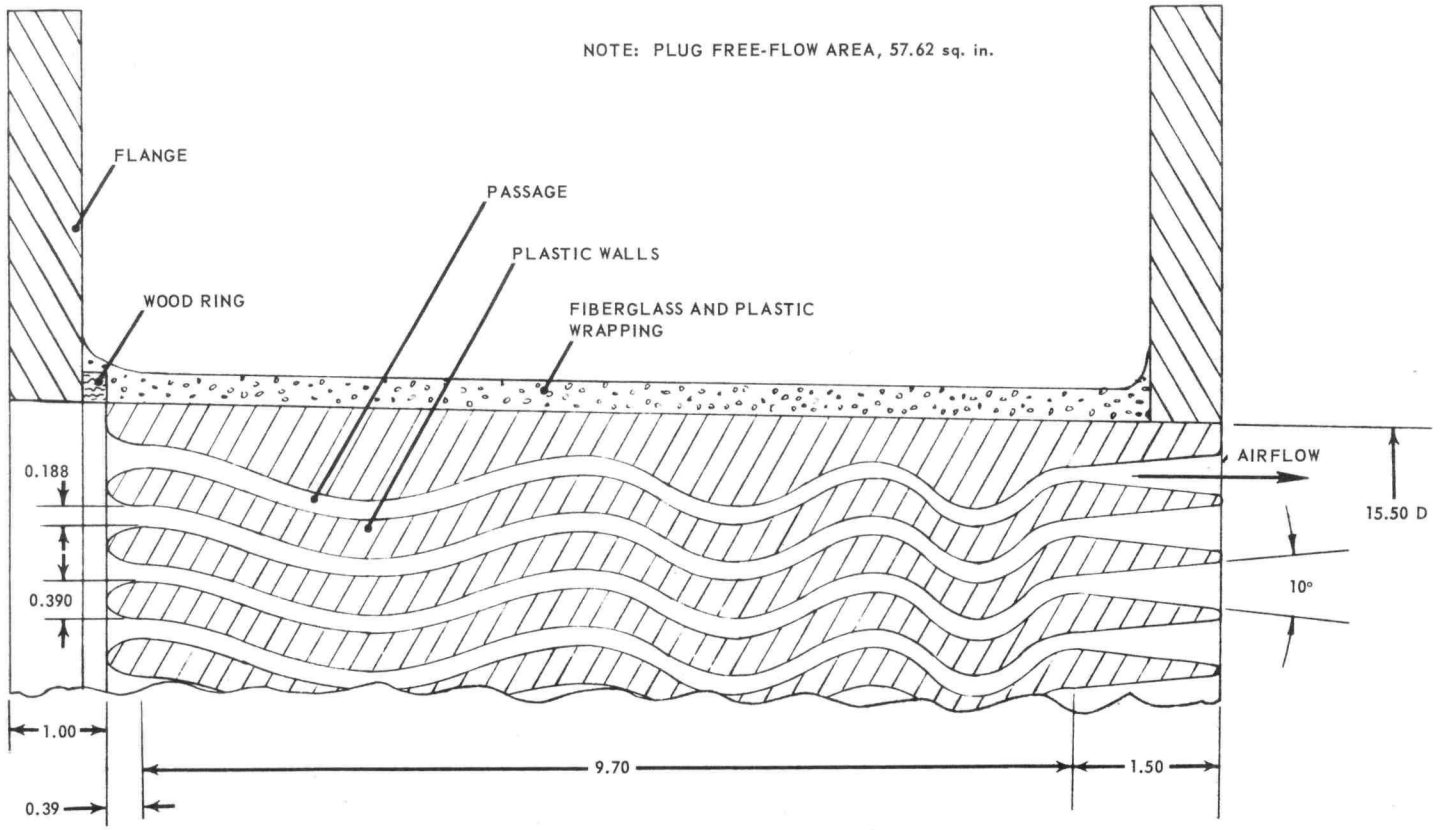

Fig. 3.21 – Horizontal section through front porous plug. View from top.
1/4-scale XMA-1 powerplant

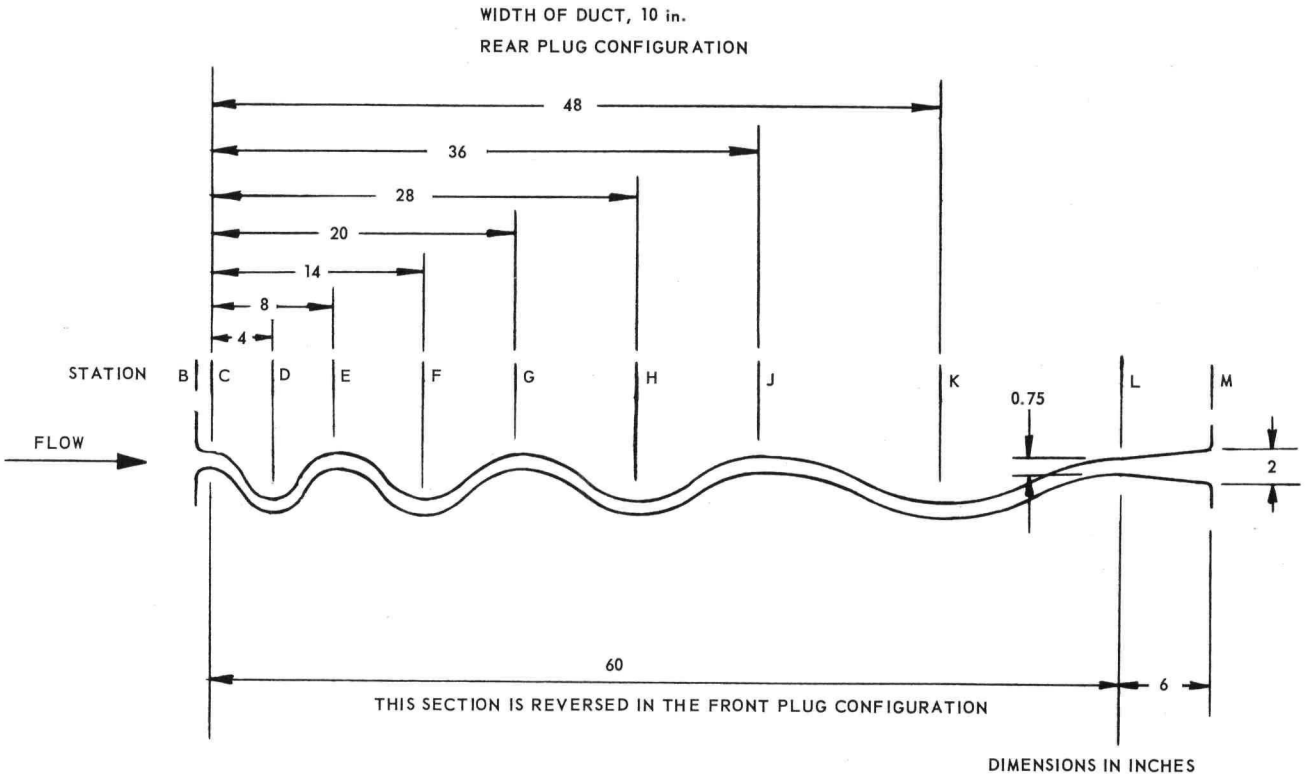

Fig. 3.22 – Serpentine duct

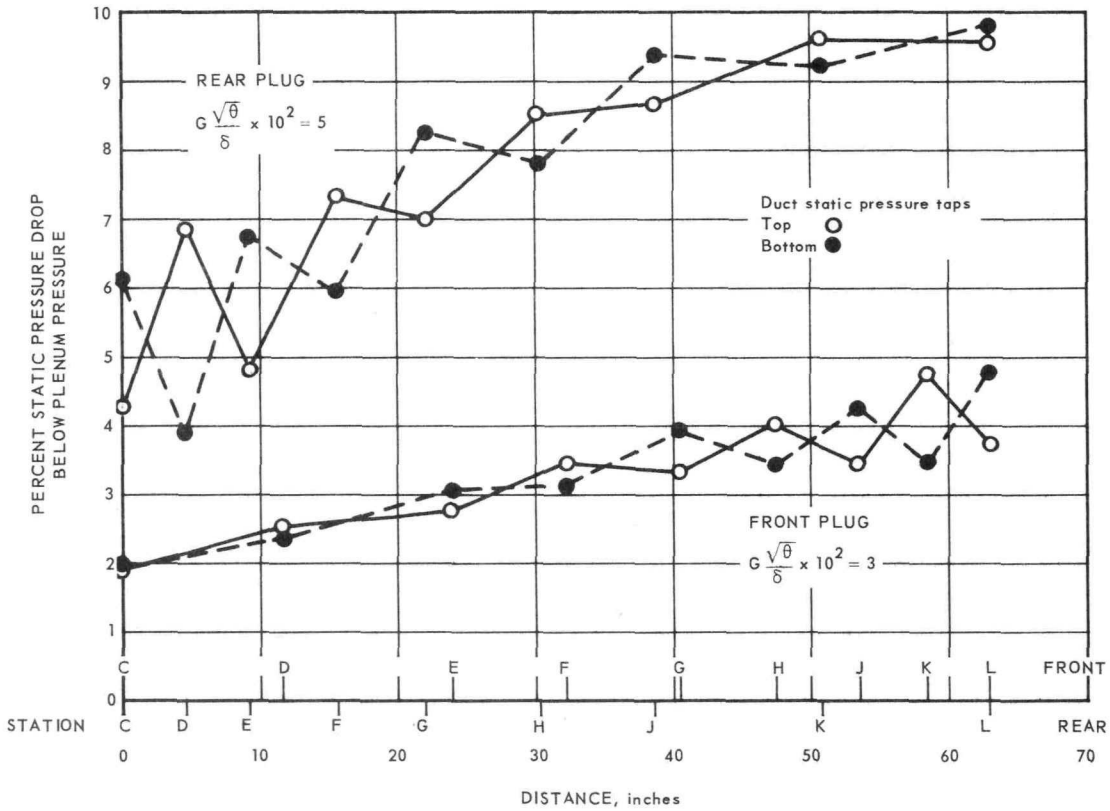

Fig. 3.23 – Variation of wall pressure within serpentine duct

order to determine the relative effect of roughness on the friction factor. These results indicated the friction factor may increase depending on surface condition, from 10 percent to 110 percent (constant hydraulic diameter) over that of a passage having smooth walls. However, it is expected that the increase in friction factor, over the smooth-wall passage, will be 10 to 30 percent for the actual component.

An experimental study was made to determine the pressure drop and flow distribution in a portion (from compressor discharge annuli through the reactor) of a 1/4-scale model of the XMA-1 power plant.[92] A sketch of the model tested is shown in Figure 3.26. The results of the testing showed that the distribution of total pressure at station 11 was uniform both radially and circumferentially in either annular gap. Variation in total pressure at station 11 between the left and right annuli amounted to only 3 percent of the average dynamic pressure. In addition, the experimental results indicated that the loss in total pressure from stations 11 to 31 was about 0.5 the dynamic pressure at station 11. The loss in total pressure from stations 31 to 51 was about 0.9 the dynamic pressure at station 31.

To investigate the possibilities of improving the velocity profile at the diffuser exit of a prototype front serpentine porous plug for the XMA-1 power plant, a series of tests were performed.[93] In the preliminary study of a porous serpentine plug for the XMA-1A power plant,[90] there was a nonuniform velocity profile at the diffuser exit of a single-passsge full-scale model used in that investigation. As it is possible that the adverse velocity profile could have a detrimental effect on the flow distribution in the reactor core, as well as on the pressure loss, this test series was made in an attempt to improve the performance of the diffuser.

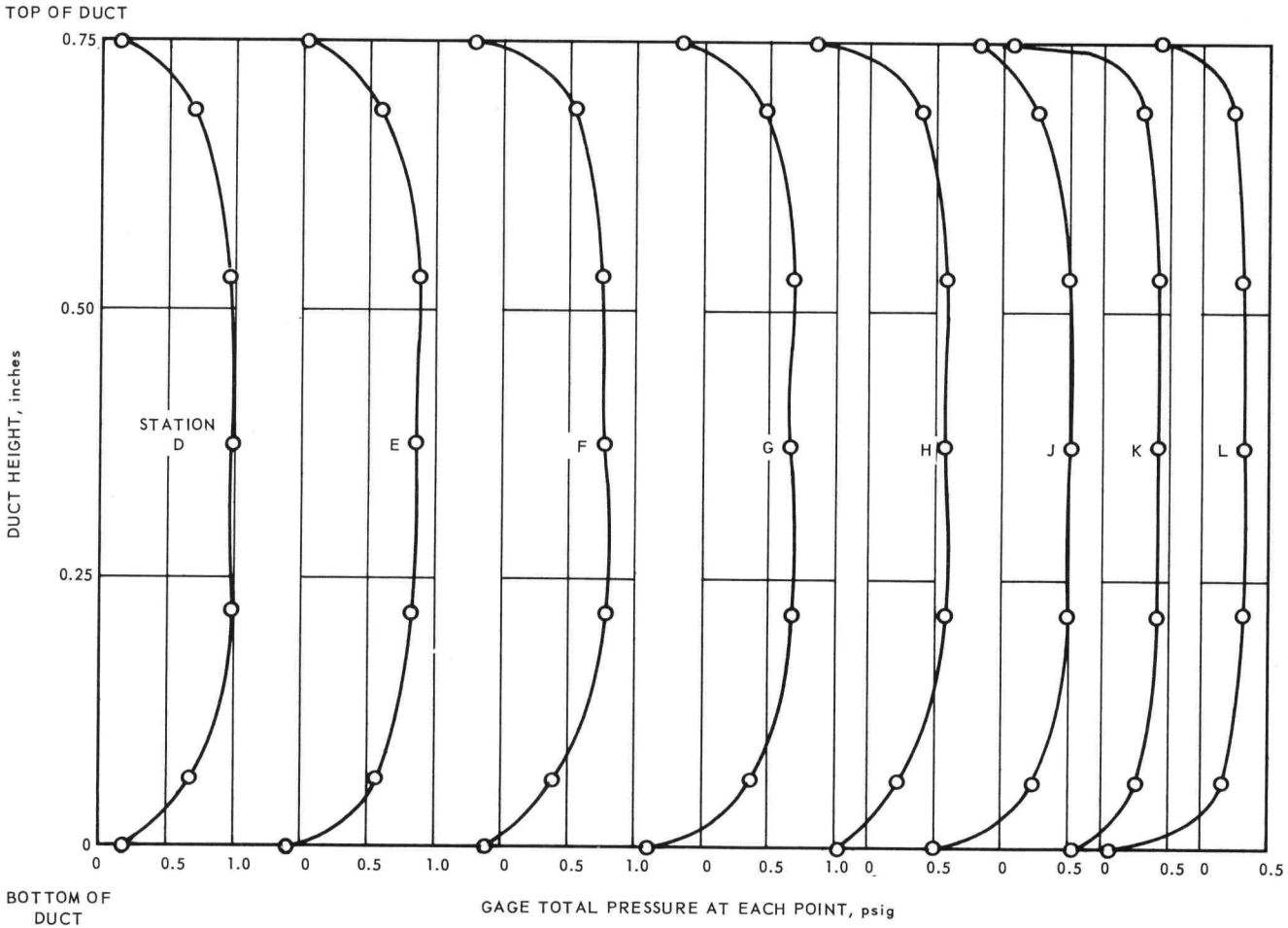

Fig. 3.24 – Front serpentine duct – gage total pressure profiles

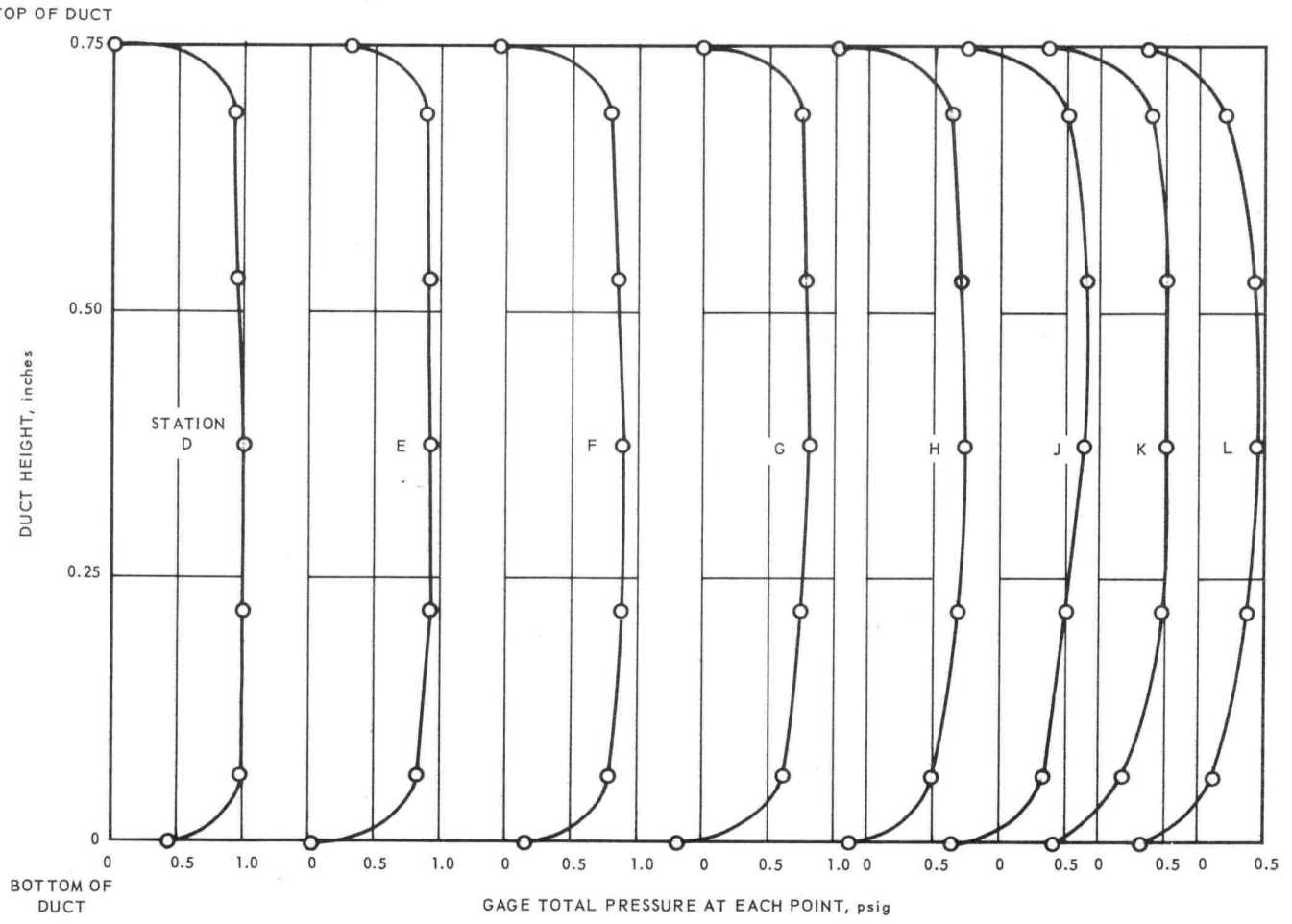

Fig. 3.25 – Rear serpentine duct – gage total pressure profiles

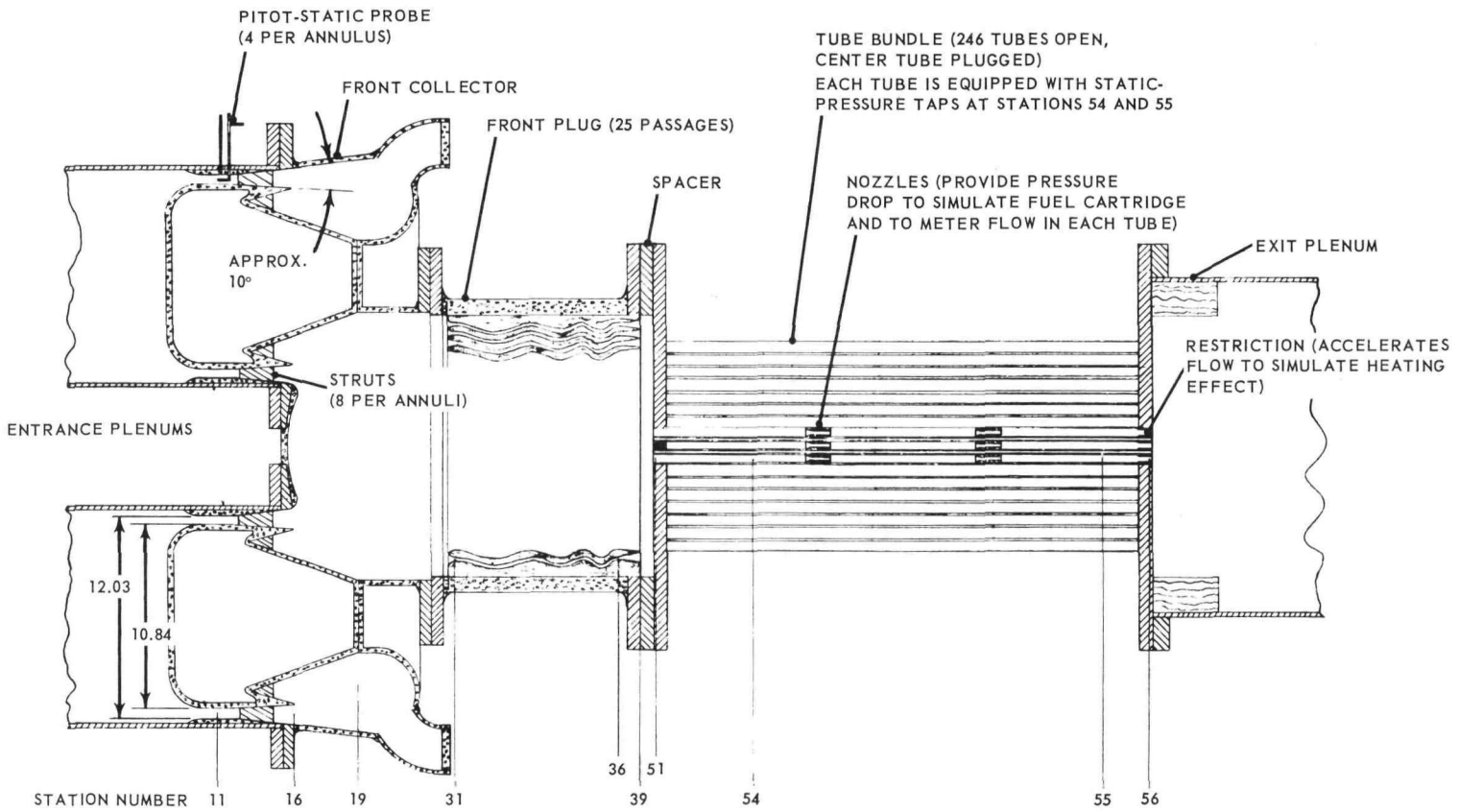

Fig. 3.26 – Sketch of front end of XMA-1 power plant – quarter-scale model

The results of this test were:

1. A friction factor of the order of 0.005 could be expected at the design condition; there was a definite Mach number effect on the value of friction factor.
2. No solution was found to correct the nonuniform velocity profile at the diffuser exit without increasing the total pressure loss or channeling the flow in a direction other than parallel to the reactor core centerline. Diffuser angles between 0 degree and 20 degrees were tested. Several were inclined at angles of 5 degrees, 10 degrees, and 15 degrees. Other geometries using such schemes as splinters or combinations of straight sections preceding the diffuser were investigated.

Results of flow tests on a 1/4-scale XMA-1 model to determine effect of orientation of front and rear plugs with respect to pressure losses and core weight flow were published.[94] The conclusions were that the orientation (horizontal versus vertical wavy walls) of the front and rear plugs has little or no effect on pressure losses, and that the addition of swirl in the compressor discharge annulus also did not affect pressure losses.

The results of experimental tests conducted to determine the component and over-all pressure losses associated with the 1/4-scale XMA-1A primary airflow model were reported.[95] In addition to pressure losses, core mass-velocity ratio distribution effects were determined with a basic dual-engine system, a single-engine system, and a simulated failure of the front shield bypass valve.

The percentage of total pressure loss from compressor discharge annulus to core simulator inlet was found to be 7.7 percent, which is within the design objective of 9.7 percent. This loss is lower than expected because the performance of the compressor exhaust collector was better than anticipated. The experimental rear-end ducting losses from rear-plug inlet to the turbine inlet annulus is 7.5 percent. The design objective is 7.7 percent. The over-all result is in good agreement but the individual component losses differed somewhat from the desired objective.

An additional experimental determination of the aerodynamic characteristics of two proposed front-shield plugs for the XMA-1A system was reported.[96] This study presents the results of cold-airflow test on a single passage of two configurations of the XMA-1A front-shield plug. The difference in the model configurations is in the type of diffuser at the discharge end; one was a "strut" type as shown in Figure 3.27 and the other was a "wide-angle" diffuser and is shown in Figure 3.28.

The conclusions reached from the experimentation were:

1. The over-all pressure drop for the wide-angle diffuser front-shield plug was less than that for the strut diffuser configuration.
2. Asymmetric flow existed in the strut diffuser and appears to be chaotically turbulent and pulsating.
3. There was more airflow in the top passage of the strut diffuser than in the bottom passage.
4. The boundary layer separated from the divergent walls of the strut diffuser and the flow surfaces of the strut.
5. In the strut-diffuser configuration, a large amount of reverse flow occurred near the parallel side walls in the top passage of the diffuser.
6. The wide-angle diffuser configuration gives better performance aerodynamically and is easier to fabricate.

An experimental investigation of the aerodynamic performance of a wavy duct was reported.[97] The wavy duct tested consisted of a rectangular cross-sectional passage with an aspect ratio of 20.5:1 and having five successively reversed 60 degree bends. Results

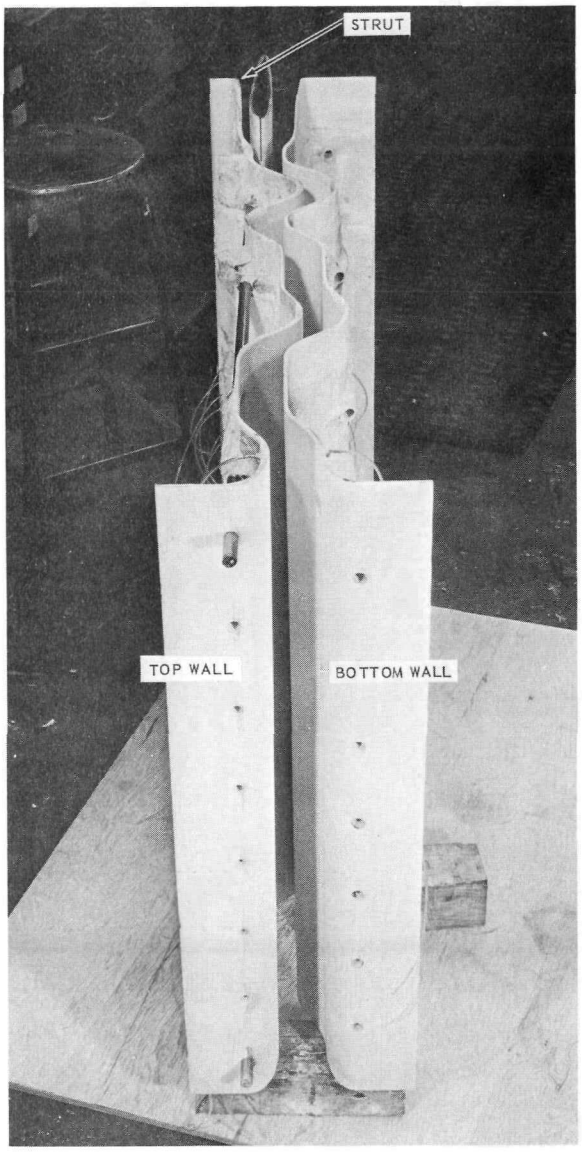

Fig. 3.27 – Full scale front plug with "strut" diffuser, XMA-1A power plant

cover a 0.9 x 10^5 to 3.4 x 10^5 Reynolds number range and a 0 to 0.48 Mach number range. For this particular configuration, the effective friction factor was about 1.7 times that for turbulent flow in a smooth tube.

The results of testing a single-passage model of a rod and tube sheet design of the front shield in order to determine over-all pressure loss and discharge flow distribution were published.[98] The total pressure loss characteristics for this particular configuration, a schematic of which is shown in Figure 3.29, were found to be less than those incurred by the previously tested 1/4-scale serpentine passage, with no apparent Mach number effects over the range of Reynolds numbers tested. The flow distribution at the passage exit was fairly uniform, the maximum variation in total pressure being approximately 0.5 percent.

The loss characteristics for a helical passage consisting of approximately 1-1/3 turns of 2.68-inch diameter pipe on a 6-inch mandrel were experimentally determined.[99] The results cover a range of Reynolds numbers from 10^5 to 7.5 x 10^5 and Mach numbers up to

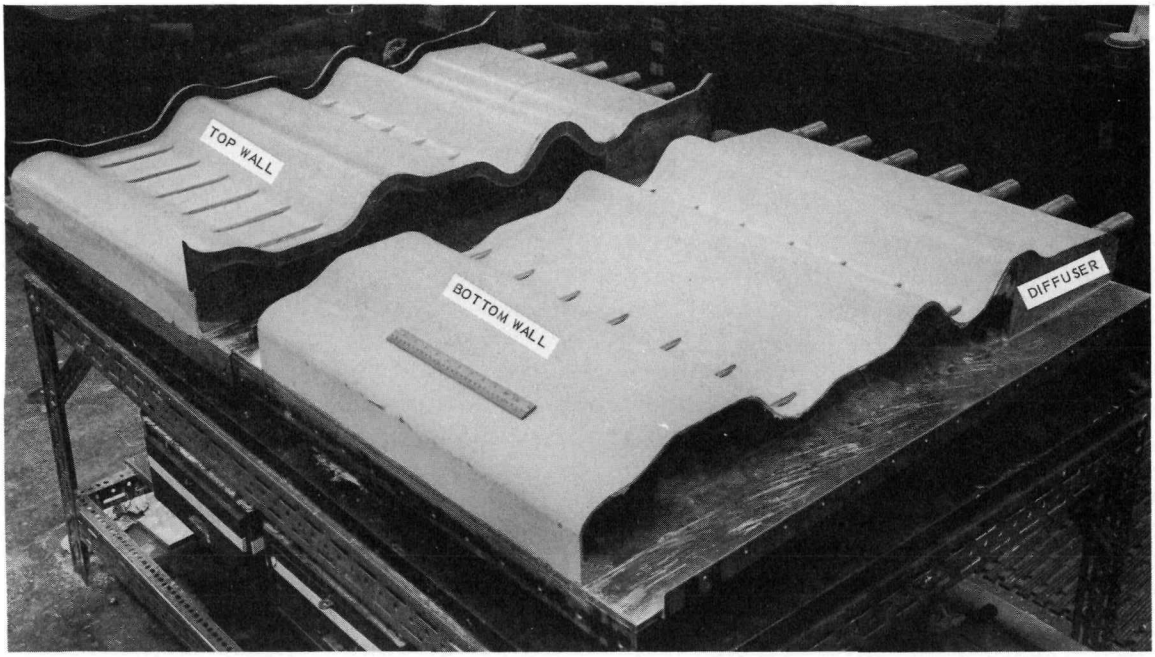

Fig. 3.28 – Full scale front plug "wide angle" diffuser, XMA-1A power plant

choke. Friction factors remained within the limits of 0.006 to 0.008 for all test conditions and are more dependent on Mach number than Reynolds number.

3.3.2.2 End Shield Cooling Technology - As previously mentioned, the HTRE series of power plants had an independent auxiliary cooling system for the shields, and there were no gross-shield cooling requirements for the primary system. The XMA-1A and XNJ140E-1 systems, however, were air-cooled by the system air flow. The method of cooling the end shields differed in these systems: the XMA-1A utilized porous-plug design and the XNJ140E-1 an annular-duct design.

In the XMA-1A, the primary airflow passed through the end shields in many parallel flow passages and in this process provided the cooling to the shielding material. No cooling tests were conducted of this configuration and heat transfer analyses were made using the "THT" computer program discussed in section 1.4.

In the XNJ140E-1 design, the primary air flowed around the outer circumference of the bulk of the end shields in an annular duct; cooling of the end shields was accomplished by bleeding small quantities of flow from the primary stream. These small quantities flowed through slots in the end shields and later were discharged back into the primary stream. Several cold-flow tests were made to evaluate the amounts and distribution of the bleed flow. No heat transfer tests were made and heat transfer analyses were performed through utilization of the "THT" and "Fantan" computer programs discussed in sections 1.4 and 1.6 respectively.

The following paragraphs summarize the more significant work accomplished:

Results of tests performed on a 1.5-scale quarter-sector model of a typical radial-cooling slot in the XNJ140E-1 front plug were published.[100] The rig was built and tested at the Aeronautics Laboratory of the United States Naval Post-Graduate School. The object of these tests was to determine pressure drop and related characteristics for this slot, especially characteristics associated with obstructions provided by control rod housings and tie-rod housings-spacer plugs. The proper shape of the slot exit, designed to

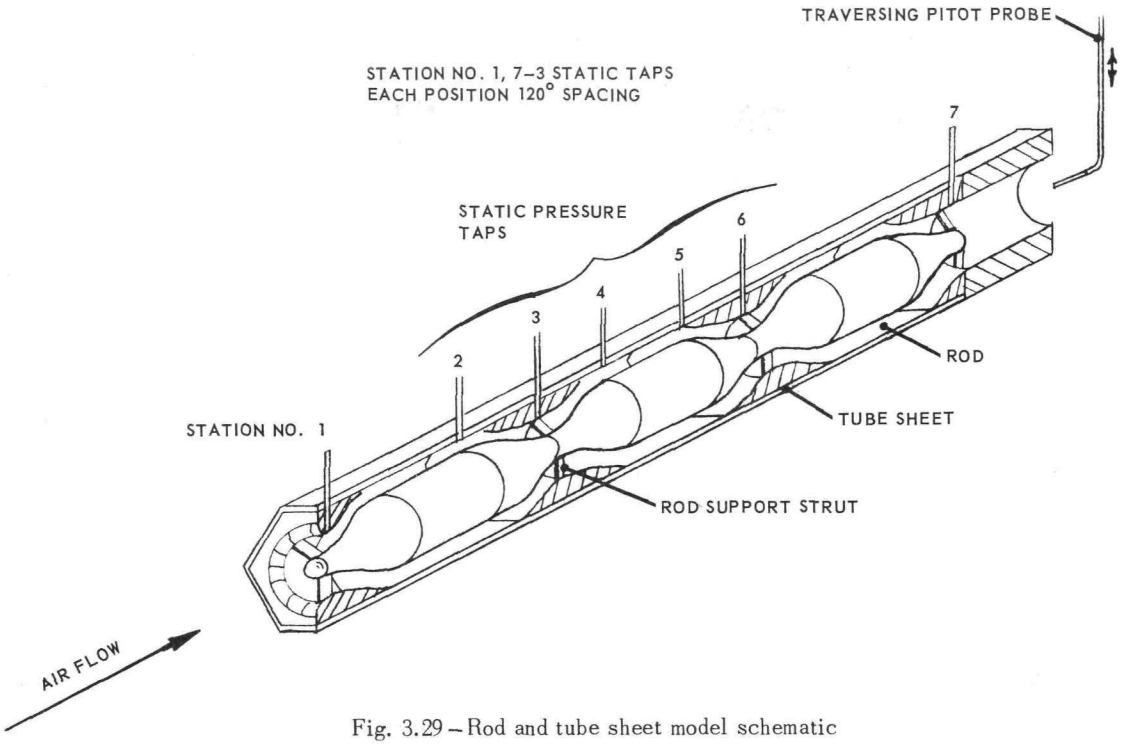

Fig. 3.29 – Rod and tube sheet model schematic

simulate dumping into a narrow collector annulus, was also investigated. The tests were run at two principal operating conditions. The first of these gave the full-scale design exit Mach number, $M_E = 0.12$, but lower-than-design Reynolds number, while the second gave full-scale design Reynolds number at greater-than-design Mach number.

The principal results of these tests were as follows:

1. The friction-pressure drop through the unobstructed slot is significantly less than that computed from one-dimensional friction-drop concepts. This would indicate that there may be a fundamental difference in the type of radial flow involved.
2. A Reynolds number effect greater than indicated from one-dimensional concepts was observed, causing a reduction in pressure drop with increased Reynolds number between the two operating conditions listed above.
3. The control rod housings and spacer blocks caused pressure drop to increase approximately 30 percent when the slot gap width was held constant. This increase was caused in the main by the large blockage of the control rod housings.
4. This increased loss due to obstructions was almost completely eliminated by enlarging the flow passage to produce constant flow area around the control rod housings.
5. With the above area enlargement, the wake behind the inner ring of spacers was the principal residual effect of the obstructions.
6. Streamlining the obstructions had no noticeable effect except to reduce the width of the wake from the inner row of spacers.
7. The best slot-exit baffle configuration consisted of rounding off the inner edge of the exit turn to 1/8-inch radius; i. e., a radius equal to one slot width, and using it as an unfilleted baffle equal in length, or overhang, to twice the slot width (the slot width in the model was approximately 1/8 inch).
8. Longer baffles and/or the use of fillets or other inner radii in the turn tended to increase the pressure drop.
9. At the highest Reynolds number practicable for these tests (the second operating condition listed above), the complete pressure drop for a feasible full-scale con-

figuration including obstructions, measured from the upstream plenum to the total pressure at the baffled exit, was approximately 70 percent of exit dynamic pressure. This is less than the pure friction effect computed by one dimensional concepts for the unobstructed slot with unbaffled exit.

It should be noted that these tests occurred in the neighborhood of a critical Reynolds number range for the clear slot. At the lower of the two operating conditions listed above, there were high-energy streams down the extreme edges of the 90 degree sector with no obstructions in the slot. This streaming did not occur when there were obstructions in the slot nor in the clear slot at higher Reynolds number. The streaming effect has not been satisfactorily explained but does not seem to be involved in the conclusions reached above.

In order to evaluate heat transfer performance in shields with a greater accuracy, additional information was needed on the effective thermal conductivity of "canned" lithium hydride used as the shielding material. As a consequence, a series of tests were performed to determine the conductivity of several different canned geometries as a function of operating temperatures.[101-104]

3.4 REACTOR COOLANT FLOW DISTRIBUTION

3.4.1 Analytical Techniques

Component flow distributions for systems of combined parallel and series flow circuits may be calculated from analysis of flow passage loss characteristics; i.e., bend losses, effect of contractions and expansions, direct friction, etc. These loss characteristics can be used with a computer program such as the Compressible Flow Network Program to evaluate the whole situation, resulting in flow distribution and pressure drop predictions. (For a description of the Compressible Flow Network Program, see section 1.7.) Typical component loss characteristics were published.[105,106]

Potential flow analysis appears well-suited for calculating the flow distribution associated with multi-channel flow into or out of a header; i.e., the effects on reactor core distribution as affected by inlet and discharge headers. A potential flow-analysis procedure and its associated computer program was published.[107]

A variation of this header distribution problem is encountered in a folded-flow system, in which flow enters a header, is turned approximately 90 degrees in the header before entering a high resistance bed, and then is turned another 90 degrees into a discharge header. A method of analysis applicable to the discharge header of this situation is given in the 90° Isothermal Folded Flow program discussion (see section 1.5).

3.4.2 Scale Model Tests of Flow Distribution

3.4.2.1 Fluid-Flow Investigations for the R-1 Reactor System - Aerodynamic characteristics of the R-1 reactor-shield primary flow path were investigated to determine if the main line of design was adequate from the flow distribution standpoint, and to determine suitable alternate arrangements necessary to correct components which were deficient. It was decided through consultation with fluid-flow authorities that simulation of Mach number would be the most important criterion in an experimental investigation, and that Reynolds number would be of lesser importance as long as the model values were maintained in the 3×10^5 or greater range. The Reynolds number of the prototype-duct flow passages would be considerably higher, but the effects of Reynolds number above 3×10^5 for this parameter were believed small. It was further decided that the flow investigation would be carried out on a 1/4-scale model in isothermal flow, and that the testing would be performed at the Langley Aeronautical Laboratory of the NACA.

The complete flow model is illustrated in Figure 3.30. This model was constructed of wood and metal and tested at interval pressures up to 15 psig. Design alternatives of the reactor inlet header plate, exit-turning guide vanes, rear strut, and control rod housings were tested as part of seven different system configurations. The results of these tests were published[108] and are summarized as follows:

1. The inlet annulus, the inlet collector-ring, the rear strut and the original design of the exit header section, all increased the mass-flow deviations from uniformity in the simulated reactor.
2. The guide vanes at the exit of the reactor were the most convenient means of reducing mass-flow deviations in the simulated reactor; by this means, the deviations in all except annulus 1 were reduced to within ±5 percent of the mean, an improvement of 38 percent relative to the complete model deviations before vane alterations.
3. Changes to the contour of the inlet header plate had little effect on the mass-flow deviations in the simulated reactor.

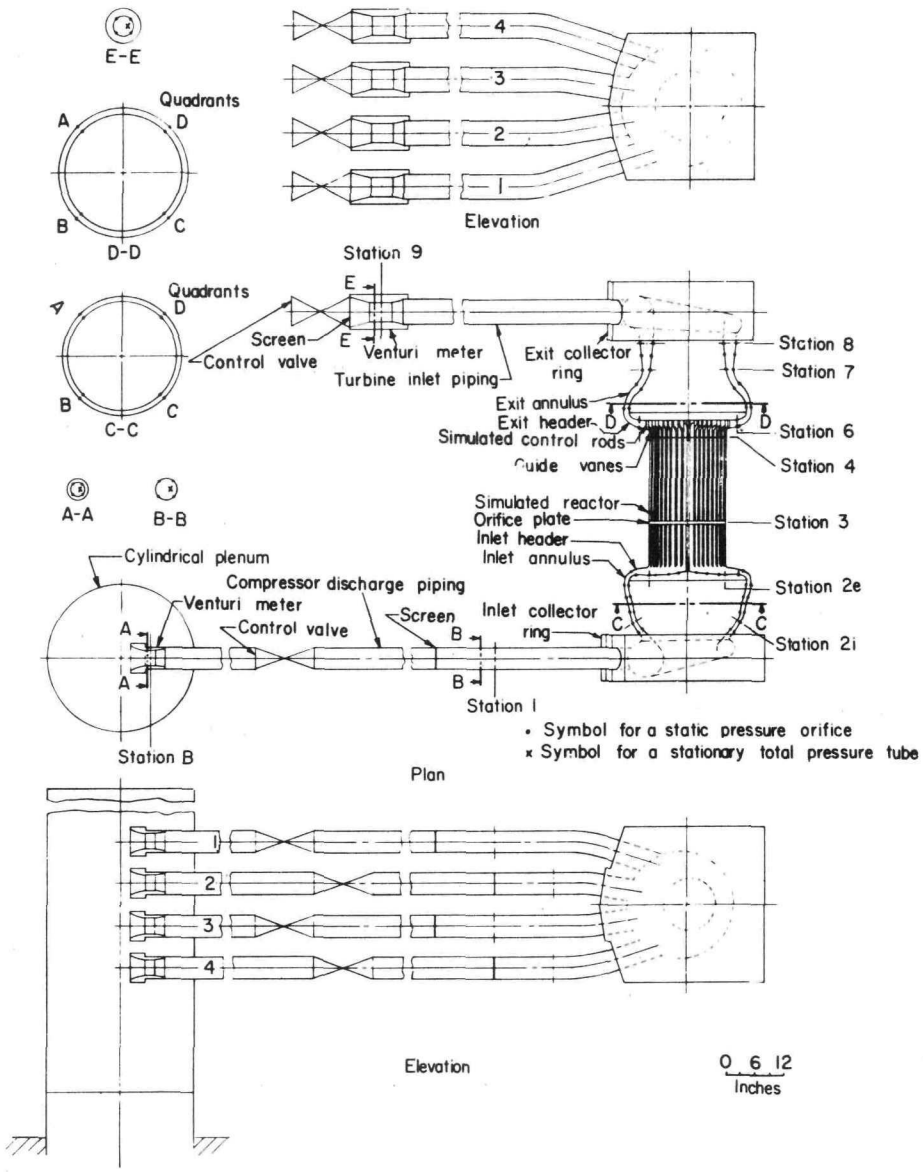

Fig. 3.30 – Diagram of the complete duct system – Test configuration 4

4. The mass-flow deviations in the reactor passages increased for the asymmetrical conditions as the number of closed compressor discharge and turbine-inlet pipes increased; with three of the four pipes closed, the velocity of airflow was essentially zero in some annuli near the center of the reactor.
5. Mass-flow deviations in the simulated reactor for all configurations tested became smaller with increasing Mach number and Reynolds number.
6. Although the inlet collector-ring established a whirl motion and considerable circumferential asymmetry in the flow, the velocity profiles in the inlet-annulus exit station (station 2e) were improved, the loss of the inlet annulus and diffuser (stations 2i to 2e) was reduced by 6.5 percent, and the loss of the inlet header section (stations 2e to 3) was increased. The net result was an increase in loss between stations 2i and 3 of 8.5 percent relative to the loss with ideal flow at the inlet annulus inlet station.
7. The expansion angle of the diffuser in the inlet-header-plate region was judged to be too high to permit satisfactory performance at full-scale Reynolds numbers. A redesigned header-plate provided an expansion angle of 12 degrees, which improved the velocity profile in the inlet-annulus exit station (station 2e), reduced the combined loss of the inlet annulus and diffuser (stations 2i to 2e) by 30 percent, and increased the header section loss (stations 2e to 3). The net result was a decrease in loss of 10 percent between stations 2i and 3.
8. Flow in each of the nine annuli of the simulated reactor 2-1/2 inches downstream from their entrance was stable with relatively high velocities near both the inner and outer walls of each passage.
9. Wakes from the rear strut and control rods were present in the exit annulus and prevented the attainment of reliable measurements at station 6.
10. The losses in the exit collector-ring were appreciably larger than losses in the inlet collector-ring. The exit collector-ring was responsible for considerable flow asymmetry in the exit annulus, particularly in a circumferential direction, and probably responsible for somewhat higher losses in all duct elements affected.
11. The measured loss coefficient for the entire model of the configuration giving acceptable mass-flow distributions in the reactor (header-plate 2, guide-vane configuration 2, and rear-strut 2) was 6.66, which was 2.4 percent less than observed with the original configuration (header-plate 1, guide-vane configuration 1, and rear-strut 1). The measured variation with increasing Mach and Reynolds number was attributed almost entirely to the orifice-plate characteristics.
12. The sampling technique used in the airflow tracing investigation proved satisfactory for this type of investigation.
13. The data indicated that paths of specific segments of airflow could be traced from the simulated reactor to a specific turbine-inlet pipe, and that, within the limits of the tests, the paths were not significantly affected by Mach number or by the concentration of Freon-12 vapor introduced.

3.4.2.2 Core Test Facility Investigation - The Core Test Facility for test of the HTRE No. 1 reactor, as described in 2.1 of APEX-903, was investigated through a 1/4-scale model to determine that the reactor airflow distribution was satisfactory. The CTF was designed for uniform reactor flow distribution and low pressure loss, and these characteristics were considered of sufficient importance to warrant the model test.

Figure 3.31 shows a schematic of the model flow system. The results of the test indicated that none of the reactor tubes should have less than 98 percent of average flow, and that the facility pressure loss would be within three percent of the predicted value.

3.4.2.3 HTRE No. 3 Model Tests - An experimental investigation was made using air at ambient temperature to determine the aerodynamic characteristics of the Heat Transfer

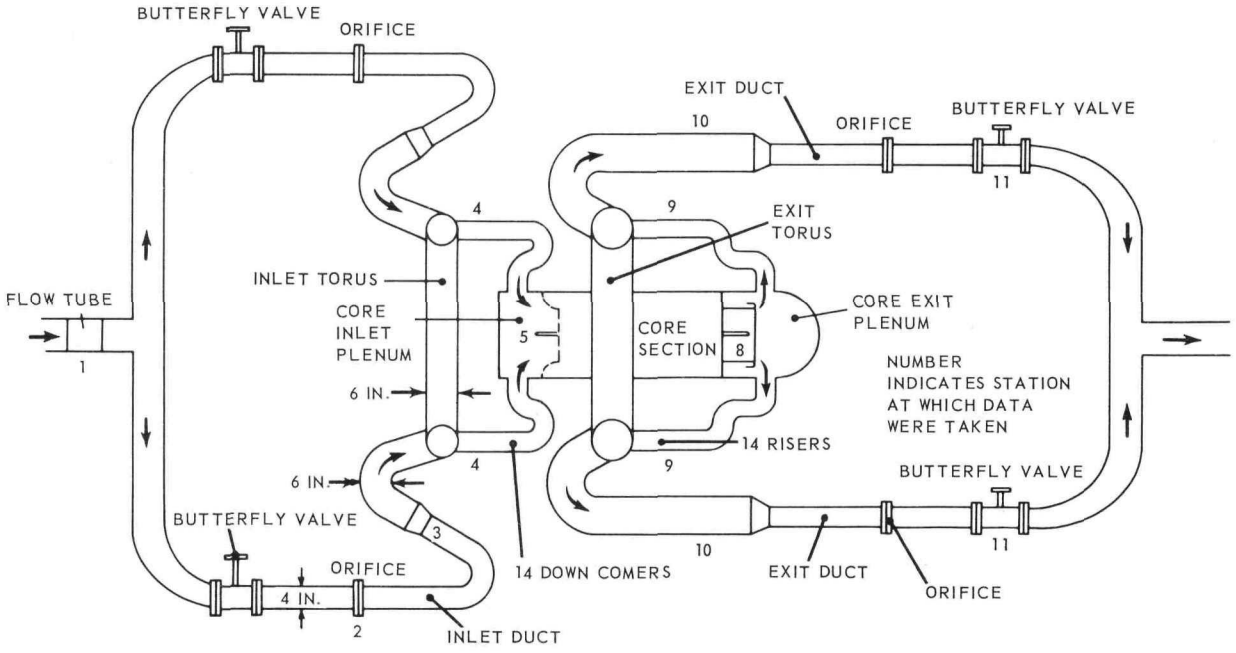

Fig. 3.31 – Flow system schematics

Reactor Experiment No. 3 by testing an approximately 1/4-scale reactor-shield mockup. A complete description of this power plant is given in APEX-904.

Because the aerothermodynamic characteristics of various shields are discussed in section 3.3, only the effects of header, or shield-plug geometry on the weight-flow distributions in the reactor core are discussed here.

Figure 3.32 is a schematic diagram of the various test configurations. Figures 3.33 and 3.34 indicate the geometries of the front- and rear-shield plugs respectively.

Figure 3.35 is a photograph of the scroll used in configuration D_3-5-4 (Figure 3.32). With the exception of the scroll and rear plug number 4, which were made of Fiberglas reinforced epoxy resin, the flow surfaces of the model were metal or Plexiglas.

Figure 3.36 indicates the terminology used to designate position in the core cross-section in these tests.

Figure 3.37 indicates the weight-flow distribution radially in the core for various front-header shapes. The tests from which these data were generated were made with the core exhausting into a plenum. Thus no rear-plug effects are present in Figure 3.37. Based on these data it would appear that plug number (or header number) 6 should be used in tests to determine the optimum rear-plug configuration. Plug number 5 was chosen however, because its geometry was closer to the geometry being considered for HTRE No. 3 and also because the pressure loss from the shield annular passage to a station inside the reactor (station 3 and 4, respectively, in Figure 3.34) was lower for plug number 5 than for plug number 6.

The weight-flow distribution radially in the core for various rear plug configurations in conjunction with front plug number 5 were presented in Figure 3.8. These tests were made with a plenum feeding the front-plug annulus. Two of the rear plugs were unacceptable because of the poor core flow distributions produced and the large pressure losses. Configuration C_3-5-4, however, produced suitable core-flow distribution and resulted in a total pressure loss which was about 53 percent less than the total pressure loss of the latter of the other two rear-plug configurations.

Data obtained with the test configuration wherein the scroll was used (configuration D_3-5-4) indicated no circumferential or radial variations in the core weight-flow distribution attributable to the scroll. In other words, essentially the same core weight-flow distribution occurred regardless of whether the front-plug annulus was fed from an upstream plenum or from the scroll. In addition, essentially the same core weight-flow distribution was measured with a configuration in which flow was introduced to the front plug through only one leg of the scroll simulating a single-engine operating condition. Thus the data presented in Figure 3.8 for configuration C_3-5-4 are also applicable for the configuration wherein the scroll was used (configuration D_3-5-4) for either 1 or 2 engine operation.

Figure 3.38 shows the weight-flow distribution in the core for the configuration in which the scroll was used. The large numbers shown in each of the tubes represent the percent of average weight-flow through that particular tube in which the number appears.

3.4.2.4 XMA-1 Flow Tests - Experimental investigations of several versions of the XMA-1 power plant were made using air at ambient temperature to determine the power plant aerodynamic characteristics. A complete description of this power plant appears in APEX-907.

The first series of tests were made using the same core simulator used in the 1/4-scale HTRE No. 3 tests, front- and rear-shield plugs of the type first considered for the XMA-1 power plant, and front and rear transition sections. In addition, compressor-exit sections and turbine-inlet sections were simulated.

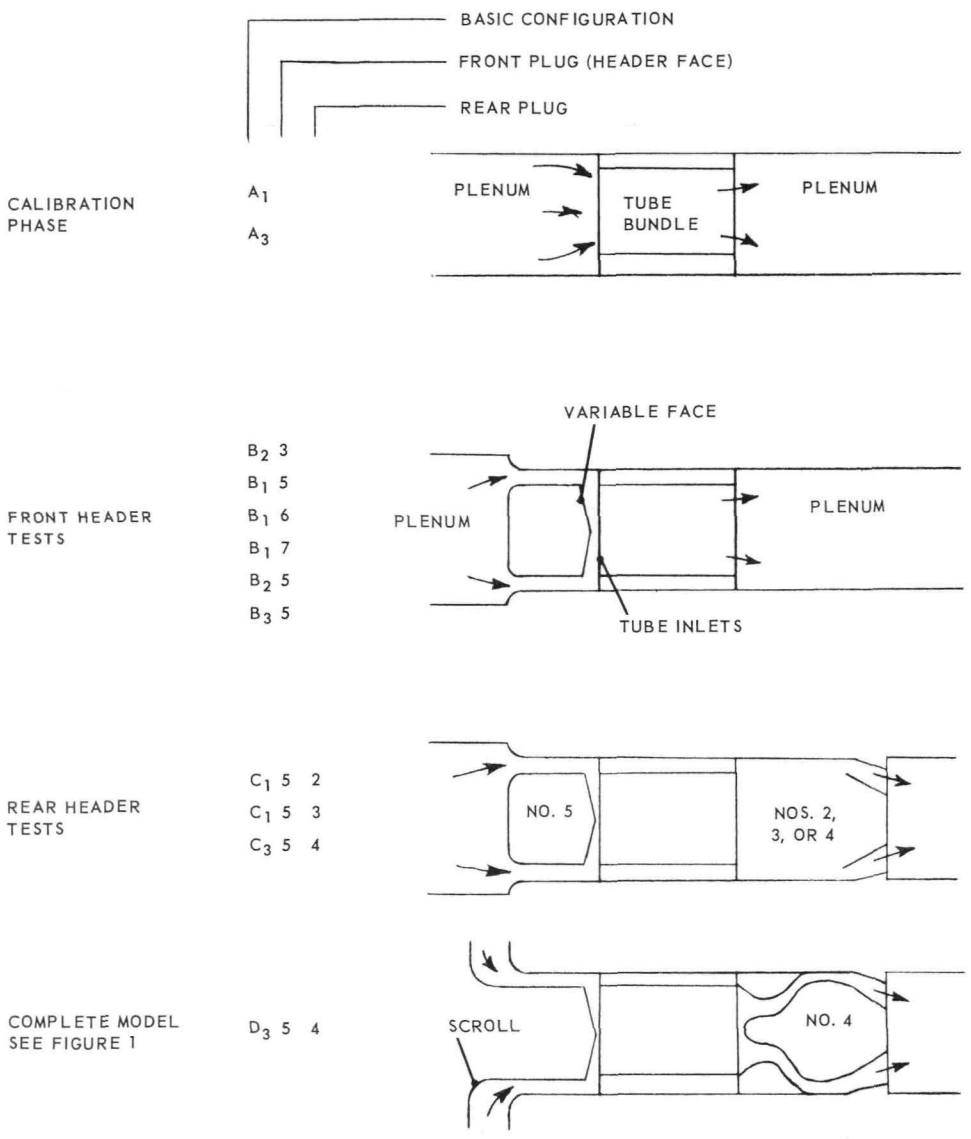

NOTE: SUBSCRIPTS
1 = SHARP EDGE TUBE INLETS.
2 = 0.2 PARTIAL RADIUS ON 8 OUTER ROW TUBES – NUMBERS B3 THRU C21.
3 = SAME AS 2 PLUS 0.1 RADIUS ON ALL TUBES.

Fig. 3.32 – Summary of test configurations

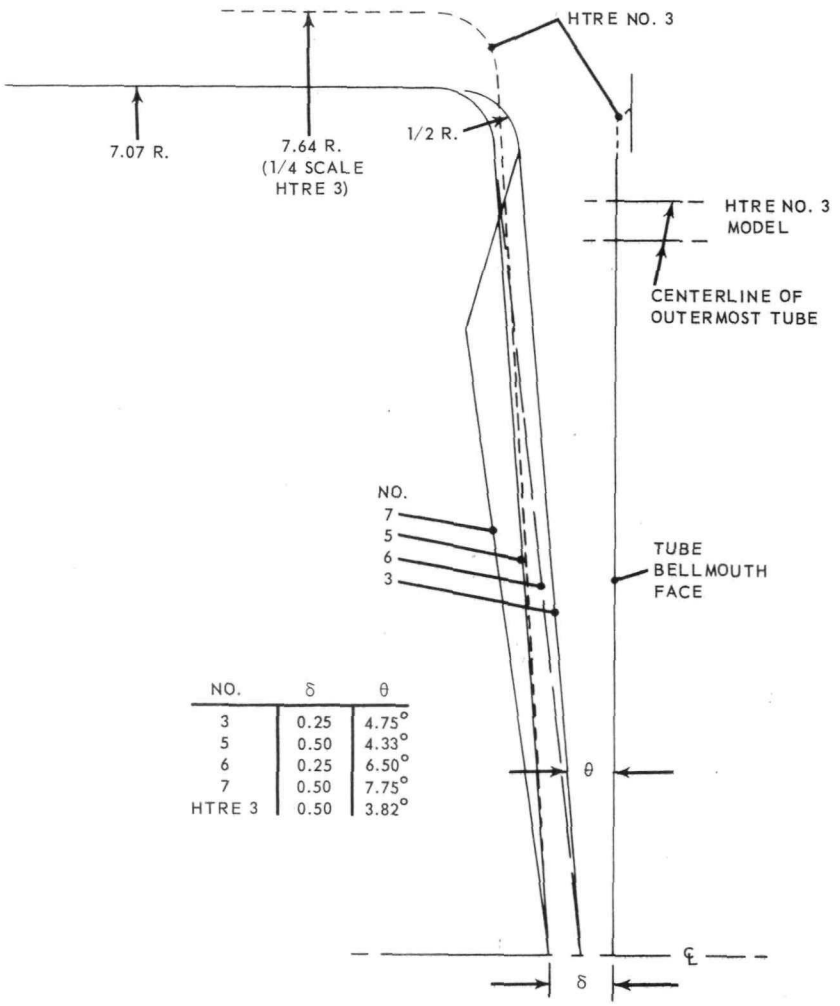

NO.	δ	θ
3	0.25	4.75°
5	0.50	4.33°
6	0.25	6.50°
7	0.50	7.75°
HTRE 3	0.50	3.82°

Fig. 3.33 – Sketch of front header face geometry

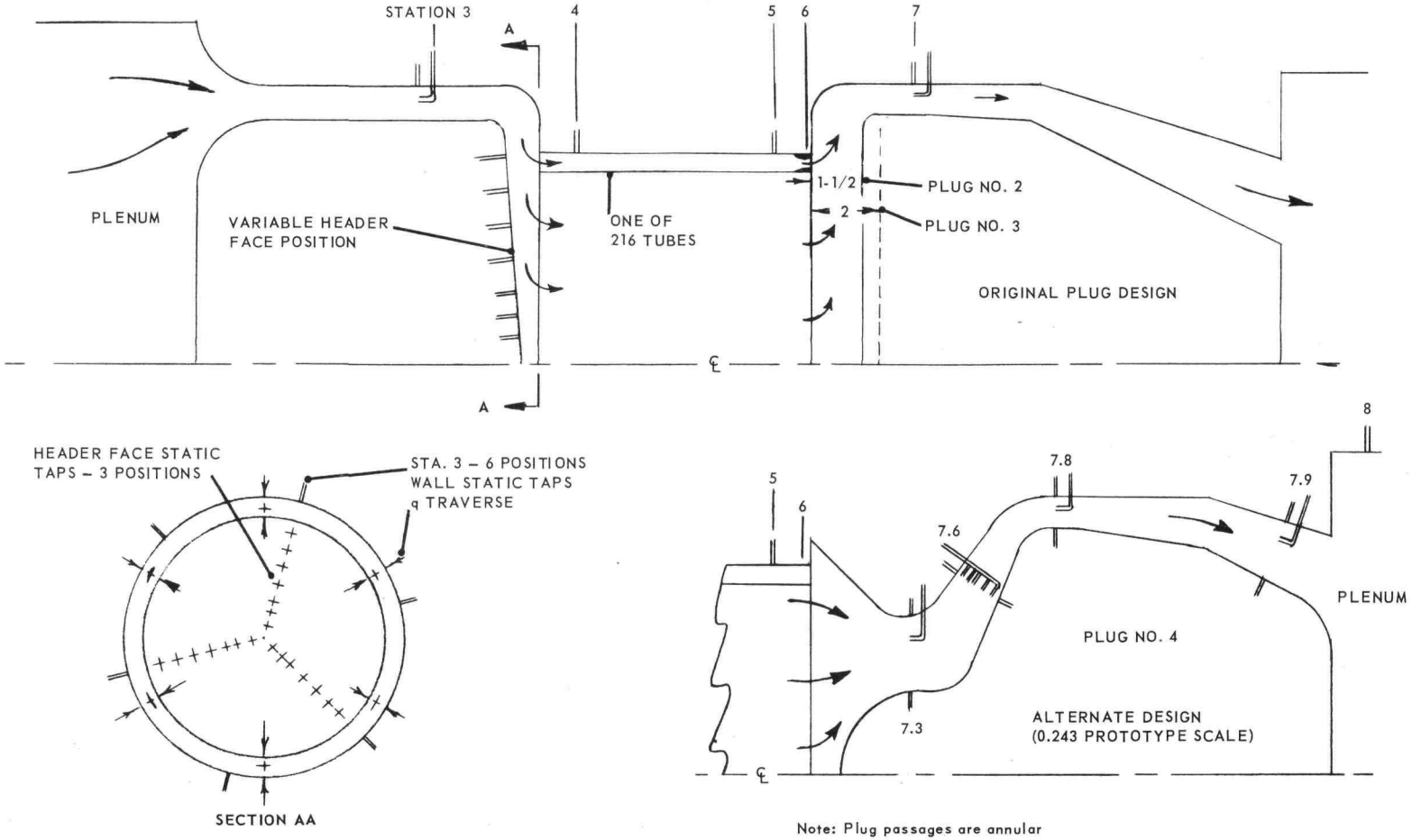

Fig. 3.34 – Sketch of model configuration for tests of various front and rear header plugs

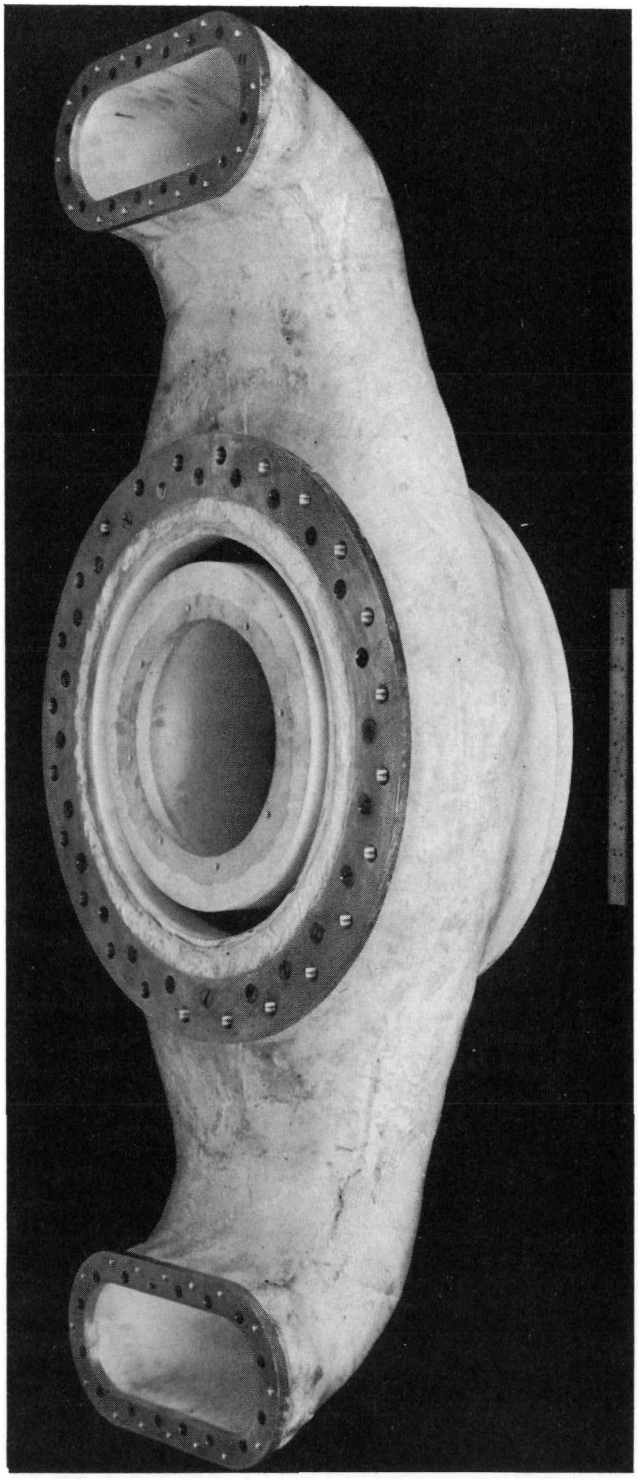

Fig. 3.35 – Front view of the front plug inlet scroll

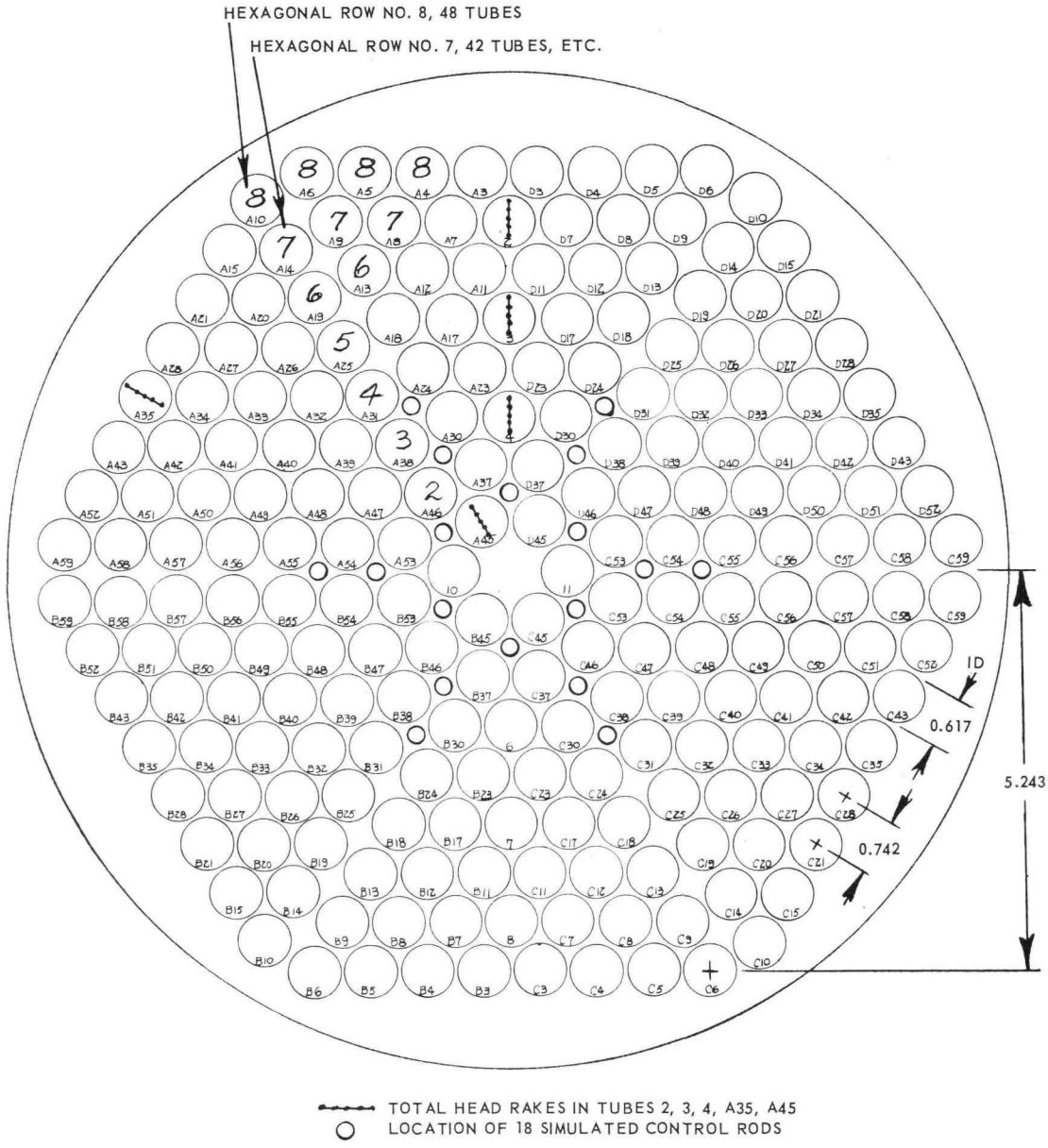

Fig. 3.36 – Sketch of front face of 216 tube core simulator as used in tests

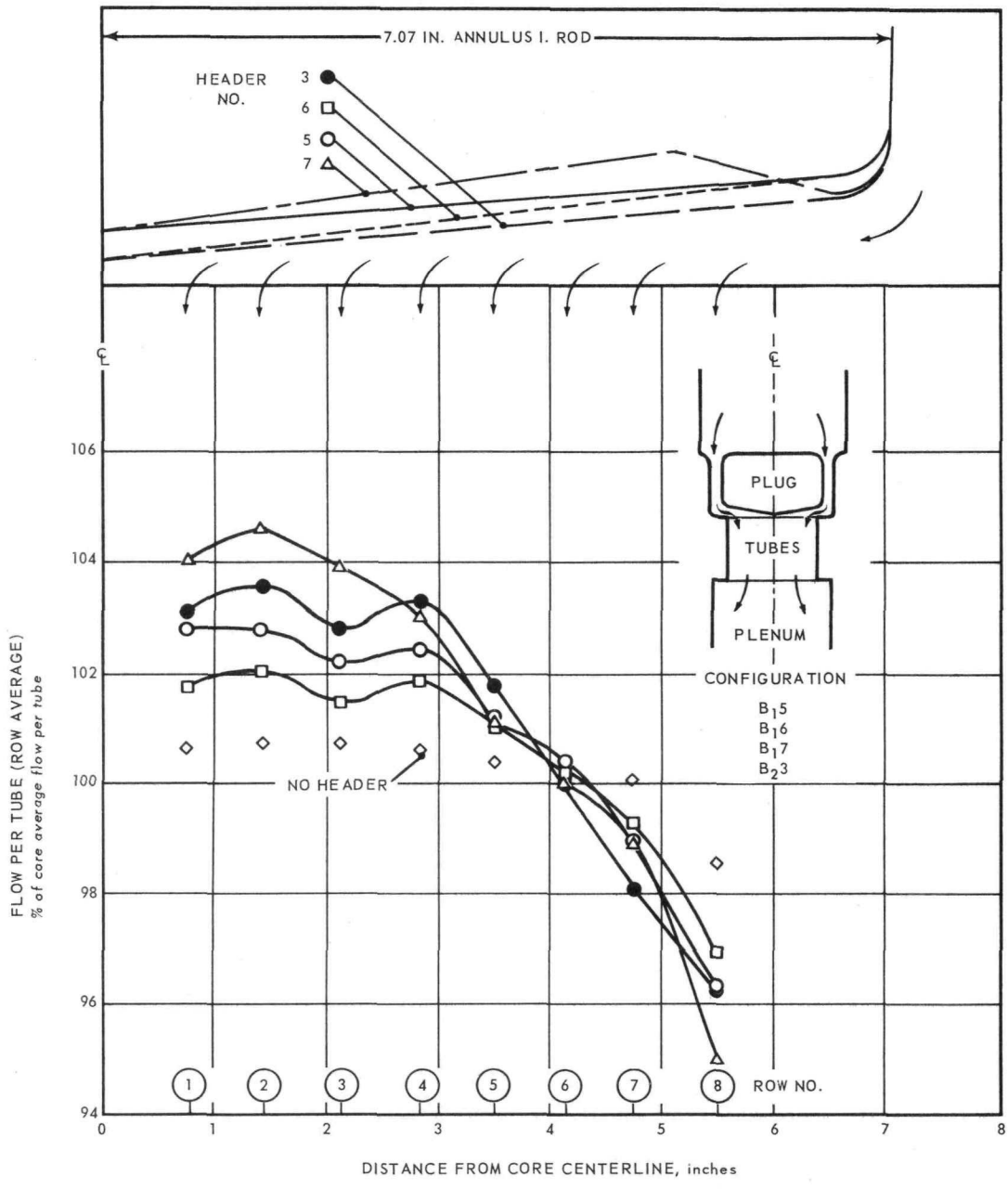

Fig. 3.37 – Weight flow distribution radially in core for various front header shapes

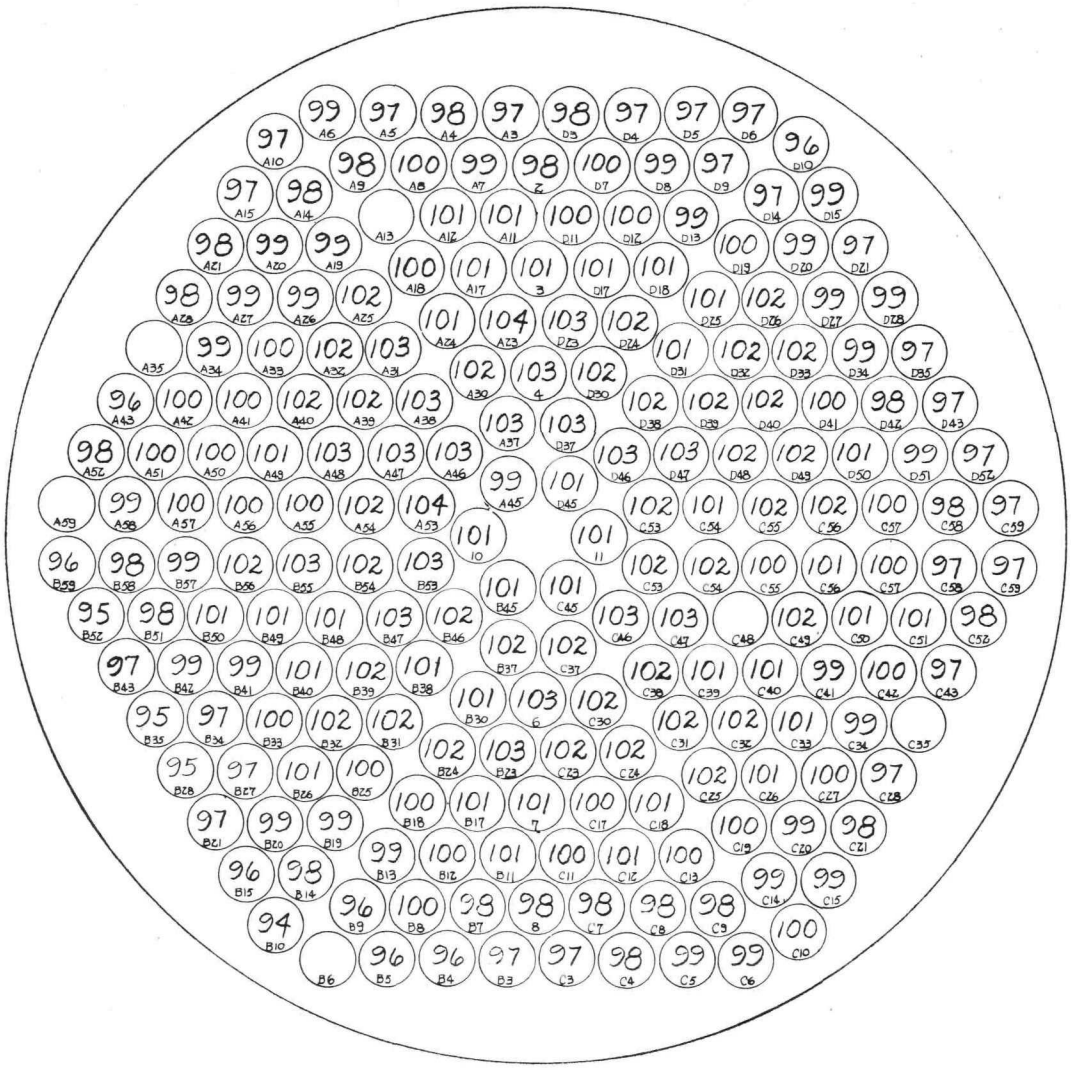

Fig. 3.38 – Weight flow distribution "D" in core for complete model configuration "D"

In a later series of tests the same compressor-exit, turbine-inlet, and front and rear transition sections were used with a new front plug, a new core simulator and a new rear plug. These front- and rear-shield plugs were of the type considered for the final version of the XMA-1 power plant. In the front plug, each flow passage was split into two passages by a strut near the downstream end of the plug. In the rear plug each flow passage was divided into 3 passages at the upstream end of the plug by 2 dividers in each passage. The new core simulator was designed with 151 tubes (the core simulator used for the first series of XMA-1 tests had 247 tubes).

After fabrication of the new core simulator was started, the power plant core design was changed. The new core still had 151 tubes but the tube diameter was increased, resulting in a larger effective core diameter. Accordingly, 30 additional tubes were added at the outer periphery of the new core simulator design. This change resulted in a configuration with approximately the correct effective core diameter and free-flow area, but the geometry was incorrect. No detrimental effects were associated with these deviations.

In the first series of tests, investigations were made to determine the effects on the core weight-flow distribution, when front- and rear-shield plug passages were either horizontal or vertical. Additional tests were made to determine if the addition of swirl

at the compressor exit affected the core weight-flow distribution, and to determine the penalty, if any, in core weight-flow distribution of shortening the power plant by extending the leading edges of the front plug and the trailing edges of the rear plug into the respective front and rear collectors.

The results of these tests may be summarized as follows:

1. No change in the core weight-flow distribution except for a relocation of the below-average and above-average weight-flow regions was noted as the front plug was changed from a horizontal-passage to a vertical-passage orientation.
2. The locations of the above-average and below-average weight-flow regions was controlled by the front plug. Changes in rear-plug orientation had no effect on the core core flow distribution.
3. The addition of swirl at the compressor exit, and simulation of the extension of the front and rear plugs into their respective transition sections had no effect on the core weight flow distribution.

A typical core weight flow distribution in this 1/4-scale model of the XMA-1 system was shown in Figure 3.9. Complete results of this investigation were published.[94]

Tests in which the more up-to-date shield plugs and core simulator were used, determined the core flow distribution for the normal configuration. In these tests single-engine operation was simulated as was a front-shield or bypass valve failure. Tests were also made to determine the effects of decreasing the axial distance between the front- and rear-shield plugs and the core simulator entrance and exit, respectively.

The new core simulator design was such that all the tubes did not have the same free-flow area.[109] Accordingly, core mass-velocity distributions are presented instead of core weight-flow distributions. The mass velocity of a particular tube is defined as the weight flow through that tube divided by the particular tube entrance free-flow area.

Figure 3.39 is a typical mass-velocity ratio distribution for the revamped XMA-1A 1/4-scale model system. The variation is approximately ±6 percent from average.

Figures 3.40 and 3.41 are the mass-velocity distributions for the simulated bypass valve failure and the simulated single-engine operating condition, respectively. The respective variations in mass velocity are approximately ±12 percent and ±10 percent from average.

Additional tests indicated that mass-velocity distribution in the core was essentially unchanged by decreasing the axial distances between the shield plugs and the core. The following configurations were tested:

FULL-SCALE
AXIAL SPACING

Front	Rear
3 in.	3 in.
2.5 in.	2.5 in.
1.5 in.	1.5 in.
1.0 in.	1.25 in.
1.0 in.	0.25 in.

Complete results of the investigation using the more up-to-date XMA-1 shield plugs and core were published.[95]

3.4.2.5 Reversed Primary-Cycle Air Circuit Configuration - The reversed primary-cycle air circuit (sometimes called the offset configuration) comprises a flow geometry wherein the compressor discharge air flows through an annular passage between the shield and the reflector. The air is then turned 180 degrees into the core. A description of this power plant is presented in APEX-908.

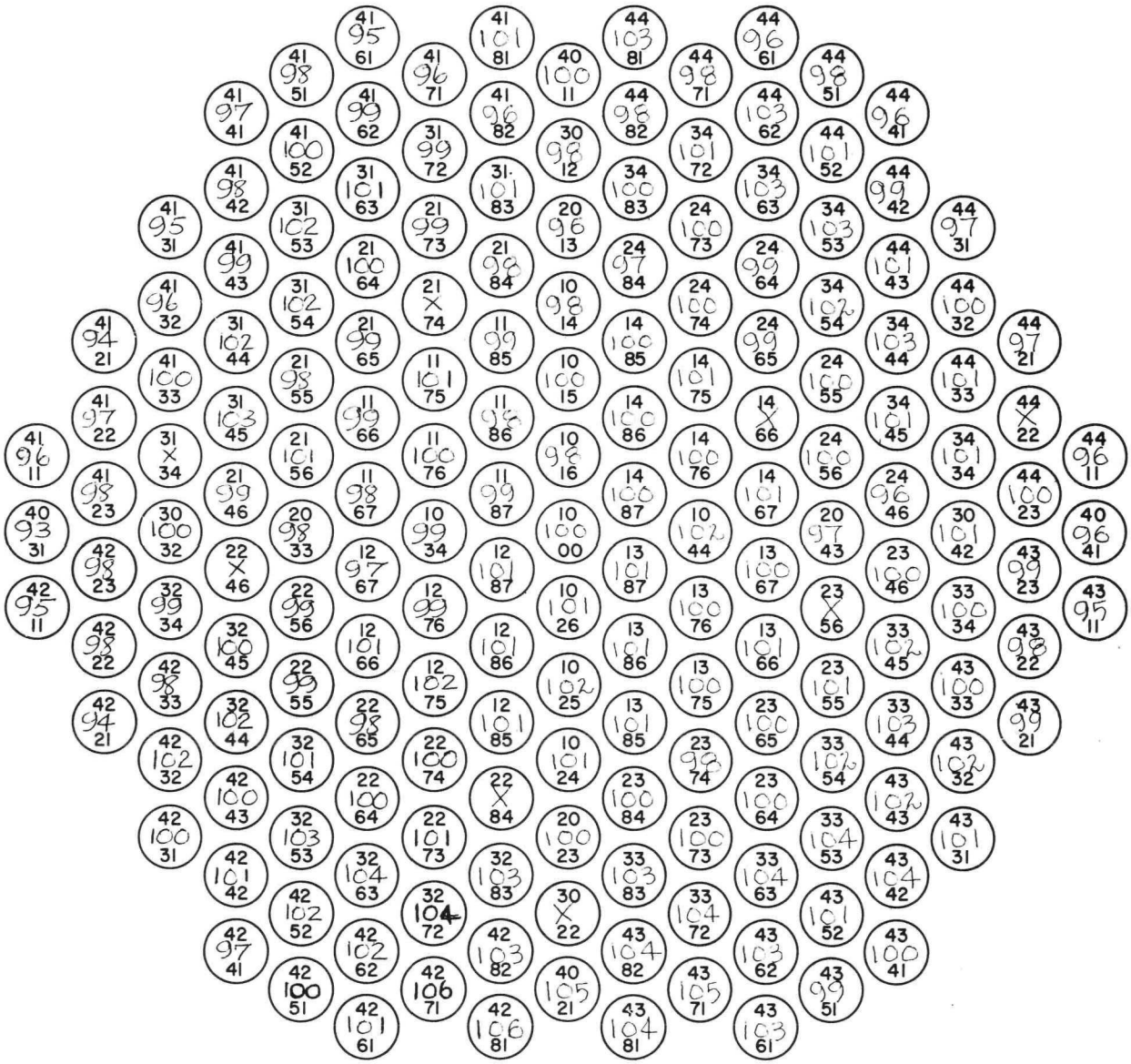

Fig. 3.39 – Mass velocity ratio distribution test with a strut-type front shield plug in final version of XMA-1A quarter-scale model

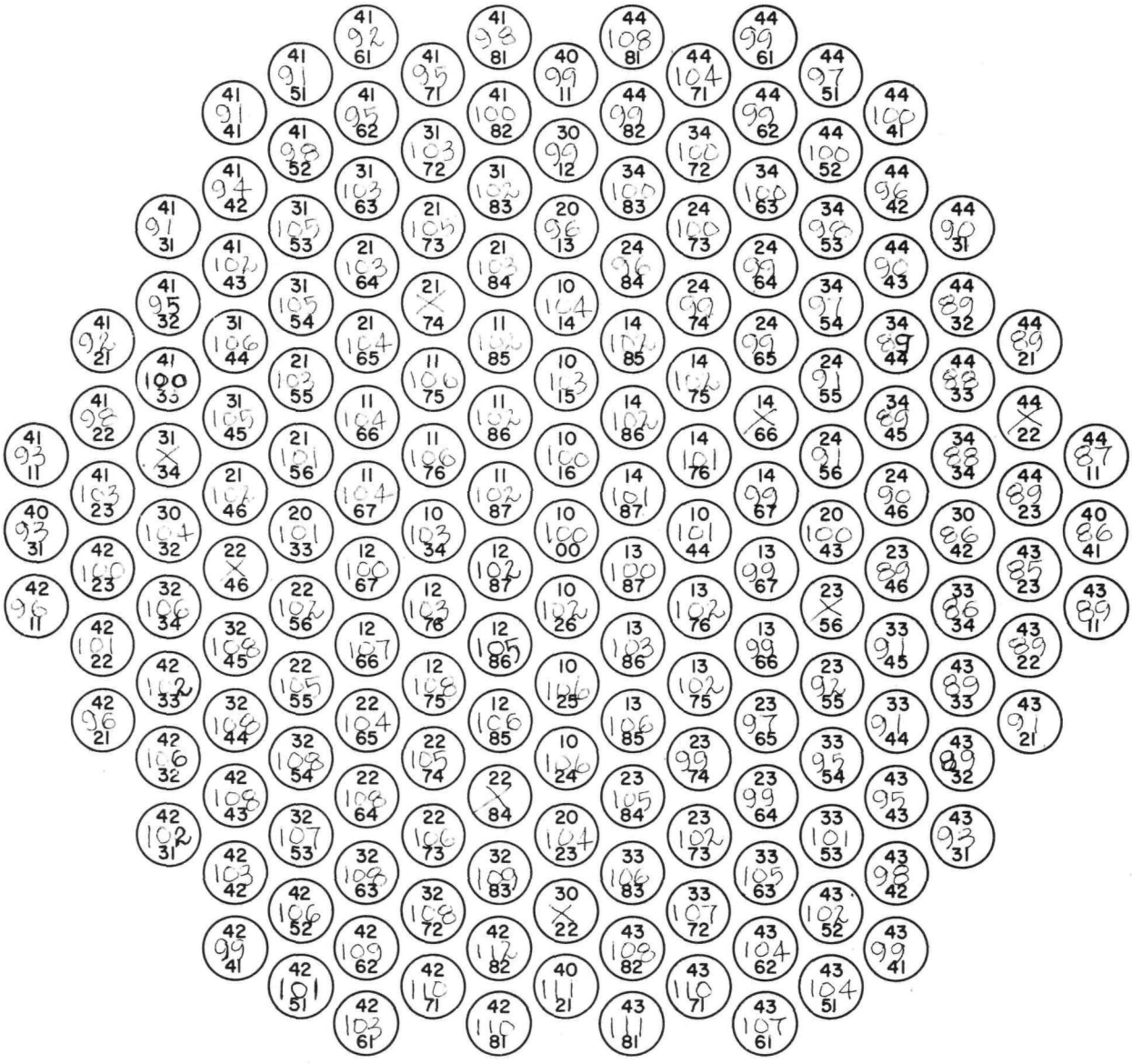

Fig. 3.40 – Mass velocity ratio distribution with a simulated front shield bypass valve failure in final version of XMA-1A quarter-scale model

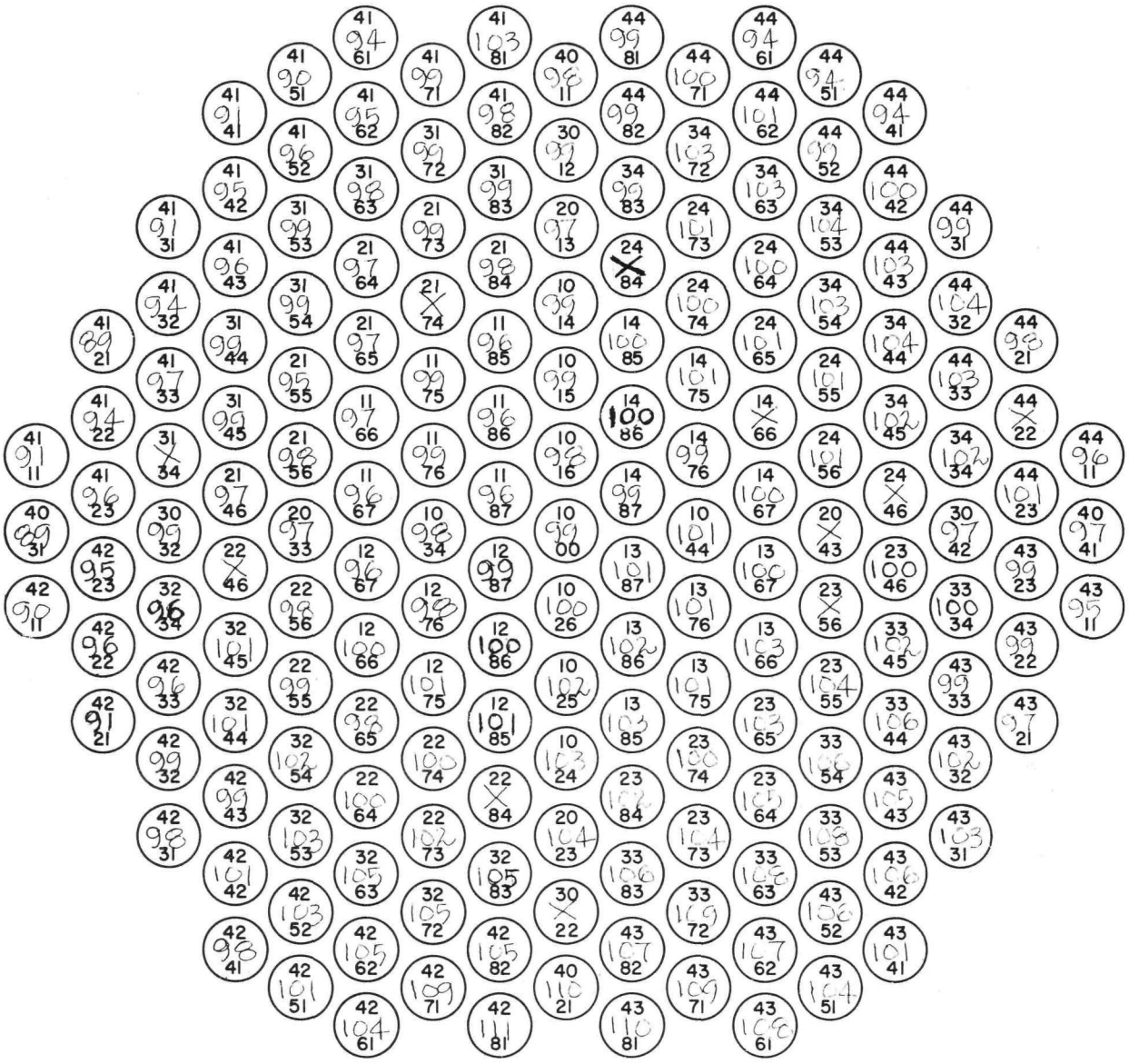

Fig. 3.41--Mass velocity ratio distribution with a simulated single engine operation in final version of XMA-1A quarter-scale model

IBM 704 computer program, Flux Plotting and Contour Search, and ANP digital computer programs 189 and 190, were used to obtain a potential flow design of an annular ring, three vanes, and a header geometry in an attempt to obtain a configuration which would achieve aerodynamically-controlled turning of the air to provide uniform radial and circumferential flow distributions in the reactor.

A schematic diagram of the test setup for 180 degrees annular-vaned turn and header combination was shown in Figure 3.18.

The core simulator used for these tests is the same one used for the HTRE No. 3 tests and the first XMA-1A tests. However, pressures (and consequently the flow) were measured in only about one-third of the core-simulator tubes.

The weight-flow distribution over the face of the core for a typical test condition is shown in Figure 3.42. For this same test condition, averages were made of the available readings in each hexagonal row. Figure 3.43 depicts the variation of these averages with core radius.

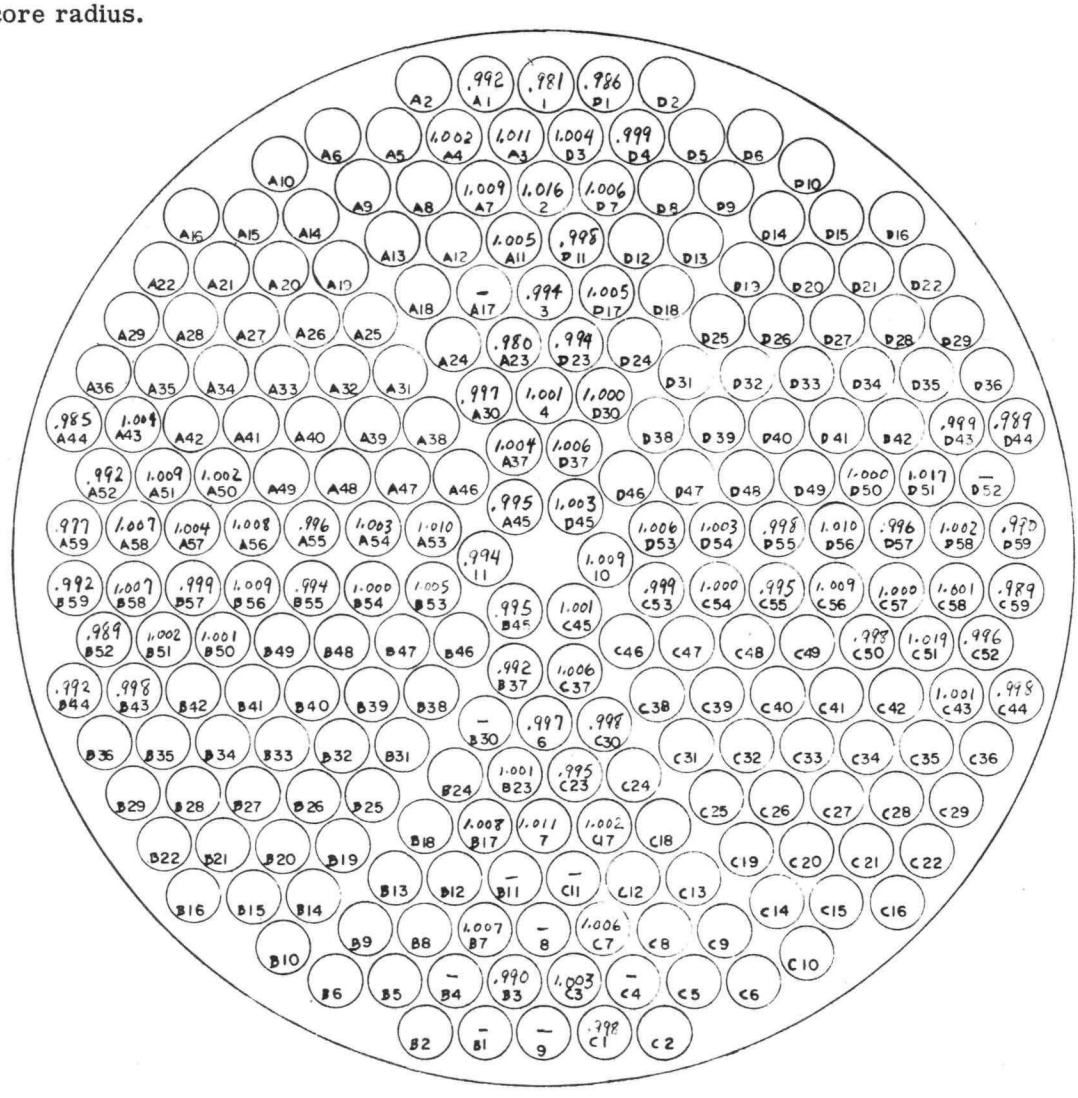

Point 3
M = 0.0976
Average deviation from average = 0.0060

Fig. 3.42 – Typical weight flow ratio (local to average) distribution over core face in reversed primary cycle airflow circuit configuration

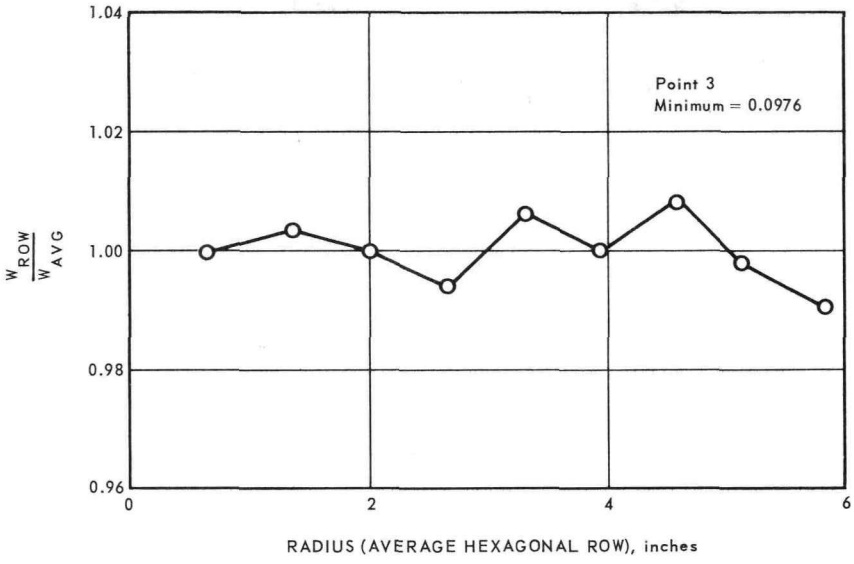

Fig. 3.43 – Variation of the average flow in a hexagonal row with core radius

Two additional investigations were made with this model. In the first, only the innermost vane was retained. For the last, no vanes were used.

Figures 3.44, 3.45, 3.46, and 3.47 represent typical weight-flow distributions over the face of the core, radially in the core, and for the single-vaned and no-vane configurations respectively.

Complete results of the reversed primary-cycle air circuit configuration investigations were published.[83, 84]

3.4.2.6 XNJ140E-1 Model Tests - Cold-flow tests of the XNJ140E-1 power plant were made to establish the basic geometry of header and collector shapes necessary to obtain an acceptably uniform core flow distribution. A complete description of this power plant is given in APEX-908. The complete cold-flow test results were published.[86]

The same core simulator used for HTRE tests, some of the XMA-1 tests, and the offset configuration tests, was used in this investigation. Thirty-seven tubes, which would have been covered by the shaft-alley simulation, were blocked, leaving 210 open tubes. The flow was measured in approximately 100 of these tubes. Figure 3.48 is a photograph of the front face of the core simulator as used in this investigation.

To answer questions which arose concerning the matching of the many air jets ejecting from the tube bundle into the collector an insert, consisting of seven small tubes, was molded into the exit of each of the 210 open tubes of the core simulator. This obtained approximately the correct scaled-flow exit-jet diameters existing at the time of the model design freeze data. Figure 3.49 is a photograph of the rear face of the modified core simulator.

The ratios (A_3/A_1) and ($L/\Delta R$) were used to define the variations in front- and rear-plug geometries, respectively. A_3/A_1 is defined as the ratio of the inlet header area to the annulus area at the front plug entrance. $L/\Delta R$ is defined as the mean axial spacing of the rear collector from the exit plane of the core simulator divided by the difference between the inner and outer radii of the core simulator.

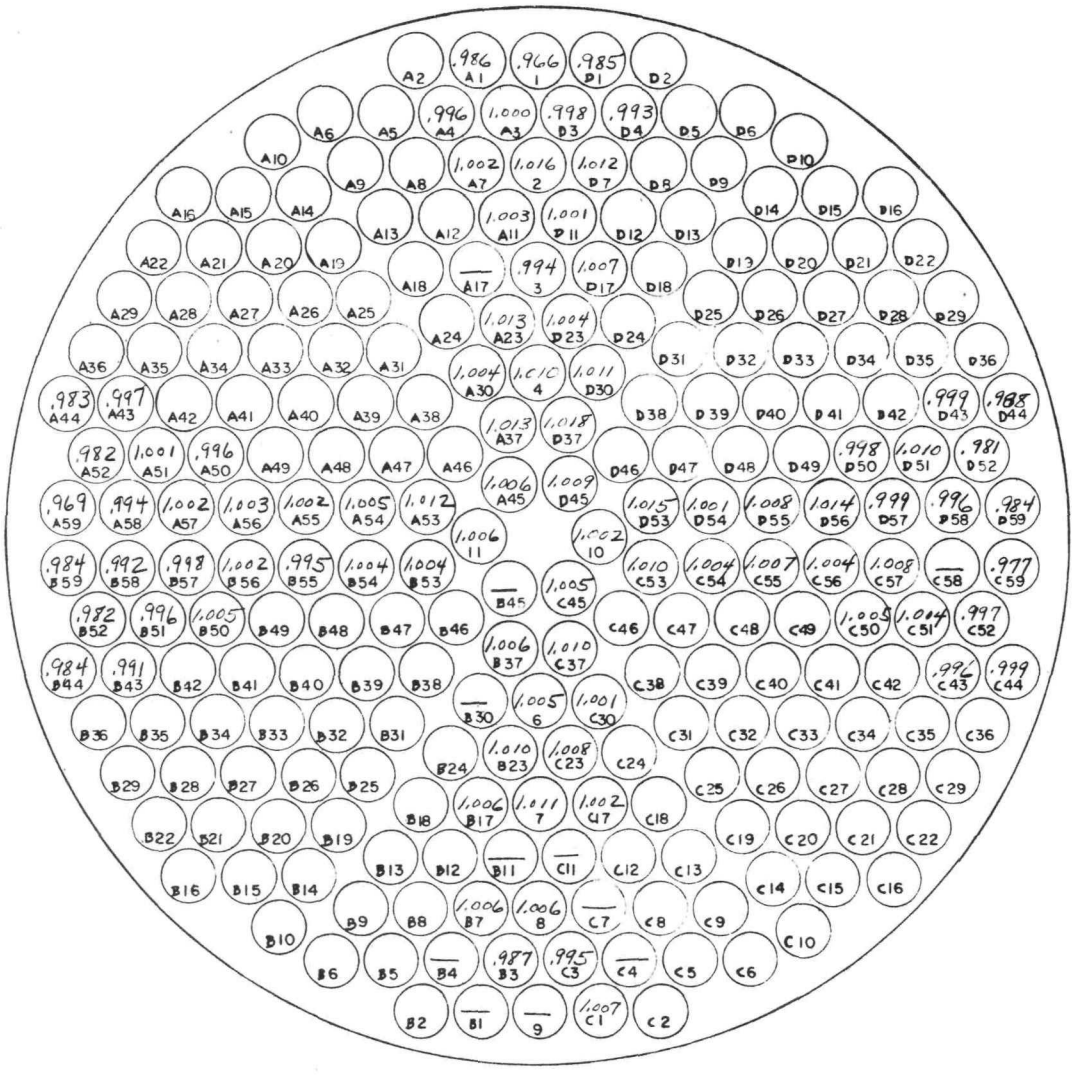

Point 43
M = 0.0991
Average deviation from average = 0.0079

Fig. 3.44 – Typical weight flow ratio (local to average) distribution over core face single-vaned reversed primary cycle air circuit configuration

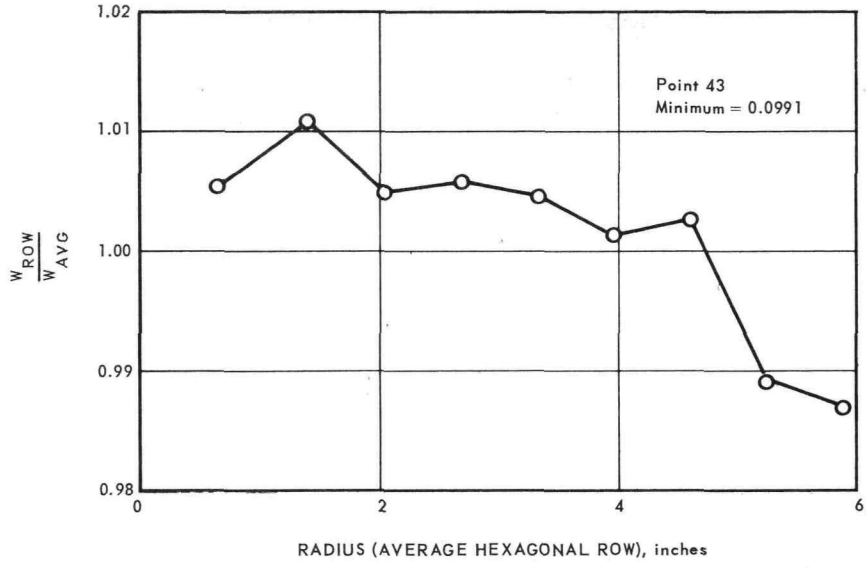

Fig. 3.45 – Variation of the average flow in a hexagonal row with core radius for the single-vaned configuration

Figures 3.50 and 3.51 show details of the model. The schematic of the model was shown in Figure 3.20. The following table shows the various configurations which were tested:

Configuration Number	A_3/A_1	$L/\Delta R$
1	1.21	0.5
2	1.21	0.4
3	1.21	0.3
4	0.96	0.3
5	0.96	0.4
6	0.96	0.5
7	0.72	0.5
8	0.72	0.4
9	1.51	0.6
10	1.21	0.6
11	1.21	0.7
12	1.51	0.7

Figure 3.52 is an indication of the core flow distribution obtained with the various model configurations. The ordinate, percent deviation $(W_{R_{max}}-W_{R_{min}})/W_{ave}$, is the difference, expressed in percent, between the maximum and minimum hexagonal row averages of weight-flow, divided by the average weight-flow per tube. These values are plotted as a function of $(L/\Delta R)$ for various values of (A_3/A_1).

The radial weight-flow distribution in the core for configuration 1 is shown in Figure 3.53.

The results of this investigation indicate that for each header design there is a particular collector shape which permits a core weight-flow distribution more uniform than those obtained with other collector shapes. Configuration 1, $(A_3/A_1) = 1.21$ and $(L/\Delta R) = 0.5$, produced the most uniform core weight flow distributions.

Three additional investigations were made with this model using configuration 1. In the first two investigations it was found that extracting up to 20 percent of the flow through a series of holes in the outer wall of the front plug annulus, or injecting up to 6 percent of the primary flow into the annulus near the core at the inner wall of the rear plug had no significant effects on the flow distribution.

In the final investigation, it was found that a simulated compressor discharge swirl angle of 30 degrees provided an unacceptable core weight-flow distribution. A swirl angle of 10 degrees, however, caused no significant changes in the core weight-flow distribution compared to that obtained with no swirl.

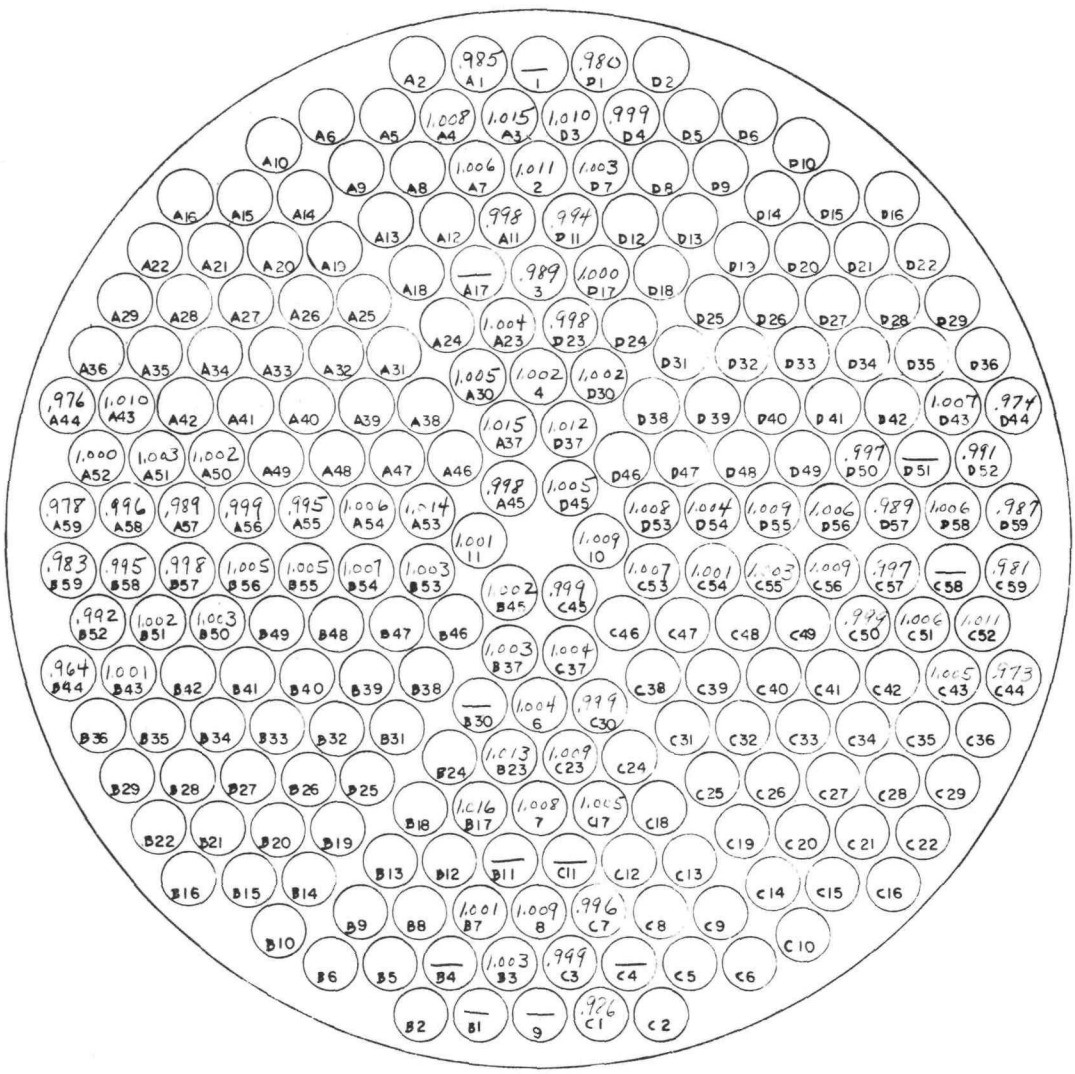

Point 74
M = 0.099
Average deviation from average = 0.0075

Fig. 3.46 – Typical weight flow ratio (local to average) distribution over core face in no-vaned reversed primary cycle air circuit configuration

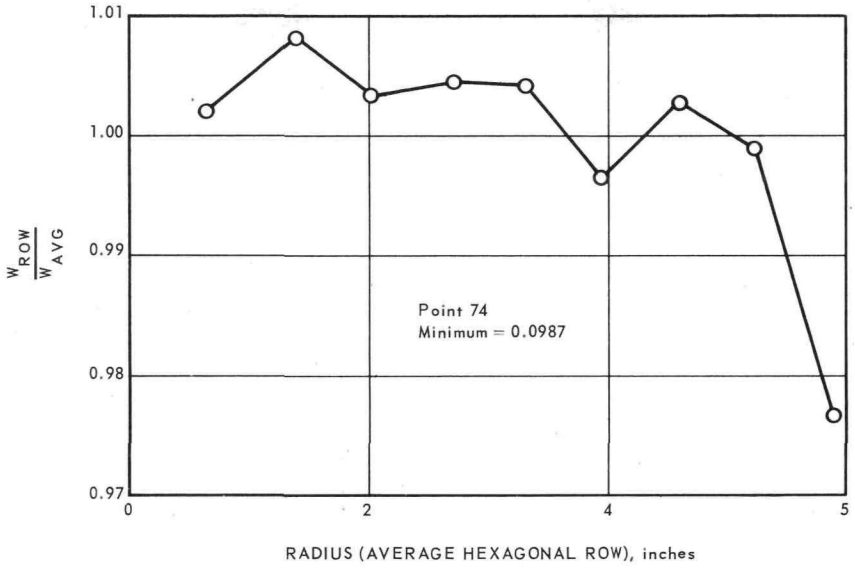

Fig. 3.47 – Variation of the average flow in a hexagonal row with core radius for the no-vaned configuration

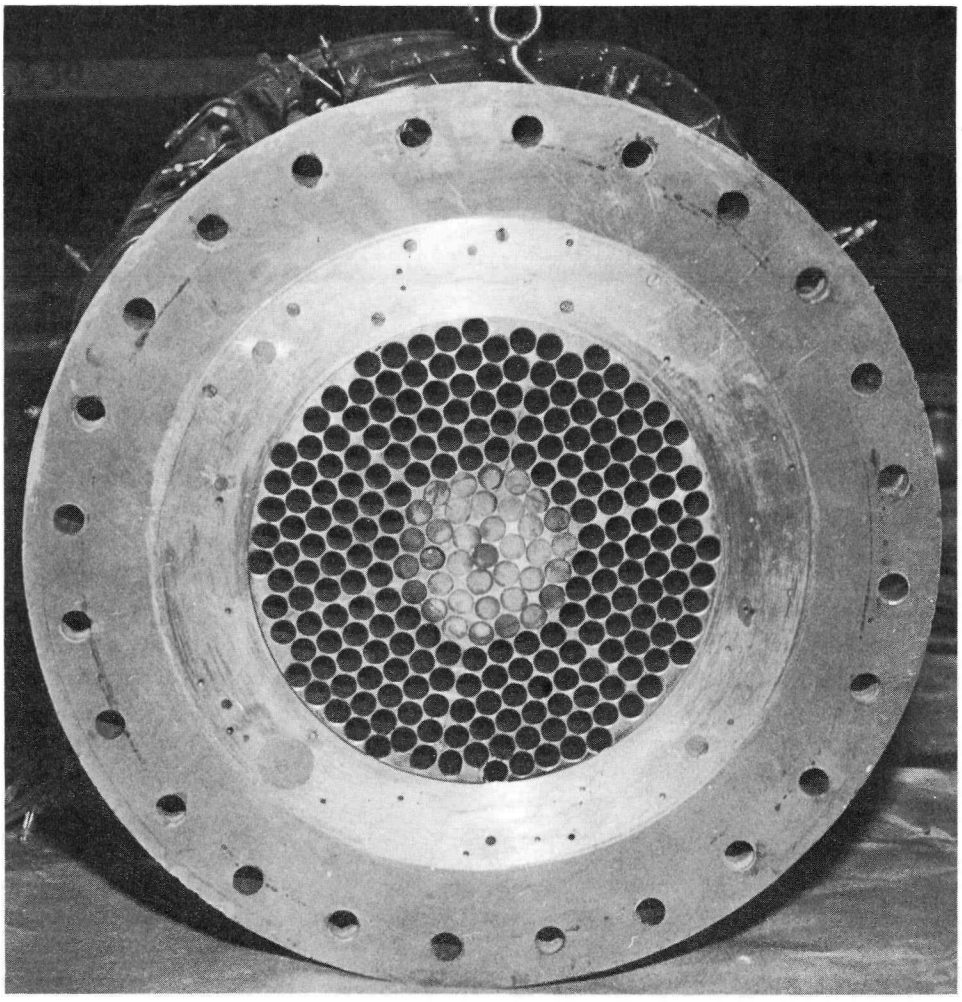

Fig. 3.48 – Front face of core simulator used in XNJ140E-1 cold flow tests

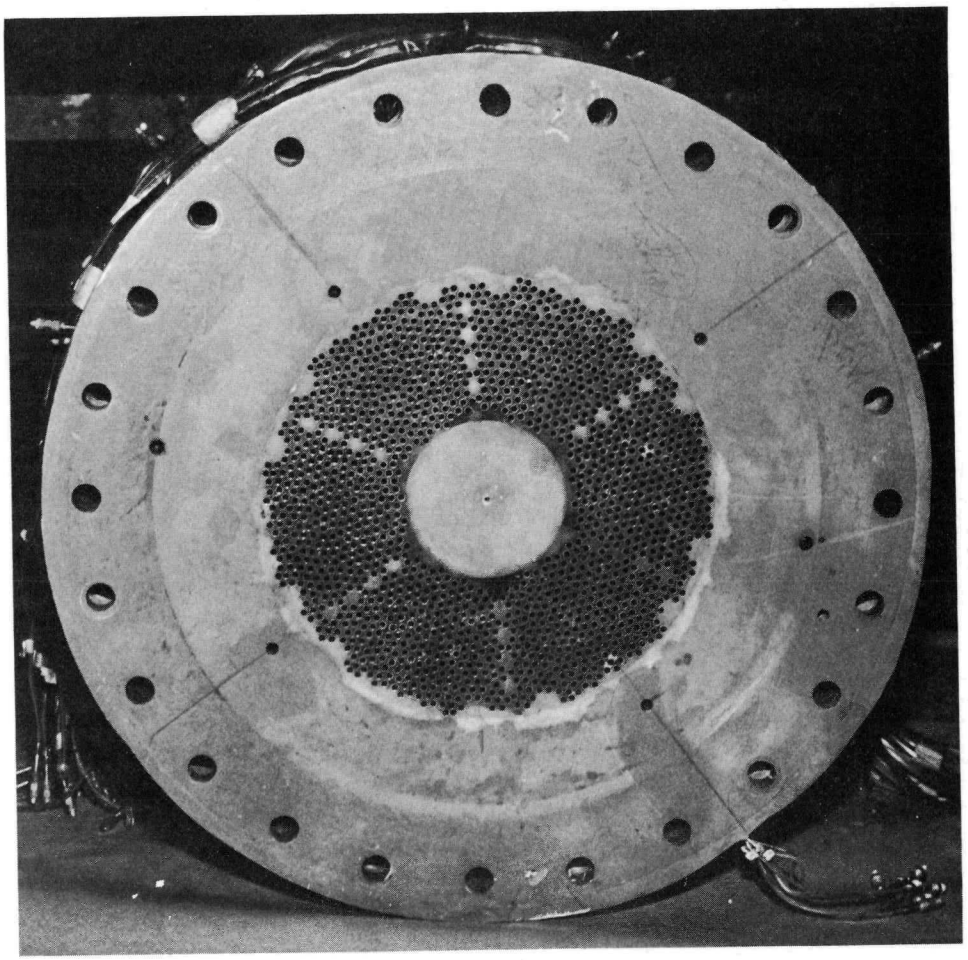

Fig. 3.49 – Rear face of core simulator used in XNJ140E-1 cold flow tests

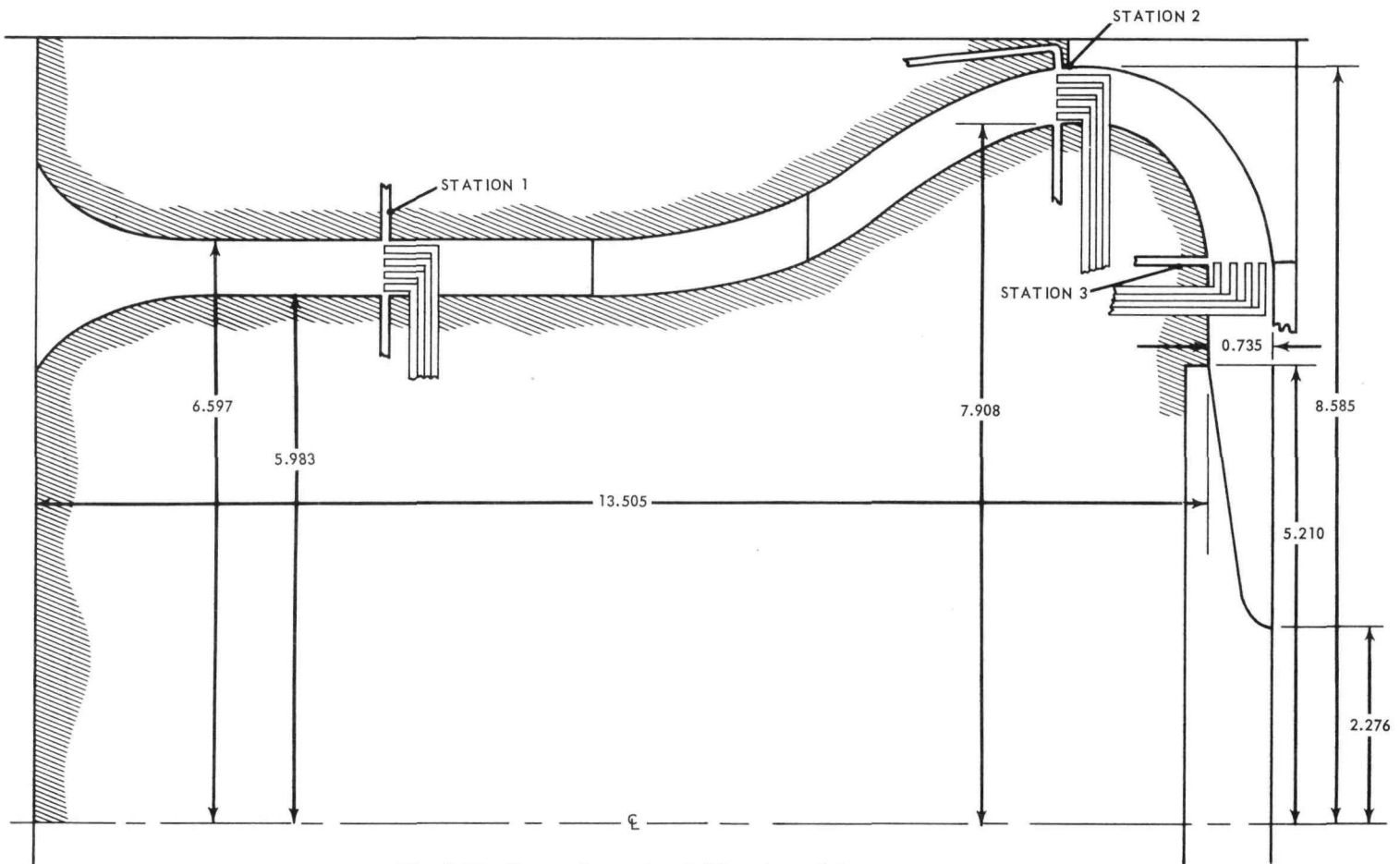

Fig. 3.50 – Front primary duct 0.27 scale model tests

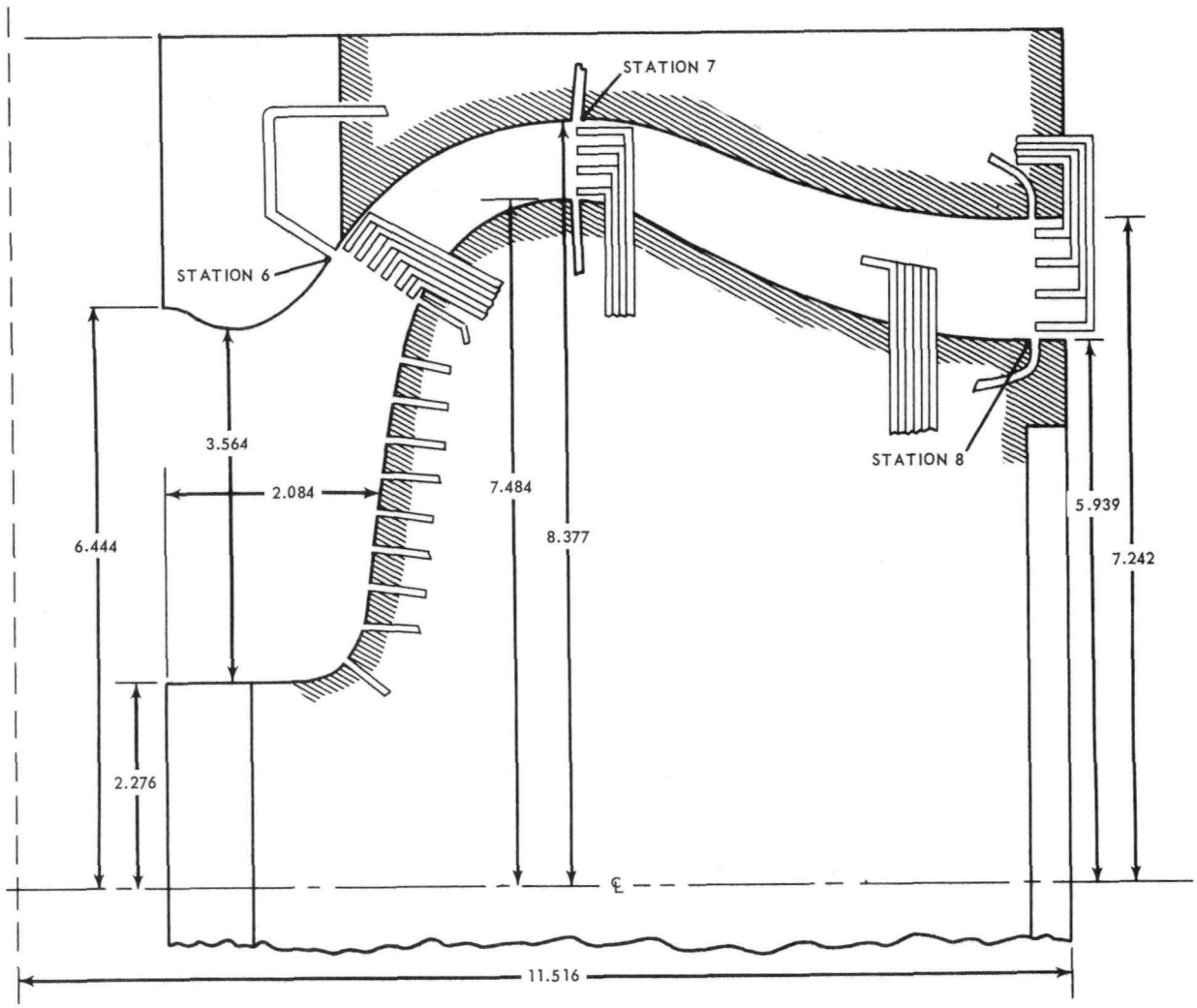

Fig. 3.51 – Rear primary duct 0.27 scale model tests

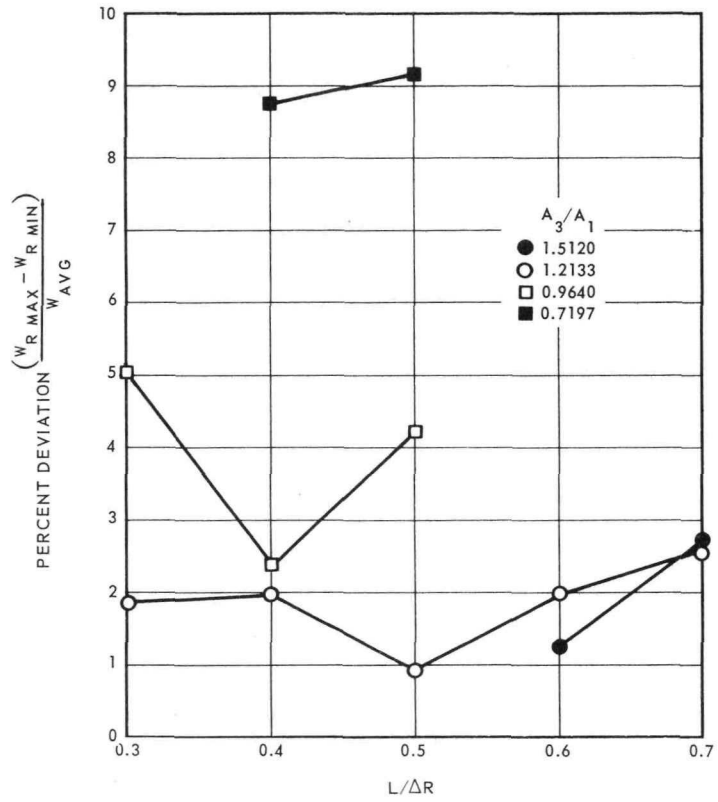

Fig. 3.52 – Difference between maximum and minimum average flows in hexagonal rows in the XNJ140E-1 model tests

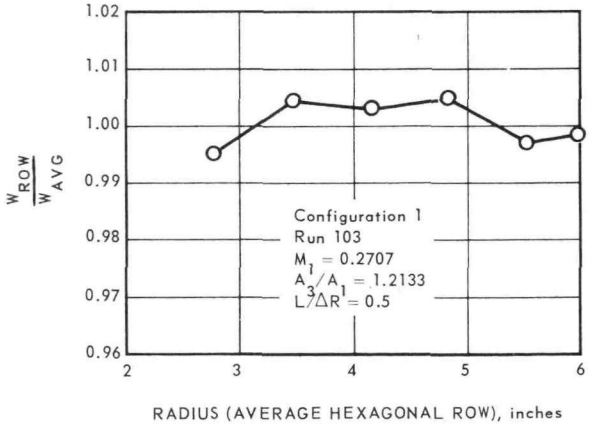

Fig. 3.53 – Variation of weight flow with radial distance

3.5 REFERENCES

1. Morgan, W. R., "Single Stage Heat Transfer and Pressure Drop Tests," GE-ANPD, APEX-132, December 1952.
2. Jay, D. J., "Correlation of Heat Transfer Experiments with Short Plates," GE-ANPD, DC 53-4-107, April 1953.
3. Jay, D. J., "Continuation of Heat Transfer Experiments with Short Plates," GE-ANPD, DC 53-4-193, April 1953.
4. Lapides, M. E. and Masters, E. B., "Summary of Single Element Rig Heat Transfer Data," GE-ANPD, XDC 54-1-78, January 1954.
5. Lapides, M. E., "Thermodynamic Analysis of a Ceramic Plate Reactor," GE-ANPD, DC 53-11-68, November 1953.
6. Masters, E. B. and Brubaker, R. C., "Reactor Design Estimating Charts Part I: Plate Type Fuel Element," GE-ANPD, DC 53-9-98, September 1953.
7. Brubaker, R. C. and Lapides, M. E., "Preliminary Thermodynamic Analysis of Pebble Bed Fuel Elements for the AC-1 Reactor," GE-ANPD, XDC 53-6-95, June 1953.
8. Lapides, M. E., et al., "Source Book for Flow Through Packed Beds," GE-ANPD, DC 54-1-75, January 1954.
9. Lapides, M. E. and Brubaker, R. C., "Summary of Results of ANPD Pebble Bed Flow Tests," GE-ANPD, XDC 54-2-101, February 1954.
10. Holowach, J., "Hydraulic Flow Test of a Folded Pebble Bed," GE-ANPD, DC 54-6-19, June 1954.
11. Lapides, M. E., "Standard Design Procedures for Ribbon Type Fuel Element," GE-ANPD, DC 54-9-17, September 1954.
12. Lapides, M. E., "Summary Report of Thermodynamic Analysis for Project 100: Part II - Fuel Elements," GE-ANPD, DC 55-7-28, July 1955.
13. Holowach, J., "Drag Forces on ANP Fuel Elements," GE-ANPD, DC 56-10-120, October 1956.
14. Moller, T. W. and Page, F. B., "Flow Device Investigation," R 56 GL 238, August 20, 1956.
15. Jones, D. L., "Fluid Dynamic Appraisal of the A-1 Fuel Element," GE-ANPD, DC 56-11-54, November 1956.
16. Hardy, L., "Pressure Drop Comparison Between XRH-1 and XRH-3 Fuel Elements," GE-ANPD, DC 57-1-6, January 1957.
17. Hardy, L., "Pressure Loss Tests of XR-27 Fuel Elements with 20^{o} Angle Ribs," GE-ANPD, DC 58-2-145, February 1958.
18. Holowach, J. and Frank, F. J., "Flow Distribution Studies Using Lead Acetate and Hydrogen Sulphide Gas," GE-ANPD, DC 57-10-39, October 1957.
19. Pugh, R. A., "Preliminary Estimate of Possible Performance Improvement Due to Flow Swirl," GE-ANPD, DC 58-5-30, May 1958.
20. Yarosh, J. G., "Friction Factor Multipliers on an X5-1B Fuel Element Cartridge Before and After Burner Rig Testing," GE-ANPD, DC 58-11-88, November 1958.
21. Yarosh, J. G., et al., "Pressure Losses and Friction Factor Multipliers In Various D102A Fuel Element Cartridge Configurations," GE-ANPD, DC 59-1-228, January 1959.
22. Yarosh, J. G., "Comparison Test for Square and Streamlined XR-27 Fuel Element Cartridges," GE-ANPD, DC 59-2-227, February 1959.
23. Lapides, M. E., "Preliminary Evaluation of Streamline Fuel Element," GE-ANPD, DC 53-10-36, October 1953.
24. Joyner, V. T. and Palmer, C. B., "An Experimental Survey of Flow Across Banks of Elliptical and Pointed Tubes," ARR(WR L-609), January 1943.

25. Heddleson, C. F., "An Experimental Determination of Total Pressure Loss of a Shaped Wire Type Fuel Element in Isothermal Flow," GE-ANPD, DC 54-10-7, October 1954.
26. Noyes, R. N., "An Experimental Determination of the Pressure Loss Through Six Different Shaped Wire Fuel Elements in Isothermal Flow," GE-ANPD, XDC 55-2-43, February 1955.
27. Noyes, R. N., "Correlation of Shaped Wire Type Fuel Element Data in Form Applicable for Prediction of Pressure Loss With Heat Addition," GE-ANPD, XDC 55-5-123, May 1955.
28. Hardy, L. and Neblett, J. W., "Heat Transfer and Pressure Drop of Two-Dimensional Wavy Passages," GE-ANPD, XDC 59-10-13, October 1959.
29. Noyes, R. N., "Subsonic Potential Flow Between Wavy Walls," GE-ANPD, XDC 59-9-121, September 1959.
30. Skirvin, S. C., "Aerothermodynamic Performance Predictions - MTR Specimen 1F36," GE-ANPD, DC 59-10-133, October 1959.
31. Manning, L., "Calibration, Friction Factor and Flow Distribution of MTR 1F36 Cartridge," GE-ANPD, DC 59-12-142, December 1959.
32. Skirvin, S. C. and Holowach, J., "The Corrugated Concentric Ring Fuel Element Development Program Milestone Report No. 1 Task 434511," GE-ANPD, DC 60-5-83, May 1960.
33. Holowach, J., "Corrugated Radial Vane Fuel Element," GE-ANPD, DC 60-5-102, May 1960.
34. Lapides, M. E., "Summary of Analysis of Heat Transfer and Pressure Drop Information and Estimates Applicable to AC-1 Fuel Elements," GE-ANPD, DC 53-3-10, March 1953.
35. Lapides, M. E., "Heat Transfer and Pressure Drop Considerations Concerning the Use of Screen Fuel Elements in the R-1 Reactor," GE-ANPD, DC 53-3-46, March 1953.
36. Lapides, M. E., "Summary of NACA Thermodynamic Tests on 8-Bank Wire Specimen," GE-ANPD, DC 54-3-2, March 1954.
37. Thomson, W. B., "P-123 Folded Flow Reactor Design Study," GE-ANPD, DC 58-9-31, September 1958.
38. Fulton, C. D. and Thomson, W. B., "A Thermodynamic Comparison of Wire, Pebble, and Plate Fuel Elements," GE-ANPD, DC 59-5-252, May 1959.
39. Tong, L. S., "Heat Transfer and Flow Friction Characteristics of Screen Matrices at High Reynolds Numbers," TR-No. 28, Stanford University, April 1956.
40. London, A. L. et al., "Heat Transfer and Flow Friction Characteristics of Crossed-Rod Matrices," TR-No. 41, Stanford University, July 1959.
41. Hardy, L. and Noyes, R. N., "Heat Transfer Characteristics of Crossed Rod Matrices at Elevated Temperatures," GE-ANPD, APEX-724, June 1961.
42. Noyes, R. N., "Investigation of a Particular Kind of Hot Spot Problem on the P-123 System," GE-ANPD, DC 59-5-223, May 1959.
43. Habel, L. W., "Temperature Perturbation Caused by Air Blockage on Screen Matrix," GE-ANPD, DC 60-11-54, November 1960.
44. Rich, T. A. and Lawrence, R. L., "The Clogging of Folded Flow Wire Fuel Elements by Atmospheric Dust," GEL, 60 GL 36, June 14, 1960.
45. Lawrence, R. L., and Rich, T. A., "Dust Collection by Wires," GEL, 60 GL 209.
46. Leoffler, A. L. and Perlmutter, M., "Turbulent Flow Through Porous Resistances Slightly Inclined To The Flow Direction," NACA TN 4221, February 1958.
47. Venneman, W. F., "Folded Flow Through Sphere Type Matrix," GE-ANPD, XDC 59-11-77, November 1959.
48. Heyda, J. F., "An Analytical Study of a Balanced Reverse Folded Flow," GE-ANPD, XDC 60-1-158, January 1960.

49. Heyda, J. F., "A Comparison of Mixed and Stratified Reverse Folded Flows," GE-ANPD, DC 61-2-76, February 1961.
50. Noyes, R. N., "A Fully Integrated Solution of the Problem of Laminar Flow in a Tube With Arbitrary Heat Flux," GE-ANPD, DC 60-3-61, March 1960.
51. Noyes, R. N., "Turbulent Heat Transfer Coefficient Development In Entrance Regions With Variable Heat Flux," GE-ANPD, DC 60-5-47, May 1960.
52. Turney, G. E., "Experimental Determination of Pressure Loss Characteristics for Various Types of Ceramic Tubes," GE-ANPD, DC 60-4-173, April 27, 1960.
53. Turney, G. E., "Flow Through Small Tubes," GE-ANPD, DC 58-2-158, February 1958.
54. Turney, G. E., "Pressure Losses for Flow Through Ceramic Tubes," GE-ANPD, DC 59-2-96, February 1959.
55. Turney, G. E., "Experimental Investigation of the Interstitial Flow In A Single Tier Hexagonal Tube Bundle," GE-ANPD, DC 60-10-88, October 1960.
56. Pugh, R. A., "Thermodynamic Analysis of Round Tube Fuel Elements," GE-ANPD, DC 59-1-54, January 1959.
57. Kaplan, B., "Analysis of Thermal Radiation and Axial Conduction Within Convective Cooled Tubular Systems With Internal Heat Generation," GE-ANPD, XDC 59-10-71, October 1959.
58. Heyda, J. F. and Hermann, R. G., "Temperature Distribution in a Cylindrical Solid With Symmetrically Placed Coolant Channels," GE-ANPD.
59. Carr, R. W. and Heddleson, C. F., "An Experimental Investigation of the Flow Characteristics of a 1/4 Scale CTF Model," GE-ANPD, June 1955.
60. Habel, L. W. and Harper, P. W., "Results of Cold Flow Performance Tests on a 1/4 Scale HTRE No. 3 Reactor Shield Mockup," GE-ANPD, DC 60-5-112, May 1960.
61. Westmacott, R. T. and Jackson, C. C., "Results of Flow Tests on a 1/4 Scale XMA-1 Model to Determine Effect of Orientation of Front and Rear Plugs With Respect to Pressure Losses and Core Weight Flow," GE-ANPD, DC 58-7-185, July 1958.
62. Lapides, M. E., "Standard Design Procedures for Ribbon Type Fuel Element," GE-ANPD, DC 54-9-17, September 1954.
63. Lapides, M. E. and Motsinger, R. E., "Generalized Thermal Design Relationships For Air In Conduits," GE-ANPD, DC 59-3-223, March 18, 1959.
64. Lapides, M. E. and Motsinger, R. E., "Generalized Pressure Loss Computations For Heat Addition To Air Flowing in Constant Area Ducts," GE-ANPD, DC 60-5-57, May 11, 1960.
65. Schoenberger, T. W., "D102A Data Book, 8th Issue," GE-ANPD, DC 59-8-22, July 29, 1959.
66. Noyes, R. N., "The Alleviation of Power Scallop Temperatures in the XMA-1A System by Thermal Diffusion," GE-ANPD, DC 59-1-55, January 1959.
67. Turney, G. E. and Jones, D. L., "Flow Through Misaligned Tubes," GE-ANPD, XDC 58-7-3, July 1958.
68. Flitner, D. P. and Jordan, L. D., "Experimental Investigations of Active Core Region Flow Paths 140E1 Reactor," GE-ANPD, DCL 61-1-88, January 1961.
69. Chandler, B. A., et al., "Effects of Surface Oxidation of Fuel Element on Pressure Loss," GE-ANPD, DC 57-9-32, September 1957.
70. Stanley, R. A. and Holowach, J., "Measurement of Longitudinal Static Pressure Profiles In Ceramic Fuel Tubes," GE-ANPD, DC 61-2-89, February 16, 1961.
71. Powell, W. C. and Yarosh, J. G., "Results of Cold Flow Tests of D102A Moderator," GE-ANPD, DC 58-6-112, June 1958.
72. Elovic, E., "D103A Moderator Temperature Analysis," GE-ANPD, DC 59-9-34, September 1959.
73. Turney, G. E. and Montgomery, H. E., "Experimental Evaluation for Pressure Losses in D103A Control Rod Cooling Passage," GE-ANPD, DC 60-2-29, February 1960.

74. Turney, G. E., "Experimental Evaluation of Pressure Losses In D140E1 Control Rod Cooling Passage," GE-ANPD, DC 60-12-52, December 5, 1960.
75. Eckard, S. E., "D140 Aft Retainer Experimental Heat Transfer Evaluation," DC 61-4-27, GE-ANPD, April 1961.
76. Mason, J. L., "Circumferential Flow Distribution of the XMA-1A External Side Shield, Entrance and Exit Plenum," GE-ANPD, DC 58-12-130, December 1958.
77. Turney, G. E., "Experimental Evaluation of Pressure-Loss-Flow Distribution Characteristics for a Proposed XMA-1A Side Shield Assembly," GE-ANPD, XDC 59-7-78, July 1959.
78. Ferris, M. J. and Roberts, J. M., "User's Manual - IBM 704 Revised XMA-1 Side Shield Program," CAPSO, GV 59-27-20, July 31, 1959.
79. Ferris, M. J. and Roberts, J. M., "Final Revision to XMA-1 Side Shield Temperature Analysis," CAPSO, GV 59-29-17, September 15, 1959.
80. Noyes, R. N., "Radial Temperature Distributions with Internal Heat Generation In Solid Rings of Large Length to Thickness Ratios," GE-ANPD, DC 55-10-61, October 1955.
81. Flock, T. G., et al., "Two Dimensional Diffuser Study," GE-ANPD, DC 56-5-83, May 1956.
82. Carr, R. W. and Heddleson, C. F., "An Experimental Investigation of the Flow Characteristics of a 1/4 Scale CTF Model," GE-ANPD, DC 55-6-113, June 1955.
83. Habel, L. W. and Asher, A. J., "Initial Results of Air Flow Tests for a 180 Degree Annular - Vaned Turn and Header Combination," GE-ANPD, DC 60-2-287, February 1960.
84. Habel, L. W. and Asher, A. J., "Results of Air Flow Tests for a 180 Degree Annular Turn and Header Combination," GE-ANPD, DC 60-7-13, July 1960.
85. Habel, L. W. and Harper, P. W., "Results of Cold Flow Performance Tests on a 1/4 Scale HTRE No. 3 Reactor Shield Mockup," GE-ANPD, DC 60-5-112, May 1960.
86. Asher, A. J. and Ratliff, A. W., "Cold Flow Air Tests Using a 0.27 Scale Model," GE-ANPD, DC 61-5-8, February 14, 1961.
87. Weeden, C. R. and Jones, R. L., "Experimental Investigation of the Aerodynamic Performance for Several Bi-Convex Strut Configurations in Ducts," GE-ANPD, DC 57-1-55, January 1957.
88. Weeden, C. R., et al., "Preliminary Investigation of the Characteristics of Air Flow Through Porous Plugs Formed by Serpentine or Bi-Convex Strut Ducts," GE-ANPD, DC 57-2-82, February 1957.
89. Habel, L. W., "Tests to Determine the Aerodynamic Performance of a 1/4 Scale Model of the Front Porous Plug XMA-1," GE-ANPD, DC 57-8-165, August 1957.
90. Christenberry, R. E., "Investigation of the Aerodynamic Performance of a Serpentine Duct," GE-ANPD, DC 57-10-56, October 1957.
91. Vesper, G. J. and Jones, D. L., "The Effect of Wall Roughness on the Pressure Loss Characteristics of a Serpentine Duct," GE-ANPD, DC 58-11-27, November 1958.
92. Harper, P. W., "Results of Flow Tests on a 1/4 Scale Model on the Front End Ducting of the XMA-1 Power Plant," GE-ANPD, DC 58-1-32, January 1958.
93. Vesper, G. J., "Diffuser Improvements Study and Internal Pressure Loss Characteristics of a Serpentine Porous Plug, XMA-1," GE-ANPD, DC 59-4-21, April 1959.
94. Westmacott, R. T. and Jackson, C. C., "Results of Flow Tests on a 1/4 Scale XMA-1 Model to Determine Effect of Orientation of Front and Rear Plugs with Respect to Pressure Losses and Core Weight Flow," GE-ANPD, DC 58-7-185, July 1958.
95. Westmacott, R. T., "Results of Tests to Determine Pressure Losses and Mass Velocity Ratios for a 1/4 Scale XMA-1A Test Model," GE-ANPD, DC 60-1-20, January 1960.
96. Vesper, G. J., "Experimentally Determined Aerodynamic Characteristics of Two Proposed Front Shield Plugs - XMA-1A," GE-ANPD, DC 60-4-159, April 1960.
97. Harper, P. W. and Bray, A. P., "Experimental Investigation of the Aerodynamic Performance of a Wavy-Duct," GE-ANPD, DC 56-8-142, August 1956.

98. Jones, D. L. and Mason, J. L., "The Pressure Loss Characteristics of a Single Passage Full Scale Model of the Rod and Tube Sheet Type Porous Plug," GE-ANPD, DC 58-7-184, July 1958.
99. Harper, P. W. and Bray, A. P. "Experimental Investigation of the Aerodynamic Performance of a Helical Duct," GE-ANPD, DC 56-8-124, August 1956.
100. Bell, R. W., "Report on Flow Tests in the 1.5 Scale Model of a Typical Radial Cooling Slot in the Front Plug of the D140E-1-Phase I," GV 765, February 24, 1961.
101. Davis, R. S., "Thermodynamic Property Tests of Lithium Hydride - Phase I," GE-ANPD, DC 60-6-71, June 1960.
102. Asher, A. J. and Ratliff, A. W., "Thermodynamic Property Tests of Lithium Hydride - Phase II," GE-ANPD, DC 60-12-132, December 1960.
103. McKee, D. J., "Investigation of the Effective Thermal Conductivities For A Finned Coolant Tube Lithium Hydride Specimen," GE-ANPD, DC 61-1-22, January 1961.
104. McKee, D. J. and Manning, L., "Investigation of the Effective Thermal Conductivity of Cast Lithium Hydride," GE-ANPD, DC 61-5-68, May 1961.
105. Heddleson, C. F., Brown, D. L. and Cliffe, R. T., "Summary of Drag Coefficients of Various Shaped Cylinders," GE-ANPD, APEX-229, April 1957.
106. Cliffe, R. T., Faron, F. S., et al., "Pressure Losses Within Ducting Systems and Components for Incompressible Flow," GE-ANPD, DC 59-1-156, January 1959.
107. Asher, A. J., "Notes on the Use of the Field Mapping Program," GE-ANPD Library File No. 61-1412, January 19, 1959.
108. Wood, C. C. and Henry, J. R., "Aerodynamic Characteristics of a 1/4 Scale Model of the Duct System for the General Electric P-1 Nuclear Power Plant for Aircraft," NACA RM SL 55 G 29B, August 15, 1955.
109. Jones, D. L., "Design and Aerodynamic Calibration of the 1/4 Scale XMA-1A Model Core Simulator," GE-ANPD, DC 59-4-148, April 1959.

4. INSTRUMENTATION

Much of the information summarized in the previous section is dependent upon measurements of temperature, flow and pressure. This section provides a short discussion of the problems, limitations and estimated accuracy of temperature measurements. Information on instrumentation of specific power plants is given in the appropriate volume, APEX-902 through 908. (See APEX-901 for listing of contents of all reports.) A more comprehensive summary of fuel element temperature instrumentation is given in APEX-912.

4.1 TEMPERATURE MEASURING DEVICES

The difficulty of physically reaching fuel element materials being tested in a reactor, the high temperatures involved and the requirements for high reliability have created difficult problems in temperature instrumentation. Optical or radiation methods were difficult to adapt because of the problem of bringing the radiation to the point of detection. The major effort, therefore, was expended to adapt thermocouples to the measurement of fuel element surface temperatures.

The problem of temperature instrumentation of fuel elements is divided into three parts, according to the type of fuel element, as follows:

1. Fuel elements formed basically from thin metallic materials.
2. Fuel elements formed from small diameter (0.04 inch) metallic wires.
3. Fuel elements formed from essentially pure ceramic materials.

In the case of thin flat surfaces, the main problem areas are:

1. The materials and design problem of fastening the thermocouple to the surface in a reliable manner.
2. Provide reliable thermocouple lead wires.
3. The design should accurately measure undisturbed surface temperatures, and if this is not possible, errors must be predictable.

The fuel element surface materials of nichrome and iron-chrome-yttrium were instrumented in a similar manner. The method of attachment is to spot weld platinum and platinum - 10 rhodium wires to the surfaces. These may be bare wires insulated with hard-fired alumina beads or metallic sheathed and insulated wires. The technique of spot-welding and arrangement of the wires is very precise. The details of this method were published.[1]

Errors (fin effects) are encountered because the high-velocity air flowing over the plate cools the wire which in turn cools the plate, in the area of the thermocouple junction. Experimental work for the purpose of determining these errors was published.[2] Errors were found to be proportional to the difference in temperature between the fuel plate and the air temperature and a function of the mass-flow velocity over the surface. The passage through which the air is flowing, the thickness of the fuel plate, the diameter of the thermocouple

wires, and the thermal conductivities of the plate and wires also influence the error. Methods of modifying the experimental data to determine errors for other plate thicknesses, materials and geometry were published.[3] A theoretical analysis of the cooling effect of wires attached to thin plates in which there is heat generation was reported.[4] For the conditions assumed, the errors were approximately 10 to 20 percent of the temperature difference between the flowing air and the fuel plate.

When thermocouples are spot-welded to the fuel sheet, the effective junction is assumed to be at the surface contact between the fuel sheet and the thermocouple wire. This effective junction should remain fixed, but under certain high-temperature conditions, it may move as a function of time due to diffusion of the materials of the fuel plate into the thermocouple wires. Graphs of thermocouple readings whose junctions are attached to iron-chrome-yttrium fuel material were published.[5] At 2000°F no shift in effective junction is evident, but at 2300°F a drop-off of 150°F is experienced over a 100-hour period.

A technique for welding Pt - 6 Rh and Pt - 30 Rh thermocouples onto iron-chrome-yttrium fuel sheet was reported.[6]

An improved technique was developed to accurately and reliably measure surface temperature with a design known as the flattened-sheath construction. The design and technique for applying this method to fuel plates was published.[1] Besides being a more rugged design it is considerably more accurate than wire-type thermocouples. Results of a test to determine the accuracy of the flattened-sheath design were published.[7] A picture of the test specimen is shown in this reference. The flattened sheath and attendant pad indicates a reading approximately 120°F higher than the wire type which agrees well with the predicted errors for the bare-wire type thermocouple.

A theoretical analysis of the errors that may be expected with the pad and ramp type thermocouple (similar to the flattened-sheath design) was reported.[8] This analysis is based on a finite-difference approach to solve the equation involving both conduction and convection. Solutions for various geometries and bounding conditions were obtained with the aid of the THT computer program (see section 2.4).

Platinum versus platinum - 10 rhodium thermocouples encased in nichrome sheaths were relatively unreliable because of differential expansion between nichrome and platinum. This fact plus the desirability of having the lead-wire expansion coefficients match the fuel element structural material (because the leads had to run the length of the structure) resulted in work to develop a thermocouple system which had thermoelements which matched that of the nichrome structural materials and the fuel elements. Work was performed at the General Electric General Engineering Laboratory to obtain a set of thermoelements to match nichrome in expansion characteristics. The calibration of the Chromel "A" versus Hoskins 875 alloy thermocouple, which resulted from this work, was reported.[9] Also shown is its relation to the platinum versus platinum - 10 rhodium thermocouple. The fabrication procedure for flattened-metallic-sheathed thermocouples made from this material was published.[10]

Three techniques of instrumentation of small-diameter fuel wires were reported.[11] One method consists of spot-welding the bare-wire ends directly to the fuel wires. This can be done, however, only with fuel element surface materials such as nichrome. For coated columbium fuel elements the technique of a centrally-located thermocouple wire can be used. A tubular platinum versus paladium thermocouple may also be used. The latter two techniques are described on pages 8 and 10, respectively, in the reference material.

The high temperatures (2300° - 2800°F) used with ceramic-fuel elements has dictated the use of thermocouple materials made entirely of the noble metals, platinum and rhodium, with ceramic insulation. The general geometrical configurations used were pub-

lished.[12] The best configuration tested so far was that called "Duax - hard fired." This method is best because it minimizes decalibrations which occur as the result of evaporation of rhodium into the platinum leg or the platinum-rhodium leg which has the lowest percentage of rhodium. This method overcomes the diffusion of rhodium by shielding each thermoelement with material of the same composition. In the use of thermocouples for high-temperature applications, care must be taken when the leads are routed through zones of high temperature. The calibration errors that may result were reported.[13] Methods of fabrication of junctions were published.[14] It is also beneficial to flame-spray the platinum and platinum-rhodium bare wire thermocouples to prevent decalibration with time.[15] The flame spraying also prevents disintegration of the sheath. A drawing showing how metallic-sheathed thermocouple material is used to instrument a reactor test of ceramic fuel elements was prepared.[16]

4.2 FLOW MEASURING DEVICES

In some of the GE-ANP experimental-flow investigations, the geometry of the test set-up was such that it was not possible to have the recommended ten diameters of straight-run pipe preceding a sharp-edge orifice. As a consequence, attention was given to the possible use of Gentile-type flow measuring tubes. Calibration tests on these tubes were reported.[17] The results of this investigation indicated that the accuracy of a flow tube was substantially affected by upstream geometry, the flow coefficient for the tube was consistently less than that recommended by the manufacturer, and that there was considerable variation of the coefficient with pressure drop across the tube.

A procedure was derived, based on a simplifying approximation, that would permit the direct computation (non-iterative) of the compressible weight-flow of air through an orifice in terms of inlet and exit pressures, the total temperature, and orifice geometry. The error in true weight-flow, caused by the approximation, was less than 1 percent for a wide range of orifice geometries and operating conditions. The derivation of the final computational equation together with a comprehensive set of orifice tabulations based on IBM solution of the equation was reported.[18]

A description of a "double-pass" Schlieren system built by GE-ANP was published.[19] In the double-pass system, light rays that pass through the test section twice by the mechanism of reflection from a single concave mirror, are cut by a knife-edge at the focal point of the mirror, and then diverge to hit the screen. The double-pass system has approximately twice the sensitivity of the conventional two-mirror single-pass apparatus and had the additional merit of simplicity and low cost.

4.3 REFERENCES

1. Bean, J. F. and Robison, A. G., "Design, Fabrication and Installation Manual for In-Pile Thermocouple Circuits," GE-ANPD, DC 60-2-275, February 1960.
2. Clark, R. H., "Calibration of Fuel Element Thermocouples," DC 55-6-12, GE-ANPD, June 1955.
3. Kuhlman, W. C., "Corrections to Indicated Temperatures of Thermocouples Attached to the MTR 121 Specimen," GE-ANPD, DC 58-11-152, November 1958.
4. Heyda, J. F., "Local Cooling of Thin Plates by Attached Thermocouples," GE-ANPD, DC 58-6-170, June 20, 1958.
5. Reis, P. E., "Induction Heater Test of Small Samples of Advanced Material," GE-ANPD, DC 59-6-28, June 1959.
6. Kuhlman, W. C., "Project 101 and 2C Thermocouple Attachment Techniques," GE-ANPD, DC 59-3-251, March 1959.
7. Controls and Instrumentation Development Quarterly Task Report April through June 1959, DC 59-6-10.
8. Boudreaux, R. A., et al., "Pad-Type and Air Thermocouple Evaluation," GE-ANPD, DC 58-11-151, November 1958.
9. Hintze, A. S., "Chromel A versus Hoskins 875 Thermocouple Calibration," GE-ANPD, DC 59-10-120, October 1959.
10. Glasgow, J. W., "Fabrication of Chromel A versus Hoskins 875 Alloy Thermocouples," GE-ANPD, DC 59-10-202, October 1959.
11. Kuhlman, W. C., "Instrumentation of Metallic Fuel Elements," GE-ANPD, DC 60-6-138, June 1960.
12. Freeman, R. J., "Thermoelectric Stability Pt-Rh Thermocouples - Milestone No. 1 Report," GE-ANPD, XDC 60-12-28, December 1960.
13. Freeman, R. J., "Distributed Goebeck Effect at High Temperatures," GE-ANPD, XDC 60-1-166, January 1960.
14. Freeman, R. J., "Coaxial Thermocouple Investigation Report No. 1," GE-ANPD, DC 58-7-79, July 1958.
15. "Control Design Quarterly Task Report January through March 1961," DC 61-3-6.
16. "Controls and Instrumentation Development Quarterly Task Report January through March 1960," DC 60-3-10.
17. Carr, R. W. and Heddleson, C. F., "Calibration of Gentile Flow Tubes," GE-ANPD, DC 55-9-116, September 1955.
18. Hardy, L., "Orifice Tabulations and Curves," GE-ANPD, DC 59-6-186, June 1959.
19. Hardy, L., "Operational Characteristics of a Double Pass Schlieren System," GE-ANPD, DC 58-4-169, April 1958.

5. MISCELLANEOUS SUPPLEMENTARY INVESTIGATION

This section is a brief comment and reference identification of some investigations which were supplementary to the aerothermodynamic analyses and experiments performed in development of the direct cycle aircraft nuclear power plant and its components.

5.1 ANALYTICAL STUDIES WITH GENERAL APPLICABILITY TO REACTOR AEROTHERMODYNAMICS

A procedure was reported for determining the temperature field in a non-concentric annulus when the heat released from the bounding, circular, cylindrical walls is of unequal strength.[1] The flow is turbulent and the hydrodynamic boundary-layer is fully developed. The thermal boundary-layer starts developing at the longitudinal position where heating commences. In the analysis it is assumed that the line of maximum velocities for turbulent flow through a non-concentric annular cross section is equivalent to that for laminar flow, since the latter can be obtained exactly in the notation of a bi-polar coordinate system.

The complete closed-form solution for the case of laminar incompressible flow between non-concentric cylinders was reported.[2] The solution, in bipolar coordinates, gives the velocity as a function of position in the cross-sectional flow area.

A method for the assessment of the cross-sectional temperature distribution in unfueled ceramic tubes in the radial reflector region outside the active core was published.[3] This paper presents an exact solution for the problem of two-dimensional heat flow in an annular ring in which there is an exponential decay of internal heat generation from one terminal of the outer diameter of the ring to the other. The decay constant may be arbitrarily assigned.

A method for determining the effect of manufacturing tolerances on the temperature distribution in the cross section of a hollow fuel tube was reported.[4] Specifically, this method will predict the effect of non-concentricity of the coolant hole in the fuel tube on temperature perturbation in the solid material of the cross section. The outer boundary of the tube is assumed to be insulated, the tube-wall material has uniform heat generation, and a constant heat transfer coefficient exists on the periphery of the non-con entric coolant hole.

A source file of heat transfer data for design problems associated with nuclear reactors was reported.[5] This file deals with turbulent flow of gases in various types of ducts. The following items are discussed: heat flux and mode of heat-input effects, entrance-region effects, duct cross section effects, annular passages, heat transfer-momentum analogies, and recommendations of analytical methods used on the duct configurations considered.

5.2 EXPERIMENTAL STUDIES WITH GENERAL APPLICABILITY TO REACTOR AEROTHERMODYNAMICS

The "Coanda Effect" states that when a fluid flows from a duct discharge with both diverging and straight walls, and empties into an infinite plenum, the flow will be turned through an angle toward the diverging wall. The total pressure loss associated with this type of

expansion will be less than that of free expansion from a similar cross-section duct with an abrupt discharge. Results from exploratory experimental tests on the Coanda effect was reported.[6] From these tests it was concluded that a Coanda nozzle will deflect a stream of air leaving a pipe or duct with less than one velocity head loss in total pressure up to some critical Mach number which is a function of the radius of the diverging wall of the nozzle.

An experimental study of airflow through a duct containing staggered rows of streamline struts with axis normal to the air stream was reported in reference 87 of section 3. Biconvex struts (formed by two circular arcs) having aspect ratios of 3:1 and 5:1 were tested over a range of pitches, gaps and flow conditions. The results of this investigation are in the form of effective friction factor versus Reynolds number for the various geometries considered.

A transient technique of determining heat transfer coefficients for fuel element designs was reported.[7] Evaluation of the merit of this method was determined by comparing data taken during transient cooling of a large-scale test specimen, consisting of flat plates, to that obtained from steady-state heat transfer results. A correlation of the transient data indicated that this method gives results that are within 8 percent of recommended steady-state experimentally determined values.

5.3 REFERENCES

1. Heyda, J. F., "Heat Transfer in Turbulent Flow through Nonconcentric Annuli," GE-ANPD, APEX-391, June 1957.
2. Heyda, J. F., "A Green's Function Solution for the Case of Laminar Incompressible Flow Between Non-Concentric Cylinders," GE-ANPD, XDC 58-2-205, February 1958.
3. Heyda, J. F., "Temperature and Heat Flux in a Long Hollow Tube with an Exponential Heat Source," GE-ANPD, DC 60-10-40, October 1960.
4. Heyda, J. F., "Temperature Distribution in a Heated Cylinder with an Eccentric Hole," GE-ANPD, XDC 60-11-88, November 1960.
5. Lapides, M. E. and Goldstein, M. B., "Heat Transfer Source File Data," GE-ANPD, APEX-425, September 1957.
6. Keating, J. B., "Experimental Results of the Feasibility of a Coanda Nozzle," GE-ANPD, DC 56-11-145, November 1956.
7. Sowards, J. W. and Menkow, J. W., "Determination of Heat Transfer Coefficients by a Transient Technique," GE-ANPD, DC 58-5-71, May 1958.